

Park Unit shelves

CVIS

RESEARCH/RESOURCES MANAGEMENT REPORT SER-91/04

The Hydrogeology of Southern
Cumberland Island, Georgia

WINGS BAY

ENVIRONMENTAL MONITORING PROGRAM
CUMBERLAND ISLAND NATIONAL SEASHORE

**Please do not remove
this item from
Resource Room**

NATIONAL PARK SERVICE
WATER RESOURCES DIVISION
FORT COLLINS, COLORADO
RESOURCE ROOM PROPERTY

Prepared for DEPARTMENT OF THE NAVY
Naval Facilities Engineering Command
Washington, DC

U.S. Department of the Interior

National Park Service



Digitized by the Internet Archive
in 2012 with funding from
LYRASIS Members and Sloan Foundation

<http://archive.org/details/hydrogeologyofso00hern>

THE HYDROGEOLOGY OF SOUTHERN CUMBERLAND ISLAND, GEORGIA

Jennifer G. Herndon
Department of Geology
Georgia State University
Atlanta, GA 30303

RESEARCH/RESOURCES MANAGEMENT REPORT SER-91/04

KINGS BAY ENVIRONMENTAL MONITORING PROGRAM REPORT

DECEMBER 1991

Produced under Cooperative Agreement No. CA-5000-9-8005 to Georgia State University for the National Park Service, Southeast Region. Funding provided by the Department of the Navy under Interagency Agreement No. IA 5000-8-8002 with the National Park Service.

NATIONAL PARK SERVICE
WATER RESOURCES DIVISION
FORT COLLINS, COLORADO
RESOURCE ROOM PROPERTY

Dr. Stephen V. Cofer-Shabica
Program Officer
Cooperative Research Unit
Institute of Ecology
University of Georgia
Athens, GA 30602

U.S. Department of the Interior
National Park Service
Southeast Regional Office
75 Spring Street, S.W.
Atlanta, GA 30303

PREFACE

Cumberland Island National Seashore was established in 1972 to preserve the scenic, scientific and historical values of the largest and most southerly island off the coast of Georgia. It is well known for its marine turtles, abundant shorebirds, dune fields, maritime forests, fishing, marshes and tidal creeks and flats, and historic structures. The St. Marys Inlet, at the border between Florida and Georgia, is a Federally maintained entrance channel to the Intracoastal Waterway, ports at Fernandina, Florida, and St. Marys, Georgia, and the US Naval Submarine Base at Kings Bay, Georgia. Construction of coastal engineering works and channel dredging over the past 100 years have had noticeable effects on the St. Marys Entrance, Cumberland Island, Georgia and Amelia Island, Florida. In the early 1960's, Kings Bay was selected as the Navy's home port for Poseidon-class submarines. In the mid-1970's Kings Bay was selected to homeport the Navy's new class of Trident submarines. In upgrading the Kings Bay base from the smaller Poseidon submarines, it was necessary to deepen, widen, and lengthen the entrance channel to Kings Bay. The five year, Kings Bay Environmental Research Program was conceived in 1986 by the U.S. Departments of Interior and Navy. This Department of the Navy funded Program focuses on evaluating the potential effects on the natural resources of Cumberland Island and vicinity of the deepening of the Kings Bay Trident Submarine ship channel from 42 ft. (12.7 m) to 51 ft. (15.5 m). The channel is almost 22 miles (35.2 km) long and required the removal of approximately 35 million cubic yards (26.8 million cu m) of dredged material. The potential biophysical effects of dredging are being evaluated by the National Park Service through a series of biological and geological research projects. The Department of the Navy, through the US Army Engineers, is monitoring the physical aspects of the ocean shoreline of Cumberland and Amelia Islands and the Cumberland Sound estuary. Technical direction and guidance during the study were provided by Dr. Albert Greene, Jr., National Park Service (NPS); Messrs. Thomas J. Peeling, Naval Facilities Engineering Command (NAVFAC); John Headland, NAVFAC; Darryll Molzan, NAVFAC; Dr. Robert Dean, University of Florida, Gainesville (NPS); Dr. Stephen Cofer-Shabica (NPS); and the late Dr. William Odum, University of Virginia, Charlottesville (NPS).

The ultimate goal of this research is to document the potential for short- and long-term changes on the resources of Cumberland Island and Cumberland Sound estuary related to channel dredging. The work described in this report is one of a series of National Park Service studies directed towards this goal.

Stephen Cofer-Shabica

ABSTRACT

A hydrogeologic investigation of southern Cumberland Island was conducted to determine the effect of channel dredging on the groundwater quality in the Pliocene-Miocene aquifer. As a part of the study 10 wells were installed on the southern portion of the island. Three wells were installed at two cluster sites and four wells were installed at a third cluster site.

The aquifers of interest included the Miocene sand aquifer, the Pliocene-Miocene aquifer, and the surficial aquifer. Water-level measurements during high tide indicate that the horizontal gradient of the surficial aquifer was toward the southwest and the Pliocene-Miocene aquifer was toward the west. The direction of groundwater flow within the Pliocene-Miocene aquifer may change in response to fluctuating tides and storm surges.

An aquifer test performed in the Pliocene-Miocene aquifer indicated that the transmissivity of the aquifer ranged from 235 to 650 ft²/d, the hydraulic conductivity ranged from 34 to 94 ft/d, the storage coefficient ranged from 1.05×10^{-5} to 5.6×10^{-5} , and the diffusivity ranged from 5.9×10^3 to 3.5×10^7 ft²/d. Test data indicated that lateral and vertical heterogeneities existed in the aquifer. The seepage velocity of the Pliocene-Miocene aquifer ranged from 0.049 to 0.085 ft/d

The surficial aquifer was in a steady-state condition with constant long-term recharge, equivalent discharge and no appreciable withdrawals due to pumping. Approximately 2.85×10^5 gallons per square mile recharged the aquifer each day and nearly the same amount was discharged to the low lying wetlands (1.92×10^5 gal/d), the underlying Pliocene-Miocene aquifer (8.5×10^4 gal/d), and along the coast at the seepage face (7.58×10^3 gal/d).

Analysis of hydraulic data suggest that intrusion of seawater from the channel into the Pliocene-Miocene aquifer was insignificant. The amount of freshwater discharged from the aquifer during flushing was an order of magnitude greater than the volume of seawater that intruded the aquifer. The net volume of freshwater discharged from the Pliocene-Miocene aquifer per unit area was 0.019 ft³/ft² d (0.142 gal/ft² d).

ACKNOWLEDGEMENTS

I would like to thank my thesis advisor, Dr. Ram Arora, for his direction in this thesis. Appreciation is extended to my committee members Dr. Seth Rose, Dr. V.J. Henry, and Dr. Stephen Cofer-Shabica for their reviews and comments. A very special thanks is extended to Robert Randolph for his advice, direction, and reviews. Sincere gratitude is extended to Woody Hicks and Rick Krause of the U.S. Geological Survey for their reviews and suggestions. Gratitude is extended to my colleagues at the U.S. Geological Survey for their support and encouragement during this endeavor. I would like to thank Barbara Milby, Mike Pecker, Alan Cressler, and Steve Wilson for their invaluable assistance with the aquifer test.

Sincere thanks is extended to the National Park Service maintenance crew for their pleasant assistance on several odd jobs on the island. Without their help, many jobs would not have been completed successfully. I would also like to thank Dave Brackett for building and calibrating the flow meter used in the study. A very special thanks goes to Willis G. Hester for his generous help and advice in drafting my figures. Special thanks goes to Gary Davis for his incredibly good advice and reviews of my thesis. Sincere thanks is extended to Jon Olivier for his encouragement to complete my degree.

I dedicate this thesis to my parents, Johnny and Margaret, who provided abundant support and love that inspired and enabled me to complete this thesis.

TABLE OF CONTENTS

Abstract	i
Acknowledgements	ii
Table of contents	iii
Tables	v
Illustrations	vi
Introduction	1
Purpose and scope	1
Description of study area	4
Climate	4
Previous work	5
Geologic framework	7
Geomorphology	7
Regional island geology	8
Local geology	21
Miocene series	21
Pliocene series	28
Holocene and Pleistocene deposits	29
Methods of investigation	30
Surface geophysics	30
Drilling methods	31
Well design and construction	32
Well development	36
Borehole geophysics	39
Natural gamma	39
Electric logs	40
Spontaneous potential	40
Single point resistance	41
Grain size analysis	42
Aquifer test	42
Step drawdown test	43
Multi-well aquifer test	43
Analysis of surface geophysics and well site location	45

Hydrogeologic framework	53
Miocene sand aquifer	53
Pliocene-Miocene aquifer	55
Surficial aquifer	62
Aquifer interaction	66
Analytical model	68
Aquifer test	72
Interpretation	75
Hantush-Jacob method	78
Straight line method	87
Streltsova.	87
Bixel-Van Poolen.	89
Discussion	97
Potential for seawater encroachment due to channel dredging	103
Conclusions	108
Future work	111
References	112
<u>Appendix</u>	
A. Grain size analysis data	117
B. Core descriptions	119
C. Estimation of hydraulic conductivity based on grain size analysis	133
D. Density corrections	138
E. Leakage and analytical model calculations.	142
F. Step drawdown	147
G. Derivation of the diffusion equation	154
H. Aquifer test data and calculations for transmissivity and storage values	158
I. Tidal effects	171
J. Calculations for potential seawater intrusion	180

TABLES

1. Well construction summary.	37
2. Groundwater level summary for June 28, 1990.	58
3. Percent seawater and water density at each well.	59
4. Transmissivity and storage values of the Pliocene-Miocene aquifer	86
5. Transmissivity, hydraulic conductivity, and seepage velocity values of the limestone and sand zones of the Pliocene-Miocene aquifer.	96
A1. Raw grain size analysis data.	118
H1. Drawdown data for KBMP 7, December 8, 1989.	159
H2. Recovery data for KBMP 7, December 10, 1989.	160
H3. Drawdown data for KBMP 11, December 8, 1989.	161
H4. Recovery data for KBMP 11, December 10, 1989.	162
H5. Drawdown data for KBMP 12, December 8, 1989.	163
H6. Recovery data for KBMP 12, December 10, 1989.	164

ILLUSTRATIONS

	Page
Figure 1. Cumberland Island, GA and surrounding geographical features.	2
2. Location and depth of channel dredging by the US Navy and well site locations.	3
3. Location of wells, Cumberland Island.	9
4. Stratigraphic section and gamma logs for wells GGS 3426, 34E10, and 34F13.	10
5. Location of boreholes and geologic sections, Cumberland Island	12
6. Geologic section A to A'	13
7. Geologic section B to B'	14
8. Altitude of the top of the Charlton Formation	15
9. Altitude of the top of the Duplin Formation	17
10. Thickness of the Duplin Formation	18
11. Altitude of the top of the clay sediments of Pleistocene age	19
12. Thickness of clay sediments of Pleistocene age	20
13. Lithology and geophysical logs at well KBMP 1, site 1	22
14. Geologic section D to D'	24
15. Lithology and geophysical logs at well KBMP 6, site 2	25
16. Geologic section C to C'	26
17. Lithology and geophysical logs at well KBMP 10, site 3	27
18. Well construction at well site 1.	33
19. Well construction at well site 2.	34
20. Well construction at well site 3.	35
21. Grain size distribution curves, in thousandths of an inch	38

22. EM conductivity surface where the coil spacing is 33 feet and coil configuration is horizontal.	46
23. EM conductivity surface where the coil spacing is 33 feet and coil configuration is vertical.	47
24. EM conductivity surface where the coil spacing is 66 feet and coil configuration is horizontal.	48
25. EM conductivity surface where the coil spacing is 66 feet and coil configuration is vertical.	49
26. EM conductivity surface where the coil spacing is 132 feet and coil configuration is horizontal.	50
27. EM conductivity surface where the coil spacing is 132 feet and coil configuration is vertical.	51
28. A. Hydrogeology at well sites 1 and 2. B. Hydrogeology at well site 3.	54
29. Potentiometric surface map of the Pliocene-Miocene age aquifer for June 28, 1990	57
30. Potentiometric surface map of the surficial aquifer for June 28, 1990.	64
31. Comparison of the Pliocene-Miocene aquifer water levels to the channel stage, August, 1990.	67
32. Conceptual model of the aquifer system, site 3	69
33. Location and depth of pumping and observation well for aquifer test, site 3.	73
34. Schematic diagram of the hydrogeology and well construction at the aquifer test site	74
35. The Theis governing equations and assumptions	77
36. The Hantush-Jacob leaky governing equations and assumptions	79

37. Comparison of well KBMP 11 drawdown data to the Hantush-Jacob leaky curve	82
38. Comparison of well KBMP 11 recovery data to the Hantush-Jacob leaky curve	83
39. Comparison of well KBMP 12 drawdown data to the Hantush-Jacob leaky curve	84
40. Comparison of well KBMP 12 recovery data to the Hantush-Jacob leaky curve	85
41. Streltsova (1988) governing equations and assumptions	88
42. KBMP 11 drawdown. Transmissivity solved for by the straight line method	90
43. KBMP 11 recovery. Transmissivity solved for by the straight line method	91
44. KBMP 12 drawdown. Transmissivity solved for by the straight line method	92
45. KBMP 12 recovery. Transmissivity solved for by the straight line method	93
46. Bixel-Van Poolen (1967) governing equations and assumptions	94
47. KBMP 7 drawdown data. Transmissivity solved for by the straight line method	98
48. KBMP 07 recovery data. Transmissivity solved for by the straight line method	99
49. Configuration of aquifer test plots with varying transmissivity and storage values	100
50. Difference in the Pliocene-Miocene aquifer head and the channel stage	

during a 24 hour period.	105
C1. Grain size distribution curves, in phi units.	135
C2. Estimation of hydraulic conductivity once d_{50} and the standard deviation are known (Masch and Denny, 1966).	136
F1. A. Plot of s/Q vs. Q to determine B and C values. B. Table of discharge, drawdown, percent of head loss due to laminar flow, and specific capacity.	149

INTRODUCTION

During the mid-seventies, the U.S. Navy initiated a channel-dredging program to facilitate Trident submarine traffic to and from the Kings Bay Naval base, located on the mainland near St. Marys, Ga. (Figure 1). The U.S. Army Corps of Engineers drilled over 300 boreholes in the Kings Bay ship channel to determine the shallow sediment and rock composition and the depth to the top of rock. Based on their log descriptions of 1984, the amount of overburden covering the Miocene limestone ranged from none in some areas near the center of the channel to as much as 54 feet* along the banks. The average thickness of the overburden was 18 feet. At that time the depth to the bottom of the channel ranged from 17 to 48 feet with an average depth of 30 feet. The Navy has since dredged the channel to a depth of 51 feet below mean sea level (Figure 2). This depth of dredging removed clay and silt deposits that protected the freshwater aquifers from seawater intrusion and in many areas breached the Miocene limestone.

The U.S. Departments of the Interior and Defense, in cooperation with Georgia State University, developed a 5-year cooperative program to evaluate the effects of channel dredging on the hydrogeological system. This thesis describes the results of the hydrogeologic investigation of Cumberland Island and determines the effect of channel dredging on the Pliocene-Miocene aquifer.

Purpose and Scope

The purpose of this investigation was to determine the effect of channel dredging on the quality of water in the Pliocene-Miocene aquifer. As part of the study, the geologic and hydrogeologic framework of southern Cumberland Island was characterized by: completing a literature and data search; installing new wells; describing core and

*1 foot = 0.3048 meters

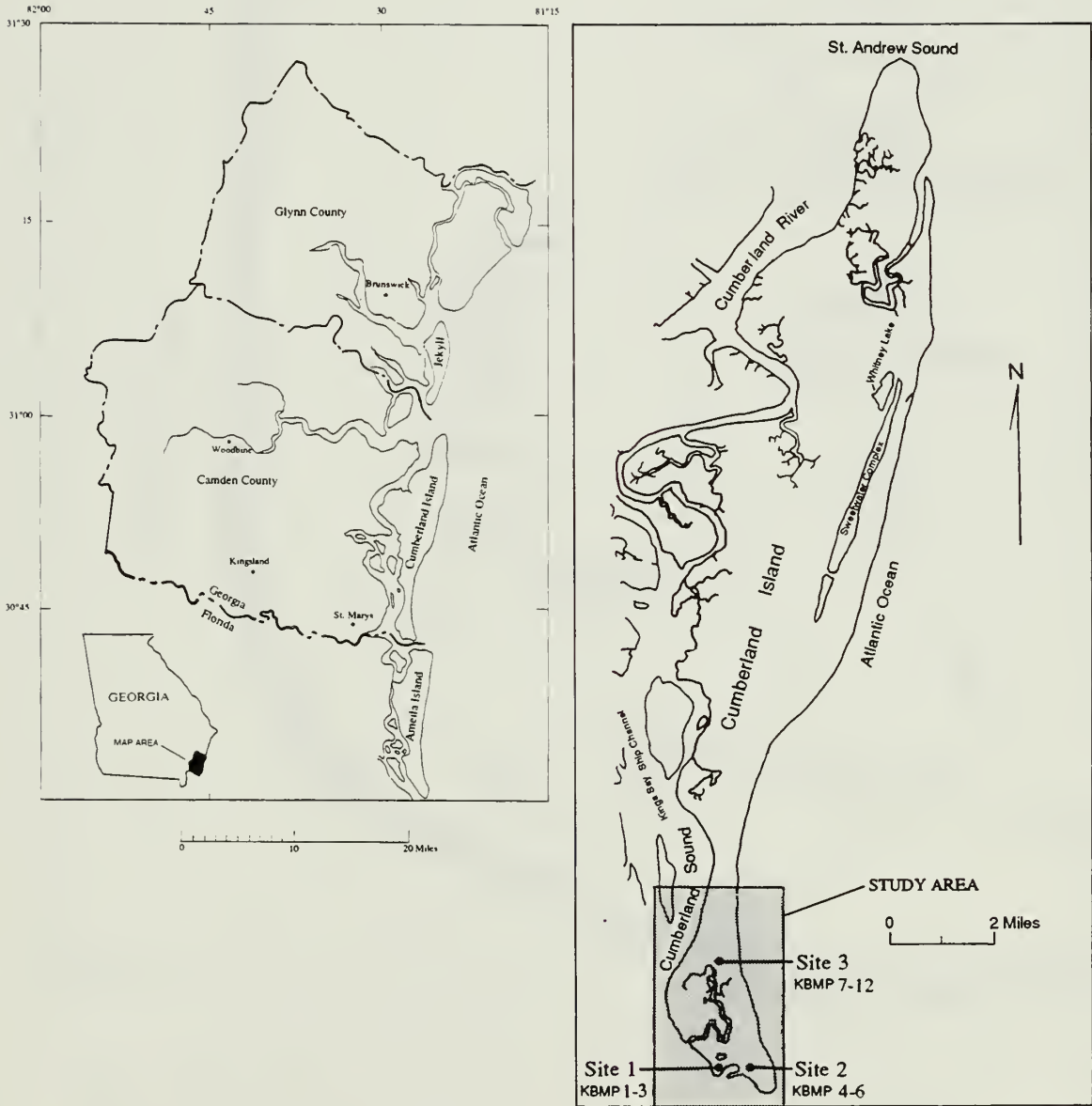


Figure 1. Cumberland Island, Ga., and surrounding geographical features.

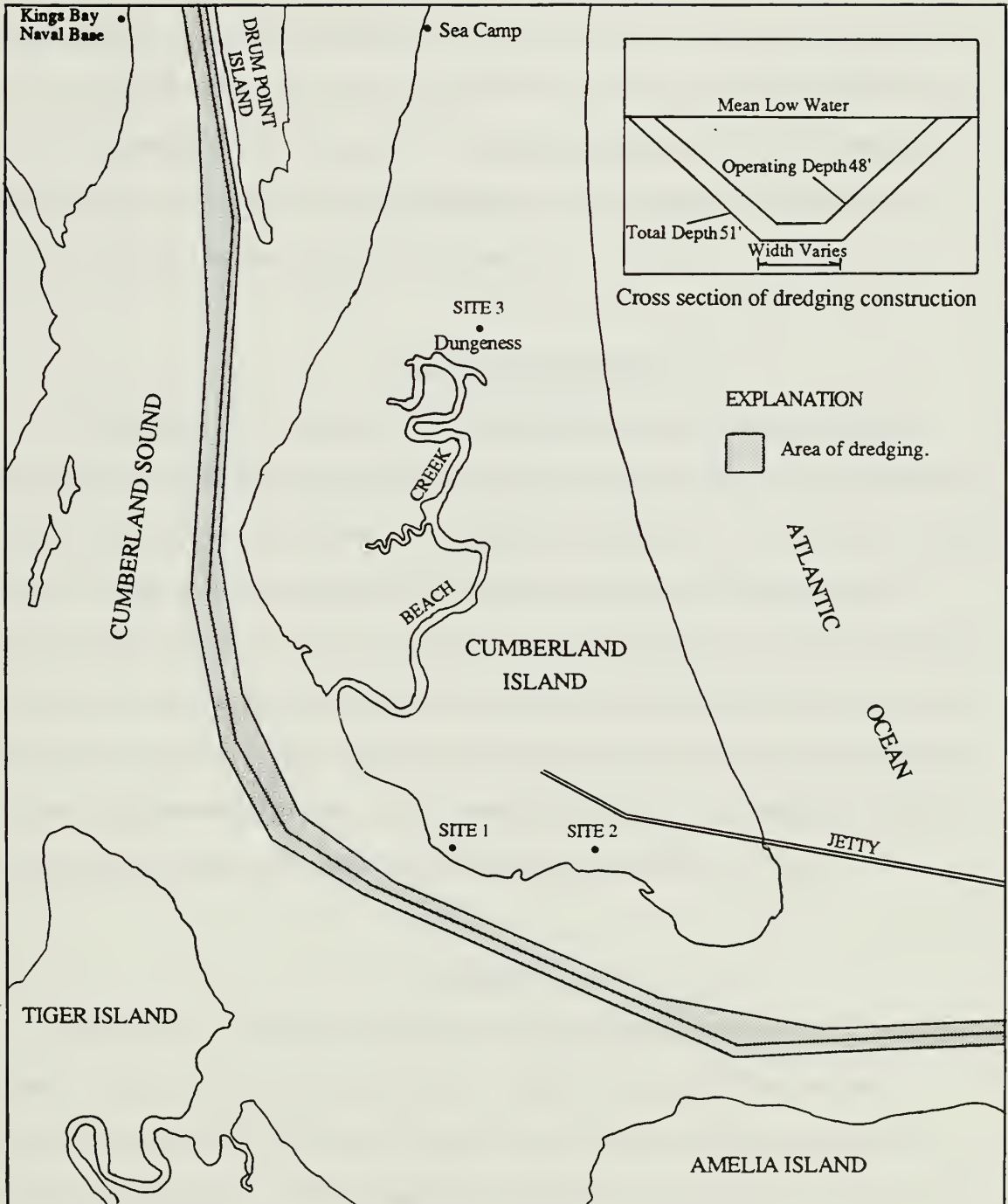


Figure 2. Location and depth of channel dredging by the US Navy and well site locations.

cutting samples; conducting surface and borehole geophysics; and constructing structure and potentiometric maps. The hydraulic properties of the Pliocene-Miocene aquifer were determined through aquifer testing. Water level data and aquifer test results were used to determine aquifer interaction and the potential for seawater intrusion into the Pliocene-Miocene aquifer from Cumberland Sound Channel.

Description of Study Area

Cumberland Island is located in the Barrier Island sequence of the Sea Island section of the Coastal Plain physiographic province. It is a compound barrier island on the Georgia coast just north of the Georgia-Florida State line (Figure 1). The island is 19 miles long and 3 miles wide at the broadest point having an area of about 60 square miles (McLemore and others, 1981). It is separated from Jekyll Island, Ga., by the St. Andrews Sound to the north and from Amelia Island, Fla., by the Cumberland Sound to the south. The study area extends from the south end of Cumberland Island to the area surrounding Dungeness and encompasses an area of 9 square miles (Figure 1). Cumberland Island is administered as a National Seashore by the National Park Service.

Climate

The island's climate is characterized by long, humid summers and mild, dry winters. The mean annual rainfall is about 52 inches of which 40 inches are lost to evapotranspiration, 6 inches to storm runoff and the remaining 6 inches are available for recharge (Brown, 1984). From the months of June through September the island receives 60 percent of the annual rainfall. The dry season occurs from October to May (Brown, 1984).

PREVIOUS WORK

Martinez (1980) described the Neogene stratigraphy of Cumberland Island including lithologic descriptions, paleontology, and thicknesses of each zone. Data were collected from core and cuttings from 18 boreholes and seismic profiles taken from the periphery of the island. McLemore and others (1981) provided a brief description of the stratigraphy from late Eocene to Holocene age and discussed the geomorphology of the island. The report also evaluated the hydrogeology of the island with emphasis on the Floridan aquifer system but did not define the hydraulic properties of these aquifers. The water quality of the Floridan and surficial aquifers was included.

Brown (1984) defined the hydrogeologic framework of northeastern Florida and southeastern Georgia. The majority of the data were collected from Fernandina Beach, Fla., and St. Marys, Ga., areas. Cumberland Island was included in the study area, but the hydrogeology of the island was not investigated. The report contained a detailed description of the hydrogeologic characteristics of the Floridan aquifer system. Also, a range of estimated transmissivity values were given for the surficial aquifer (100 to 1000 square feet per day (ft^2/d) based on lithology) and the Pliocene-Miocene aquifer (750 ft^2/d based upon aquifer testing) at Kingsland, Ga., 15 miles from the study area. The recharge and discharge areas for the upper and lower Brunswick, Pliocene-Miocene, and surficial aquifers were discussed for the region.

Miller (1986) described the hydrogeologic framework of the Floridan aquifer system, and Bush and Johnston (1988) determined the ground-water hydraulics and regional flow in its entire aerial extent. Krause and Randolph (1989) defined the hydrogeology of the Floridan aquifer system and evaluated its development potential using digital modeling. Although these investigations included Cumberland Island, they were

part of a regional aquifer evaluation and were not specific to the hydrogeology of the island.

Clarke and others (1990) provided a detailed description of the late Eocene through late Miocene age deposits along the coast of Georgia. In their report, core, cuttings, and geophysical logs were described from a well on the island. The report also described the Floridan aquifer system, the upper and lower Brunswick aquifers, and the surficial aquifer along the coast of Georgia. A map of the potentiometric surface of the Floridan aquifer (May 1985) at Cumberland Island was included.

In summary, much hydrogeologic information is available for the Floridan aquifer system in the southeast Georgia, northeast Florida area. However, information is limited for the aquifers above the Floridan aquifer system in the Cumberland Island area. Information pertaining to the characteristics of those aquifer systems overlying the Floridan on Cumberland Island generally does not exist.

GEOLOGIC FRAMEWORK

Geomorphology

The geomorphology of Cumberland Island is typical of barrier islands along the Georgia coast. From seaward to landward margin, the geomorphic provinces are the beach, foredunes, interdune meadow, back dunes, interior forest, and marshes. McLemore and others (1981) gave a thorough description of the Cumberland Island geomorphology. The following discussion is a brief synopsis of their description.

The beaches of Cumberland Island are composed of fine quartz sand. The beaches average 125 feet in width and are as much as 300 feet wide on the southeast coast due to construction of a jetty on the south end of the island in 1876. The landward margin is not as expansive as the seaward margin. The landward margin is composed of Pleistocene sands eroded from the island and clay derived from Cumberland Sound. Some areas along the seaward margin consist of the oyster *Crassostrea virginica*. However, these areas are not extensive.

The foredunes lie behind the eastern beach and extend the length of the island. The dunes vary in height from 1.5 feet to 6 feet and consist of cross-bedded fine quartz sand and some heavy minerals. In general these dunes erode during the winter and rebuild in the summer.

Interdune meadows are broad basin areas adjacent to the foredunes. The meadows receive sediment from wind-blown sand off the beach and foredunes and periodically by washover as a result of storm surges. The meadows are composed of well-sorted, fine quartz sand. Sediment remains in the interdune meadow only if stabilized by vegetation, as is the case on the south end of the island.

Back dunes lie behind the interdune meadow over most of the island's length and

extend to a maximum height of 45 feet. They are composed of well-sorted, cross-bedded, fine quartz sand and heavy minerals. The back dunes migrate to the west because of the prevailing easterly winds. Migration may be rapid where there is a lack of vegetation.

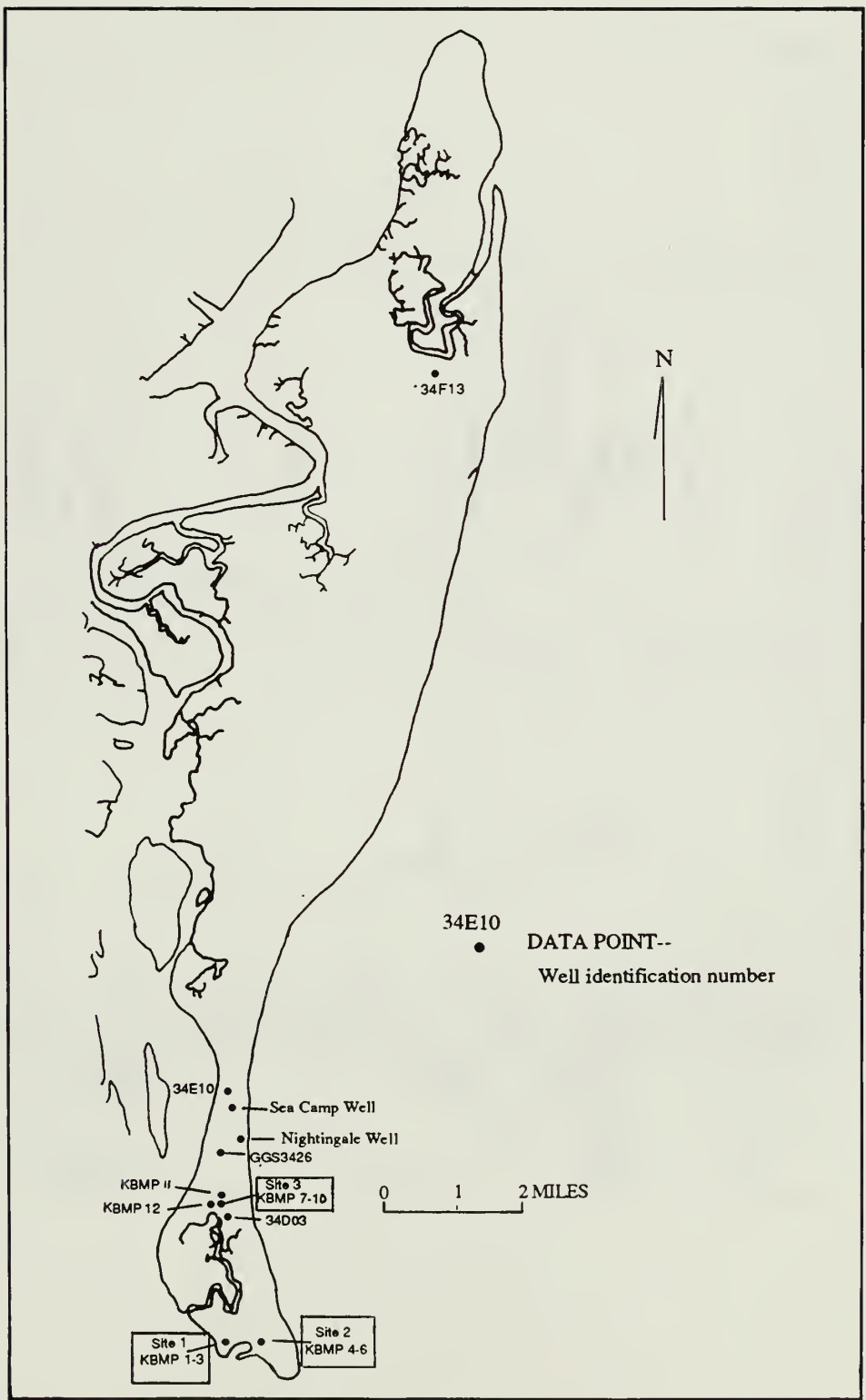
Live oaks and palmettos of the maritime forest prevent rapid migration of dunes along the Raccoon Keys salt marsh. The undergrowth of the interior maritime forest consists almost entirely of saw palmetto. The forest lies on flat rolling Pleistocene sand and is the prominent feature on the island.

The salt marshes dominate the west side of Cumberland Island which is typical of Georgia barrier islands. These marsh deposits consist of clay sediment in low-lying areas and silty sand in elevated areas such as on hammocks. The freshwater inland marshes form in areas of low topography such as Johnson Pond, or where drainage is impeded by dunes along the east coast such as Lake Whitney and the Sweetwater Complex (see Figure 1). These marshes are not influenced by tidal currents (McLemore and others, 1981).

Regional Island Geology

Cumberland Island is underlain by a thick sequence of consolidated and semiconsolidated coastal plain sediments. Lithological and geophysical data exists for a few of the deep wells (approximate total depth of 600 feet) on the island (see Figure 3 for well locations). Stratigraphy below this depth are not addressed in this thesis; only the late Eocene through Holocene age deposits are discussed herein.

The late Eocene age unit consists of the Ocala Limestone, the top of which is located 548 feet below land surface (see Figure 4). The Ocala is a massive fossiliferous limestone that contains bryozoan remains, foraminifera tests, and mollusk shells. This limestone formed in a warm, shallow-water, carbonate-bank environment (Clarke and others, 1990).



Base from McLemore and others (1981).

Figure 3. Location of wells, Cumberland Island.

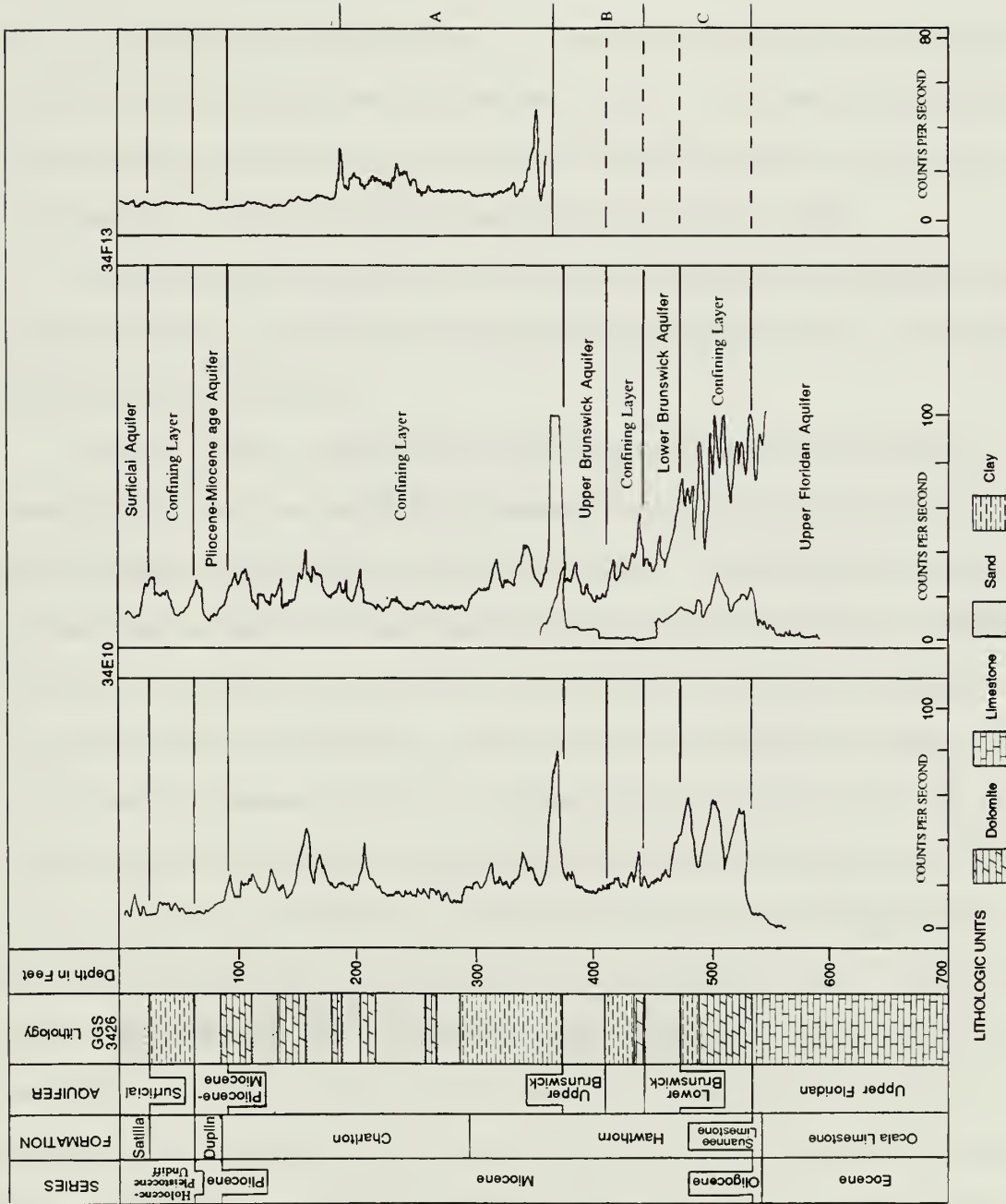
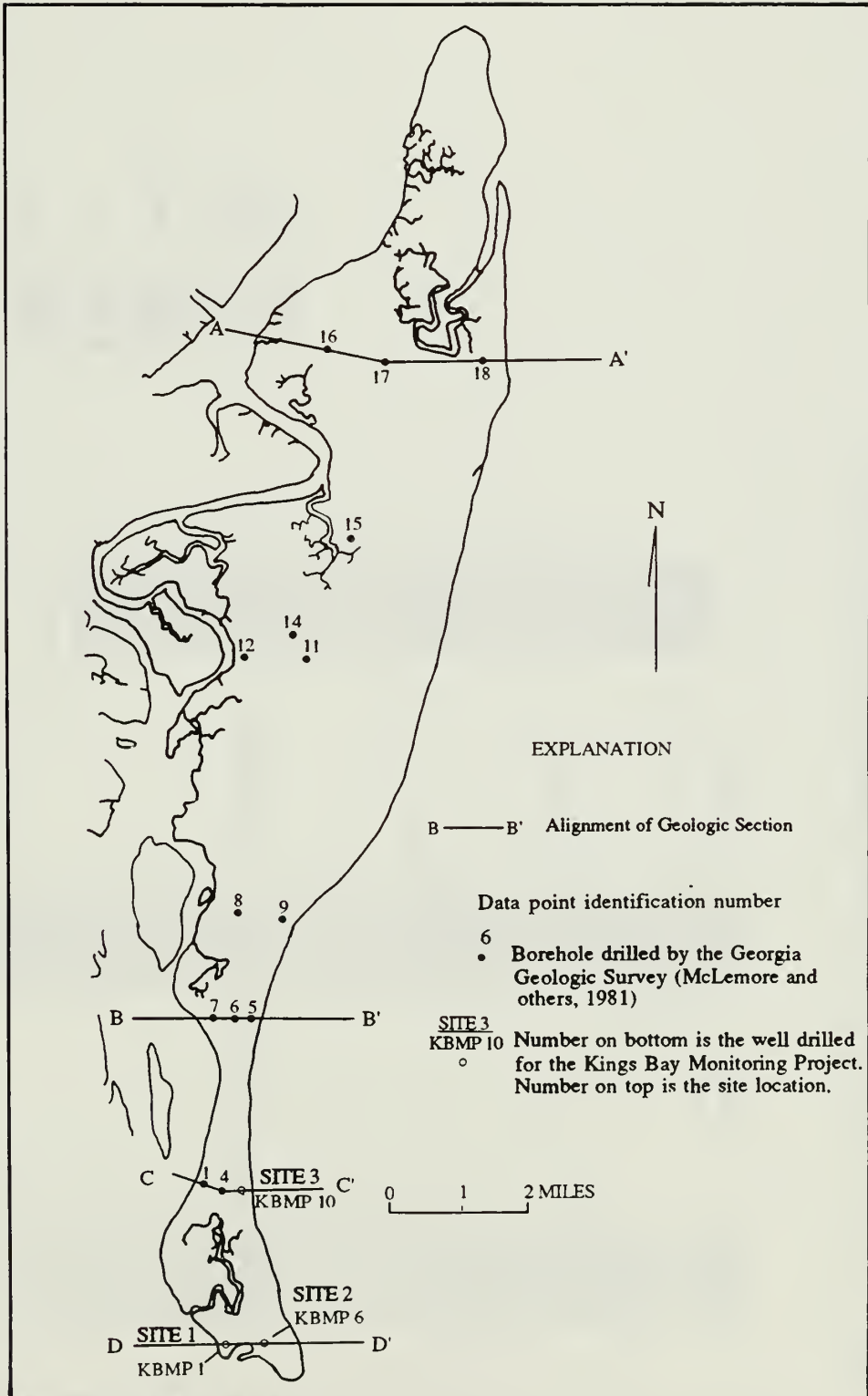


Figure 4. Stratigraphic section and natural gamma logs for wells GGS 3426, 34E10, and 34F13. (Lithologic descriptions from Clarke and others, 1990).

The Oligocene series is located at a depth of 531 feet below land surface and consists of a 17-foot section of the Suwannee Limestone (see Figure 4). The Suwannee is a phosphatic limestone and is distinguished by an abundance of miliolid foraminifera. The limestone was deposited in a carbonate bank environment (Clarke and others, 1990).

Deposits of Miocene-age consist of the Charlton and Hawthorn Formations and are composed of sand, clay, limestone, and dolomite (Clarke and others, 1990). The Miocene strata are about 458 feet thick.

Clarke and others (1990) divided the Miocene strata into three units based on paleontologic evidence and geophysical characteristics. Each unit consists of a basal carbonate layer, overlain by clay, and an upper sand layer. In descending order, these units are Miocene units A, B, C (see Figure 4). Miocene unit C is about 91 feet thick in the study area. The basal carbonate layer of unit C is composed of sandy, fossiliferous, phosphatic limestone, and dolomite. It grades upward into a silty clay and clayey silt that contains molds of diatoms. The clay layer grades upward into a poorly sorted, very fine to granule-size quartz sand containing sparse phosphate grains and dolomite rhombohedrons. Miocene unit B is about 66 feet thick and Miocene unit A is about 215 feet thick in the study area. The composition of Miocene units A and B are similar to unit C. However, the sand unit of Miocene unit A contains alternating beds of argillaceous dolostone (Clarke and others, 1990). The section of the Charlton Formation examined during this study was equivalent to Miocene unit A. Figures 6 and 7 show geologic sections from the top of the Charlton Formation to land surface (see Figure 5 for cross section location). (Figure 8 shows the altitude of the top of the Charlton Formation). According to Henry and Kellam (1988), the middle Miocene age sediments were deposited in an open marine environment. The core taken from Site 1 (see Figure 3 for site location) contained abundant marine fossils and evidence of bioturbation indicating that a shallow open marine or marginal sea



Base from McLemore and others (1981).

Figure 5. Location of boreholes and geologic sections, Cumberland Island.

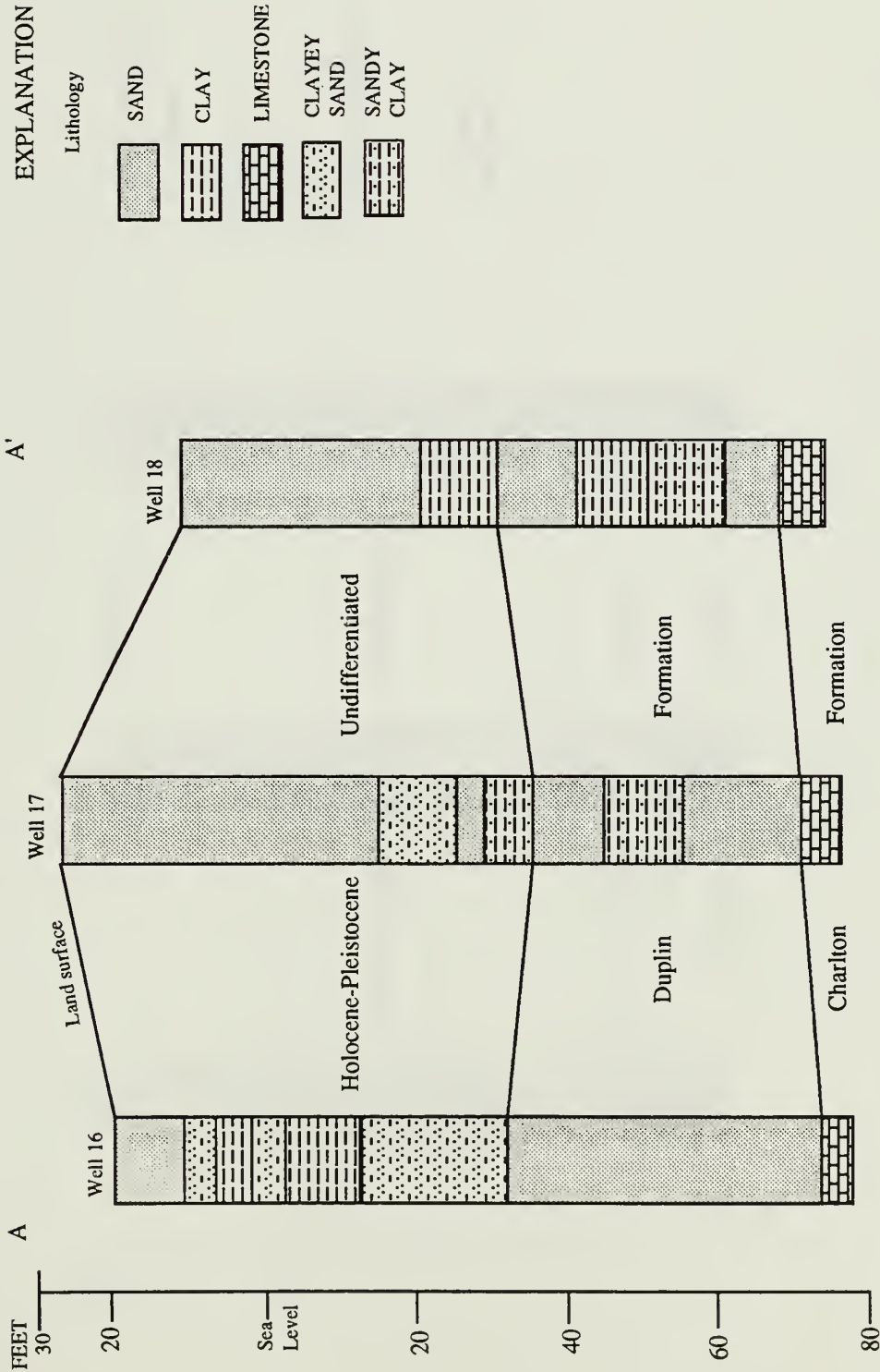


Figure 6. Geologic section A to A'. (Lithologic description from Martinez, 1980.)

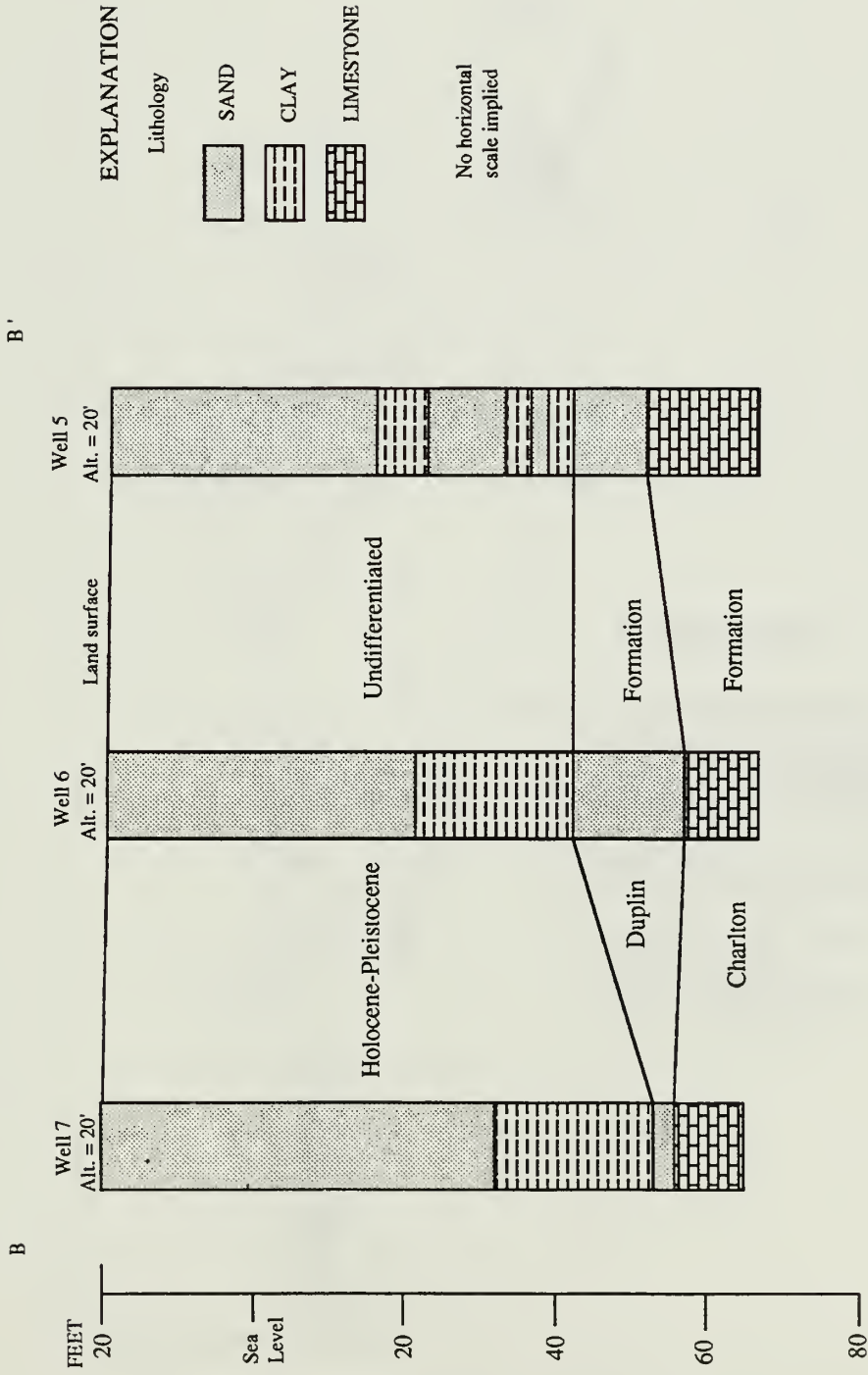
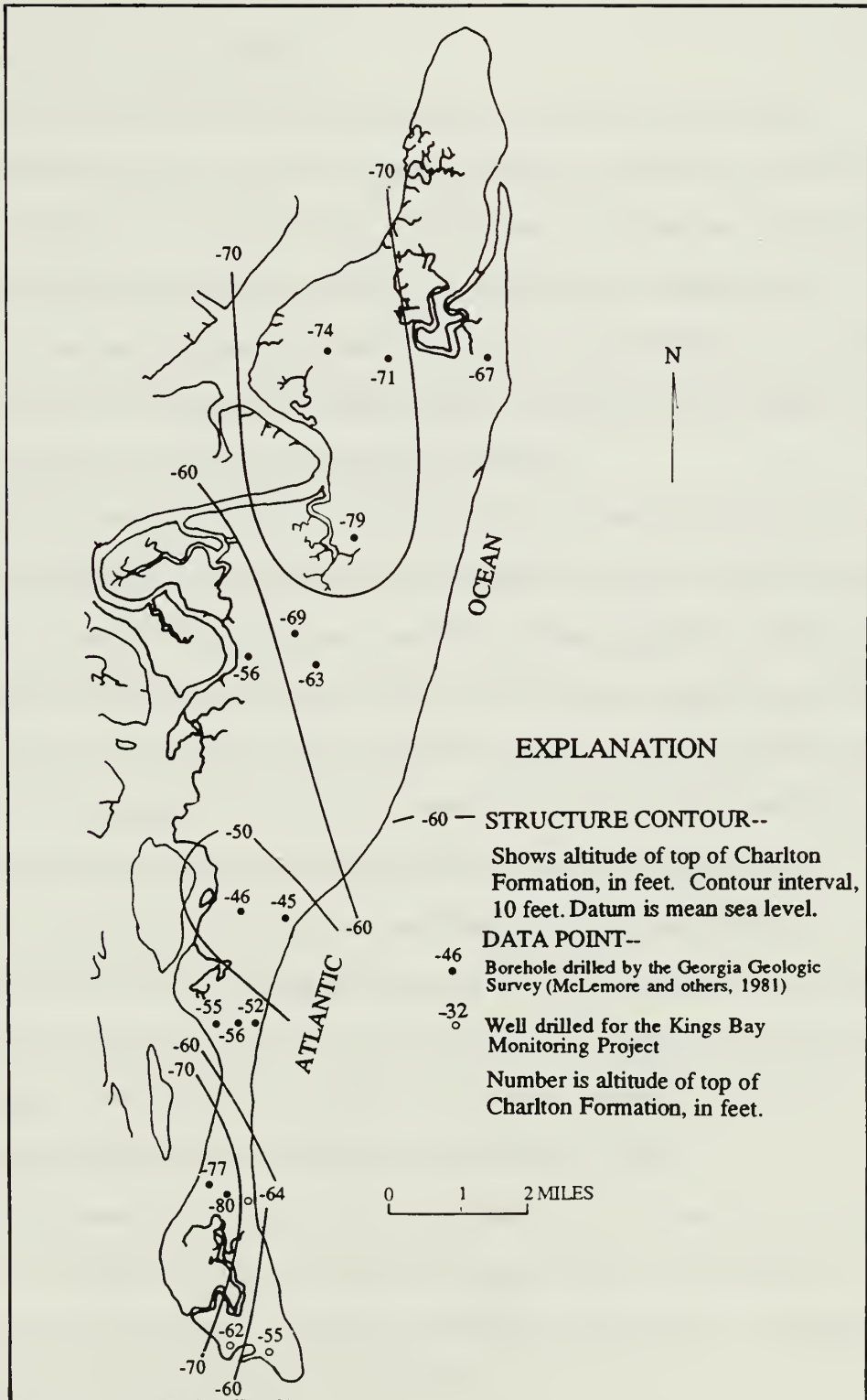


Figure 7. Geologic section B to B'. (Lithologic description from Martinez, 1980).



Base from McLemore and others (1981).

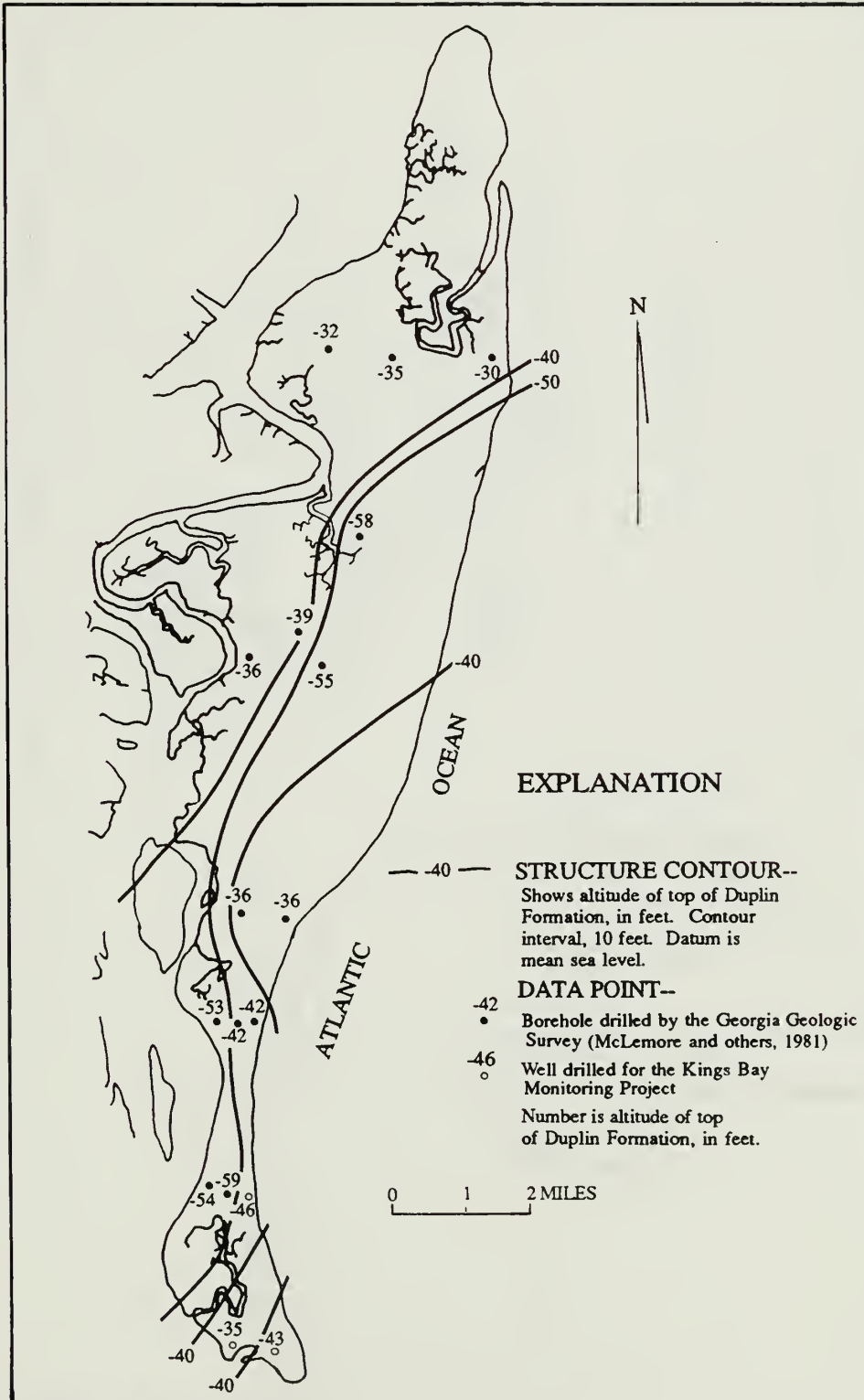
Figure 8. Altitude of the top of the Charlton Formation.

environment existed during deposition.

In the study area the middle Pliocene series is the equivalent of the Duplin Formation of southeastern Georgia and consists of well-sorted, calcareous sand which is locally gravelly (Henry and Kellam, 1988). The thickness of the formation ranges from 2 to 42 feet thick (McLemore and others, 1981). The early Pliocene sediments were deposited in a restricted basin and estuarine environment. These deposits were subaerially eroded and channel cut during middle Pliocene (Henry and Kellam, 1988). (Figures 9 and 10 show the altitude and thickness of the Duplin Formation.)

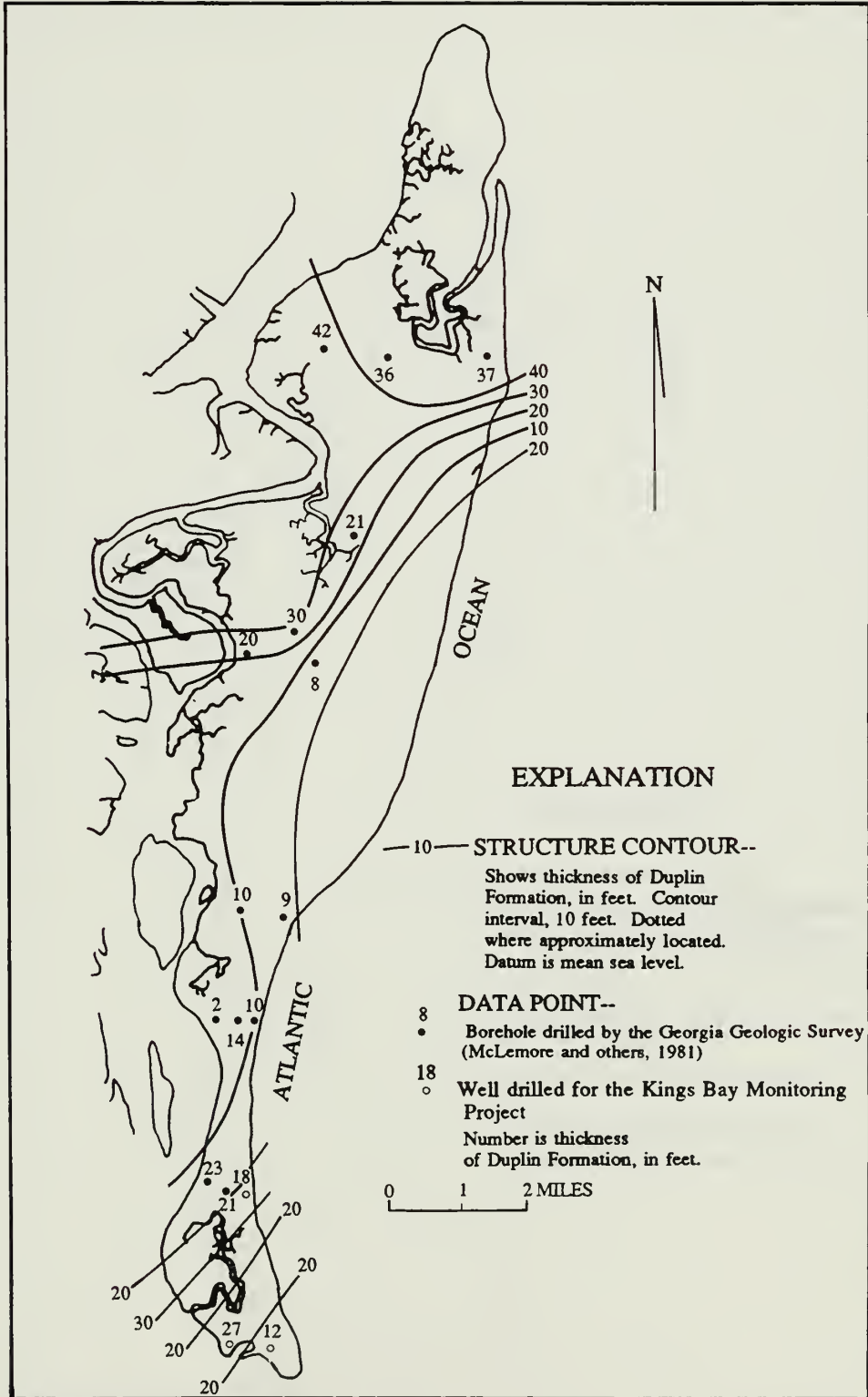
The Pleistocene age deposits consist of 22 to 62 feet of sand and clayey sand overlying 5 to 40 feet of clay and sandy clay. The Pleistocene sand is the Satilla Formation equivalent and consists of very fine quartz sand. This sediment represents barrier-island facies deposits and ranges in color from brown in the soil horizon to light brown in deeper zones. The fossil burrow *Ophiomorpha nodosa* of the shrimp *Callinassa major* is present which indicates that deposition occurred in a near-shore environment (McLemore and others, 1981). Below the sand deposits are deposits which represent back-barrier sedimentation and consist of silt, clay, and sandy clay, that range from gray to tan in color. (See Figures 11 and 12 for the altitude and thickness of the clay sediments of Pleistocene age.) Commonly, the clay is interbedded with sand ranging from less than 1 feet to about 10 feet in thickness. The lithology here indicates an estuarine back-barrier depositional environment interrupted by periods of high energy (Martinez, 1980).

The Holocene deposits occur as fine quartz sand in the beach and dune areas along the east coast. Along the west coast, the deposits consist of clays at the base of the freshwater ponds and marshes. On the island's interior the deposits occur as floodplain and stream deposits (McLemore and others, 1981).



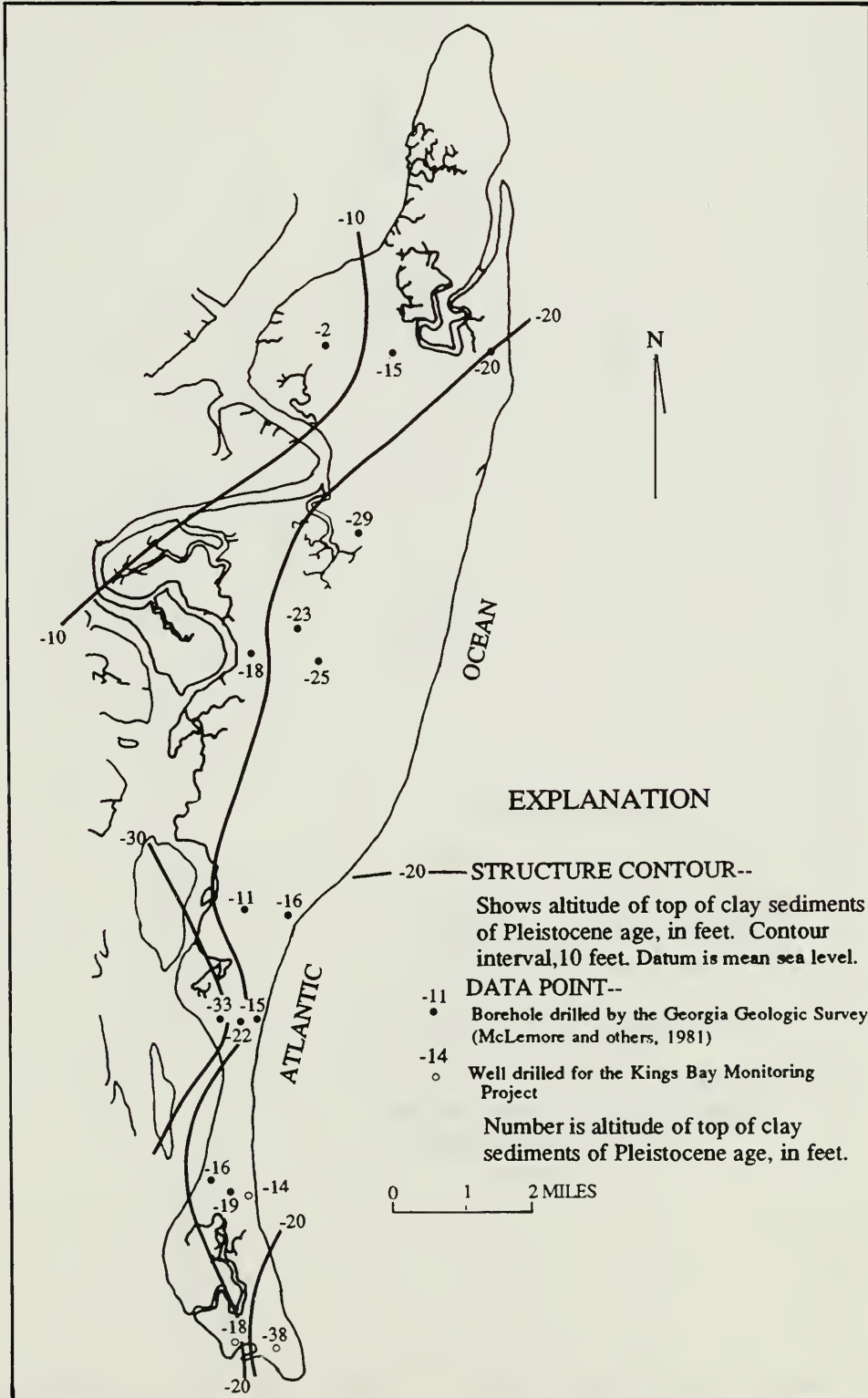
Base from McLemore and others (1981).

Figure 9. Altitude of the top of the Duplin Formation.



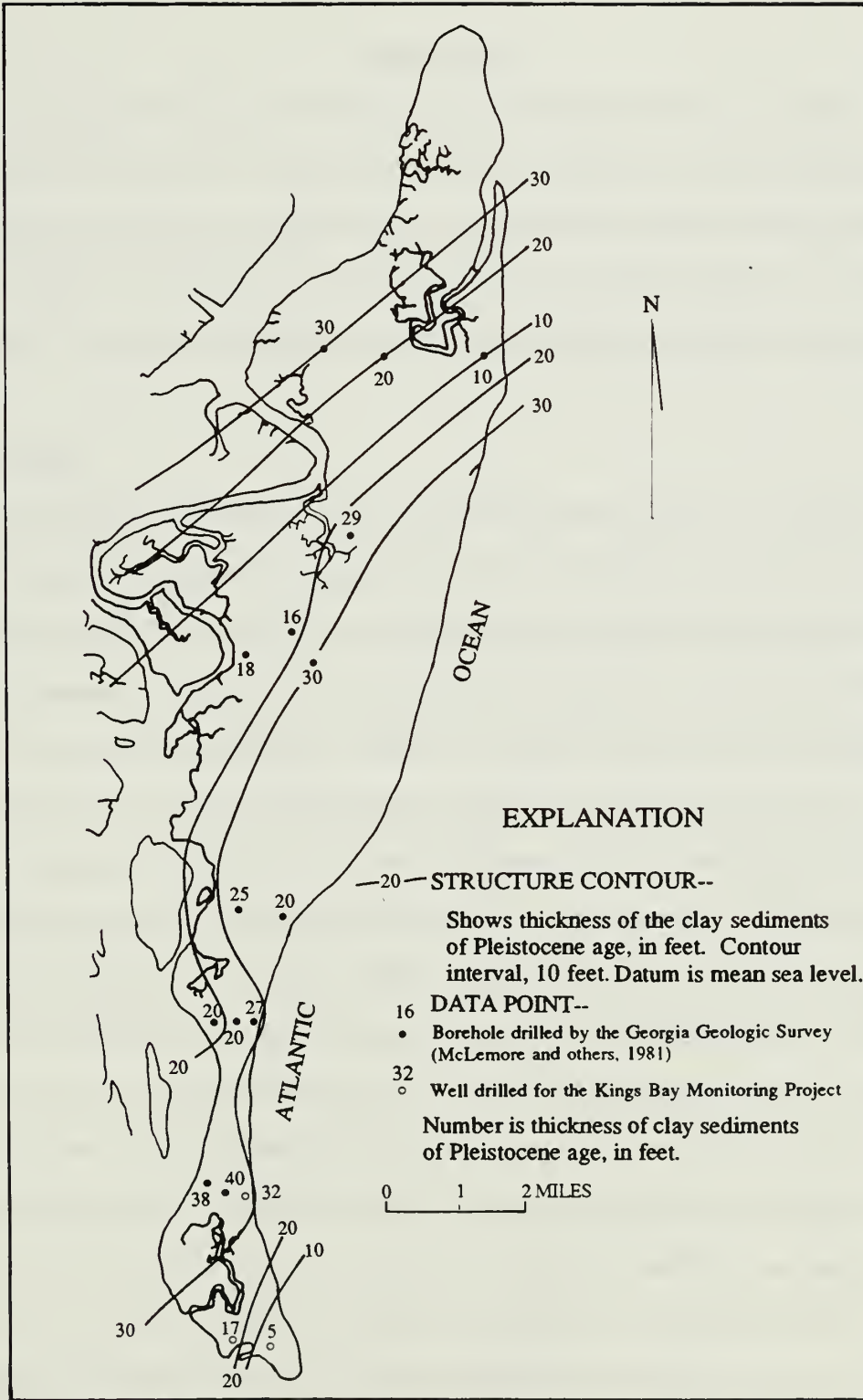
Base from McLemore and others (1981).

Figure 10. Thickness of Duplin Formation.



Base from McLemore and others (1981).

Figure 11. Altitude of the top of the clay sediments of Pleistocene age.



Base from McLemore and others (1981).

Figure 12. Thickness of clay sediments of Pleistocene age.

Local Geology

Geology from the upper Charlton Formation through the Holocene deposits were investigated in the study area. The following sections include a site specific discussion of the Charlton Formation, the Duplin Formation, and Holocene to Pleistocene deposits undifferentiated. Core samples were examined at Site 1; cutting samples were examined at Sites 1 and 2. A detailed description of the core and cuttings are provided in Appendix B.

Miocene Series

The Charlton Formation consists of alternating layers of sand, clay, limestone, and dolomite locally characterized by high concentrations of phosphate. At Site 1, the lower part of the Charlton Formation (151 to 141 feet below sea level) consists of argillaceous dolomitic limestone. The light gray section is soft, bioturbated with shell molds (20 percent). The dolomitic limestone is overlain by 10 feet of light gray, poorly indurated, to loose quartz sand. At Site 1, the SPR log was useful for determining the contacts between the quartz sand and the dolomitic limestone (see Figure 13). The sand, subrounded to subangular, varies from fine to medium (25 percent) to very coarse (60 percent). Light gray dolomitic limestone (31 ft thick) overlies the quartz sand. This section consists of fine to medium sand (35 percent), clay (35 percent), and very coarse, phosphatized calcite grains as large as 0.25 inches in diameter. The section is highly bioturbated and is locally high in phosphate content. Three feet of very light gray, calcareous clay separates the dolomitic limestone from 8 feet of dolomite. The dolomite is argillaceous (30 percent clay) with very fine to fine sand (35 percent) and very coarse quartz sand and phosphatized calcite (5 percent). The overlying zone (89 to 74 feet below sea level) consists of alternating layers of dolomite, sand, dolomitic limestone and limestone (Figure 13). This section consists of fine to medium sand (45 percent), very coarse quartz grains (7 percent)

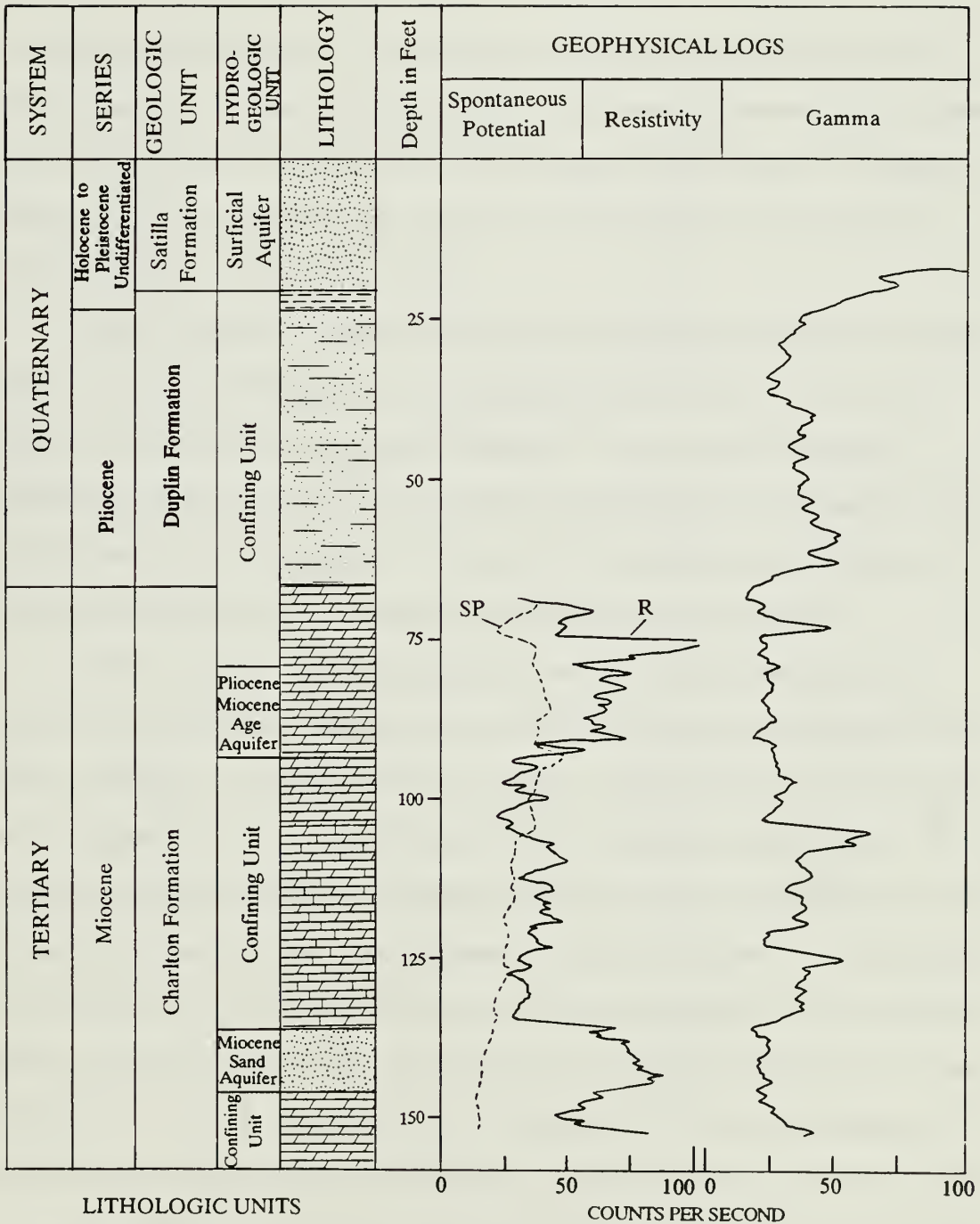
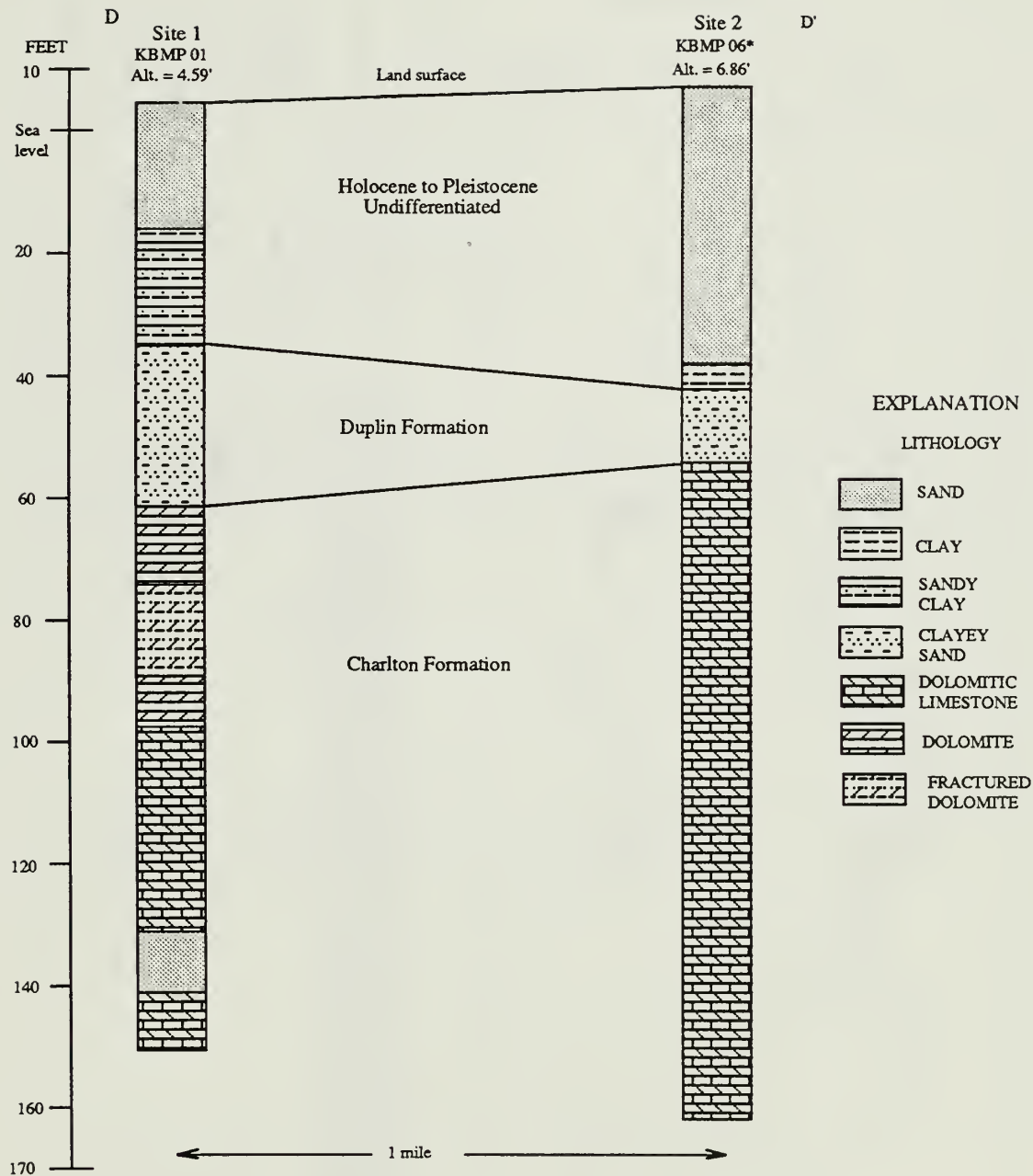


Figure 13. Lithology and geophysical logs at well KBMP 1, site 1.

and weathered shell fragments. It is highly pitted, weathered, fractured, and has good secondary porosity. Dolomite overlying the 89 to 74 foot section increases in clay content (25 percent) and is not as fractured and weathered as the underlying unit. The dolomite consists of fine sand (45 percent) and becomes very hard and dense at the top of the Charlton Formation, 61 feet below sea level.

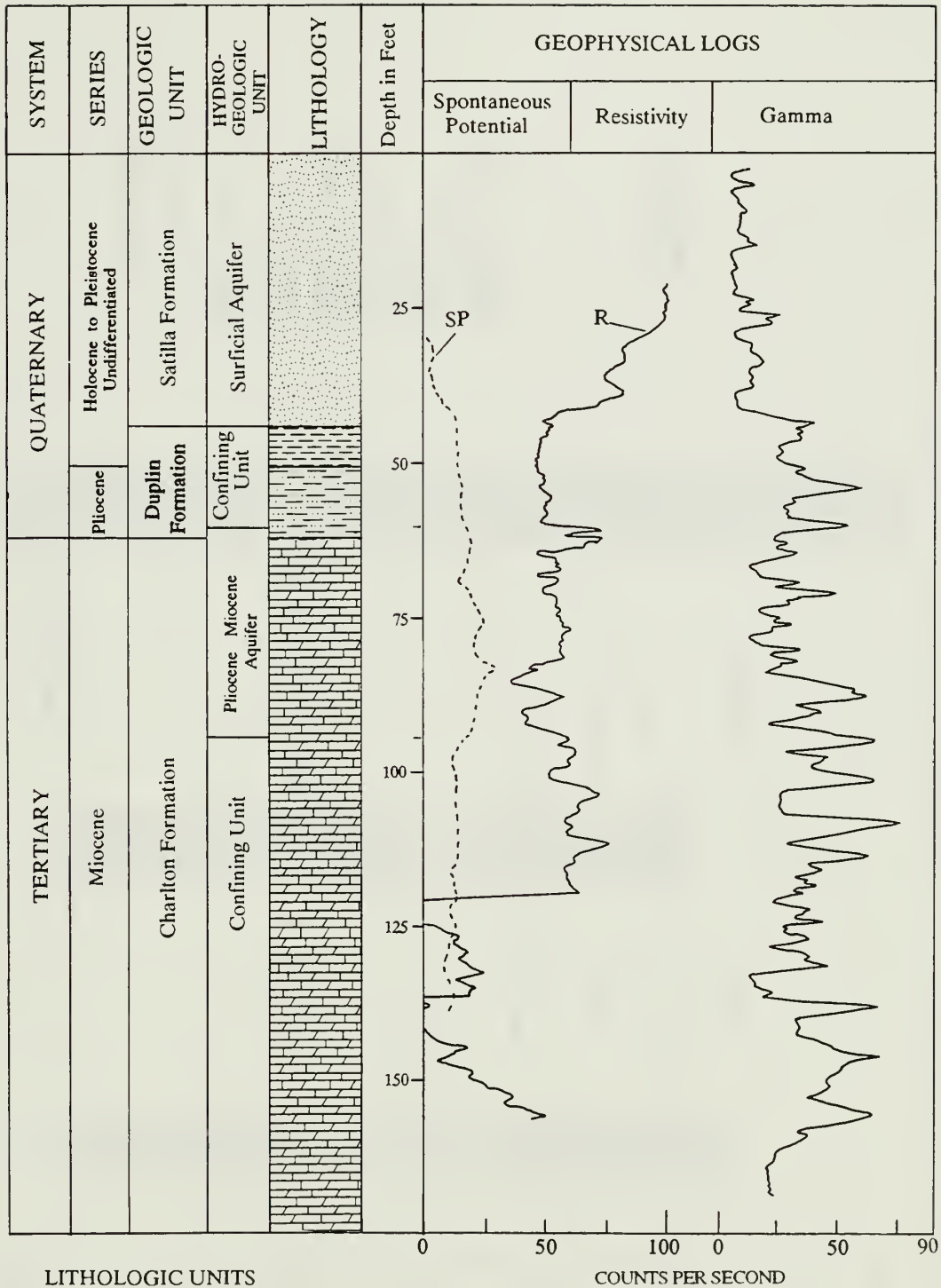
At Site 2, the upper 109 feet of the Charlton Formation were examined as cutting samples. Variations in the lithology do not exist as are present at Site 3. The section consists of olive gray dolomitic limestone (Figure 14). The dolomitic limestone is argillaceous (30 percent clay) with fine to medium sand (40 percent) subangular, broken shell fragments (5 percent) and locally contains very coarse sand to gravel (15 percent). The gamma log indicates that this zone is highly phosphatic (see Figure 15).

At Site 3, an upper 53 foot section of the Charlton Formation was examined. Figure 16 is a combination of data from Site 3 and lithologic descriptions of boreholes by Martinez (1980) that were drilled to the west of Site 3. The basal 45 feet of this section consist of alternating layers of argillaceous dolomite, clayey sand, and sandy clay. This zone contains phosphatic calcite and abundant phosphate at depths of 100 and 125 feet, as indicated by the sharp increase in natural gamma emission (see Figure 17). The light gray dolomite layers are very hard and consist of clay (30 percent) and fine to coarse sand (20 percent), subangular to subrounded. The sandy clay layers are about 40 percent clay and 30 percent fine to coarse sand, subangular to subrounded, with some shell fragments. The upper 8 feet of the Charlton Formation consists of weathered, fractured limestone with fine to coarse sand (15 percent) and shell fragments (15 percent). This layer is continuous on the island north of Dungeness based on lithologic descriptions by Martinez (1980). Core taken from the Charlton Formation contained abundant marine fossils such as *Mercenaria prodroma* cf., *Chesapecten* cf., and the brachiopod *Lingula*. *Callianassa*



*Originally well KBMP 6 was drilled to a total depth of 170 ft. below land surface. Because of partial borehole collapse, the borehole was filled, abandoned, and a new well was drilled to a total depth of 71 ft. below land surface.

Figure 14. Geologic section D to D'. Refer to Figure 5 for cross section location.



- | | |
|--|---|
|  Sand |  Sandy clay |
|  Clay |  Dolomitic limestone |

Figure 15. Lithology and geophysical logs at well KBMP 6, site 2.

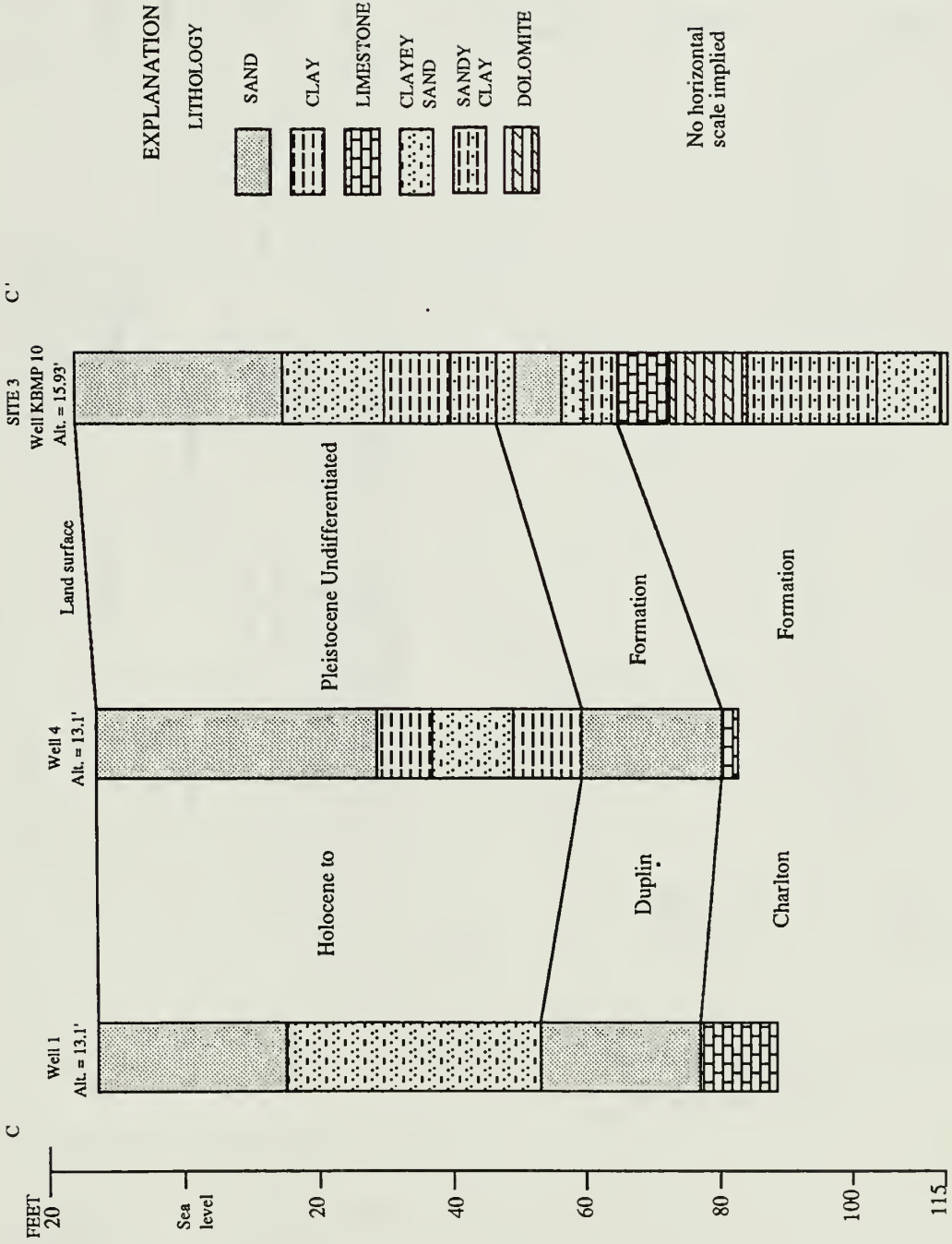


Figure 16. Geologic section C to C'. (Lithologic description of wells 1 and 4 from Martinez, 1980). Refer to Figure 5 for cross section location.

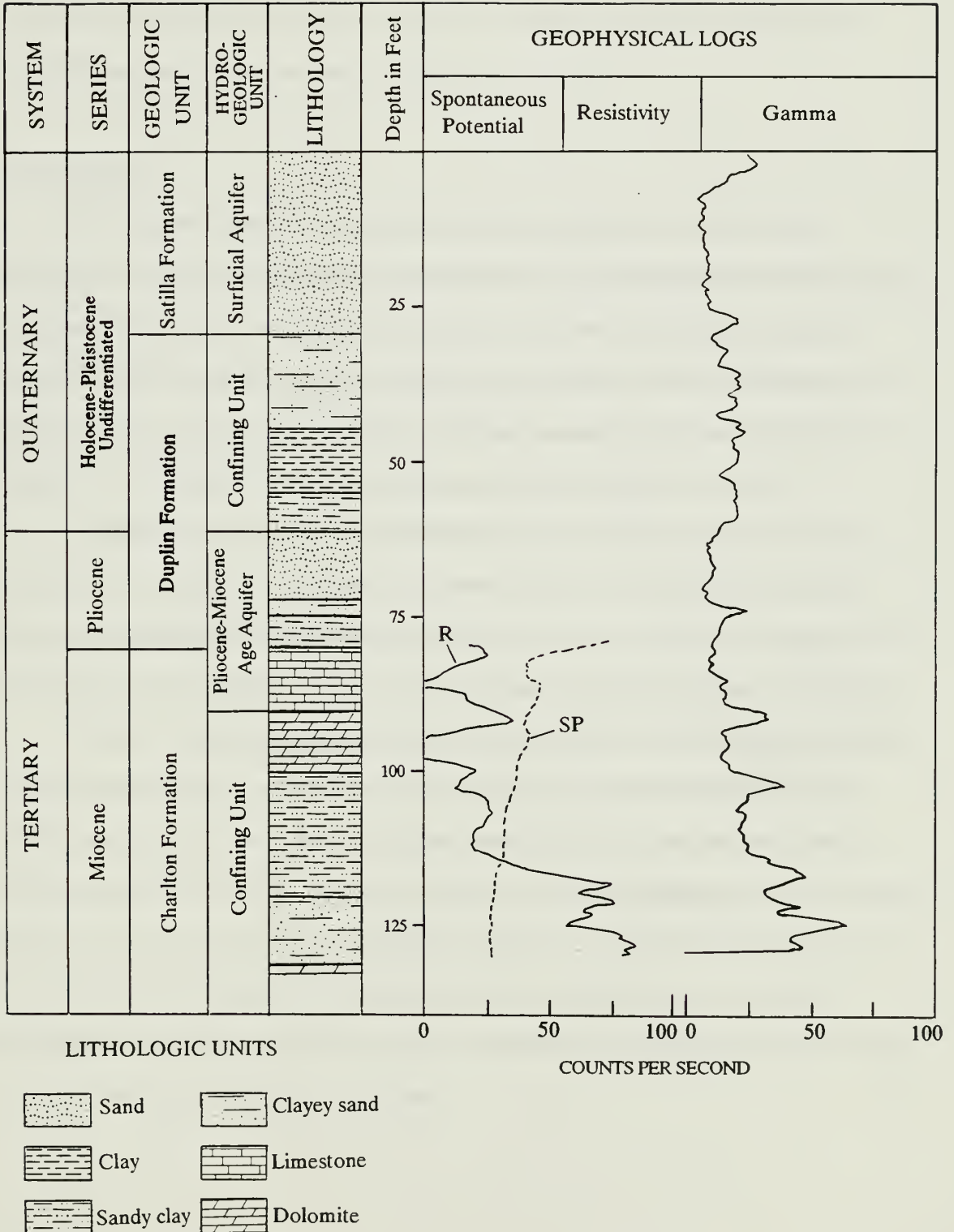


Figure 17. Lithology and geophysical logs at well KBMP 10, site 3.

burrows cf. were found in the core as well. These fauna indicate that a shallow open marine or marginal sea environment existed during deposition.

Pliocene Series

The Pliocene deposits on Cumberland Island are equivalent to the Duplin Formation. In general the formation consists of marine sand that fines upward (McLemore and others, 1981). The Pliocene deposits at sites 1 and 2 are much different than the deposits at Site 3 and those described by McLemore and others (1981) northward on the island. At these sites, the sand contains a significant amount of clay and the sediment is phosphatic as indicated by the active gamma emission (see Figures 13 and 15).

At Site 1 the deposits are 26 feet thick and consist of brown gray to olive brown clayey sand, very fine to fine (Figure 14). These deposits are slightly calcareous and consist of shell fragments ranging from a trace to 20 percent. At Site 2, the deposits are 12 feet thick and consist of clayey sand, very fine to fine with shell fragments (10 percent).

At Site 3, an unconformable contact exists between the weathered limestone of the Charlton Formation and sand of the Duplin Formation. The basal 8 feet of the Duplin Formation consists of sandy clay having very coarse quartz sand and abundant broken pecten fragments (20 percent), which is overlain by 10 feet of alternating layers of sand and clayey sand with 20 percent shell fragments (see Figure 16). The 8-foot sandy clay layer was not described by Martinez (1980), thus it likely is a localized lens and probably represents stream deposits. The stratigraphy and broken pecten shells found in the Duplin Formation indicate a near shore environment.

Holocene and Pleistocene Deposits

There are no distinguishing characteristics between the Holocene and Pleistocene sand on the south end of the island. Therefore, these deposits are referred to as Holocene to Pleistocene deposits undifferentiated. At Site 1, the basal clayey zone (17 feet thick) consists of alternating layers of sandy clay and clay. The medium gray, quartz sand is very fine, and the dark gray clay is clean. The overlying yellowish gray sand (23 feet thick) is very fine, subangular, and well sorted. At Site 2, the lower part of the Holocene to Pleistocene deposits consist of light gray sandy clay with very fine to fine sand, (35 percent) and heavy minerals (3 percent). The overlying olive gray, quartz sand (45 feet thick) is very fine to fine, and well sorted.

At Site 3, the lower part of the Holocene-Pleistocene deposits (32 feet thick) consist of alternating layers of light gray sandy clay, clean clay, and yellowish gray clayey sand, very fine. These deposits represent back barrier-island deposits. The clayey zone is overlain by 30 feet of well sorted, very fine, quartz sand which represent barrier-island deposits. Clay is completely absent in the upper section of the Holocene-Pleistocene deposits at each site (see Figures 14 and 16).

METHODS OF INVESTIGATION

Various methods were employed to collect data needed to characterize the geology/hydrogeology of the study area. Surface geophysical data provided preliminary geologic and water quality data that were used to select the most appropriate locations for the well sites. A total of 10 wells were drilled at the well sites. Three wells were emplaced in a cluster at well Site 1; three wells at Site 2; and four wells at Site 3 (see Figure 3 for location of well sites). Core, split-spoon samples, and cuttings were collected and analyzed during well drilling. Borehole geophysical logs enhanced core and cuttings data by providing information such as contacts between formations, porosity and lithology of the aquifers, and marker beds for the tops of aquifers. Surface geophysical surveys provided specific conductivity data of the shallow sediments and pore water. The hydraulic characteristics of the aquifer were determined by performing an aquifer test.

Surface Geophysics

An electromagnetic (EM) terrain conductivity meter (the Geonics EM 34-3) was used to determine the specific conductivity of the shallow sediments and formation water in the study area. The instrument measures conductivity in millimhos per meter at theoretical depths of 25 feet to 197 feet below land surface depending on the coil configuration and spacing (McNeil, 1980). Three transects were made across the southern end of the island. At each location of EM conductivity measurement, a reading for the 33, 66, and 132 feet intercoil spacing for each dipole configuration (horizontal and vertical) was taken so that data acquisition ranged from theoretical depths of 25 to 197 feet below land surface. The conductivity meter was useful for detecting cavities in limestone, mapping lithology, and locating the zone of diffusion between the freshwater and seawater.

The conductivity meter's transmitter coil receives an alternating audio frequency current which produces a magnetic field in the coil. The primary field generated by the coil propagates through the geologic medium creating electrical currents in the strata. The amount of current flow depends on the conductivity of the layers (Zohdy and others, 1974). A secondary magnetic field is produced that has the same frequency but a different phase than that produced by the transmitter coil. The secondary field is detected by the receiver coil, which cancels signals from the primary field. The strength of the secondary field is directly proportional to terrain conductivity which is a function of intercoil spacing, operating frequency, and ground conductivity (Duran, 1984).

Most of the current flow in a saturated zone is along the surface of the grains and through the pore water. The bulk conductivities of saturated sedimentary rocks are based largely on the effective porosity and formation-water conductivity. As these increase so does the bulk conductivity. For strata saturated with saline water, fluid properties dominate the EM conductivity response. In sediment saturated with freshwater, the porosity controls the bulk conductivity (Stewart, 1982).

Drilling Methods

Three well sites were selected in the study area to provide hydrogeological, stratigraphic and geophysical data in areas representing diverse hydrogeologic conditions and to monitor the water levels and water chemistry (see Figure 3 for well site locations). At each site, a cluster of three to four wells, spaced about 10 feet apart, were drilled to monitor the water-bearing zones of interest.

Drilling of well KBMP 1 (Kings Bay Monitoring Project) was initiated without the use of a drilling additive or hole stabilizers. After drilling 12 feet, the hole began to collapse and a 5 1/2 inch diameter fishtail bit and a drilling additive was used to finish the

hole to the top of rock. A biodegradable drilling mud was used which naturally decomposes after 72 hours. Split spoon samples were taken at 5 foot intervals to the top of the Charlton Formation (66 feet below land surface). The remainder of the well was cored using a steel rock bit core barrel to a depth of 146 feet with an average core recovery of 94.8 percent. At the remaining wells, cuttings were taken and analyzed at 5 to 10 foot intervals or where a significant change in lithology occurred. The core, split-spoon samples, and cuttings were analyzed for lithological and textural composition under a binocular microscope. Ubiquitous phosphate in samples was detected by directly applying ammonium molybdate. If phosphate was present, the sample turned bright yellow. The relative permeability was estimated based on sediment grain size and sorting, and for rock zones, the amount of weathering and secondary porosity. Dolomite was distinguished from dolomitic limestone by noting the abundance of dolomite rhombohedrons. Dolomite was very dense, hard, and reacted very slowly to hydrochloric acid. Dolomitic limestone was medium hard, a lighter color, and not as dense as the dolomite. Limestone reacted violently to hydrochloric acid.

The remaining wells were drilled using the hydraulic rotary method and usually a 7 5/8 inch diameter bit. Where temporary casing was used to prevent caving, a 9 3/4 inch bit was used to the top of the Charlton Formation and finished with a 7 5/8 inch bit.

Well Design and Construction

All wells were cased and screened using 4 inch polyvinyl chloride (pvc), and were capped at the base (see Figures 18 through 20). The annulus of each well was packed with sand to a distance of about 2 to 5 feet above the screen. A 2-foot bentonite plug was placed above the sand pack to seal the annular space, except in shallow, sandy zones where a plug was not necessary, or where the annular space caved in before a plug could be installed,

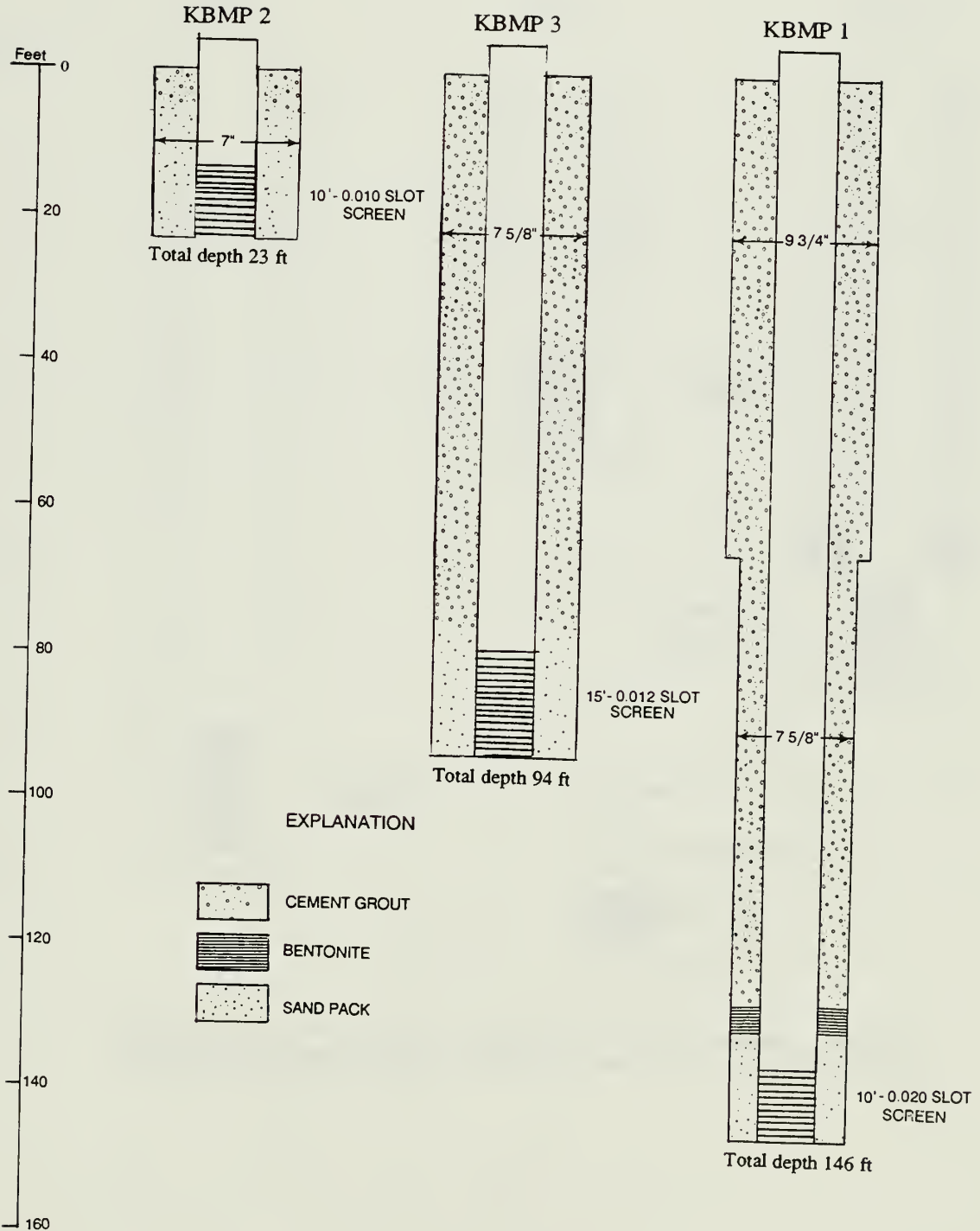
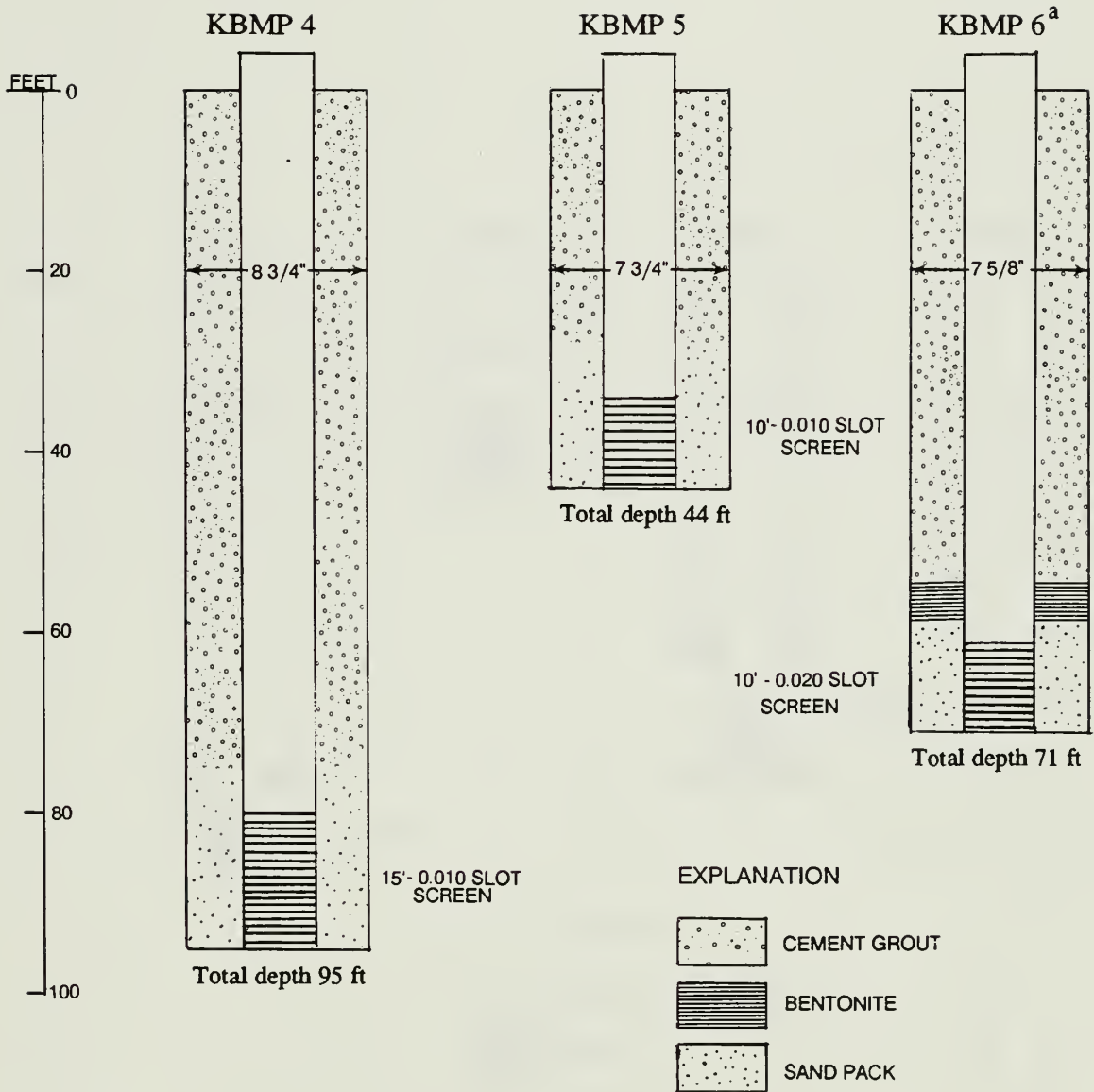


Figure 18. Well construction at well Site 1. The altitude is 4.59 feet above mean low water.



^aOriginally well KBMP 6 was drilled to a total depth of 170 ft. below land surface. Because of partial borehole collapse, the borehole was filled, abandoned, and a new well was drilled to a total depth of 71 ft. below land surface.

Figure 19. Well construction at well Site 2. The altitude is 6.86 feet above mean low water.

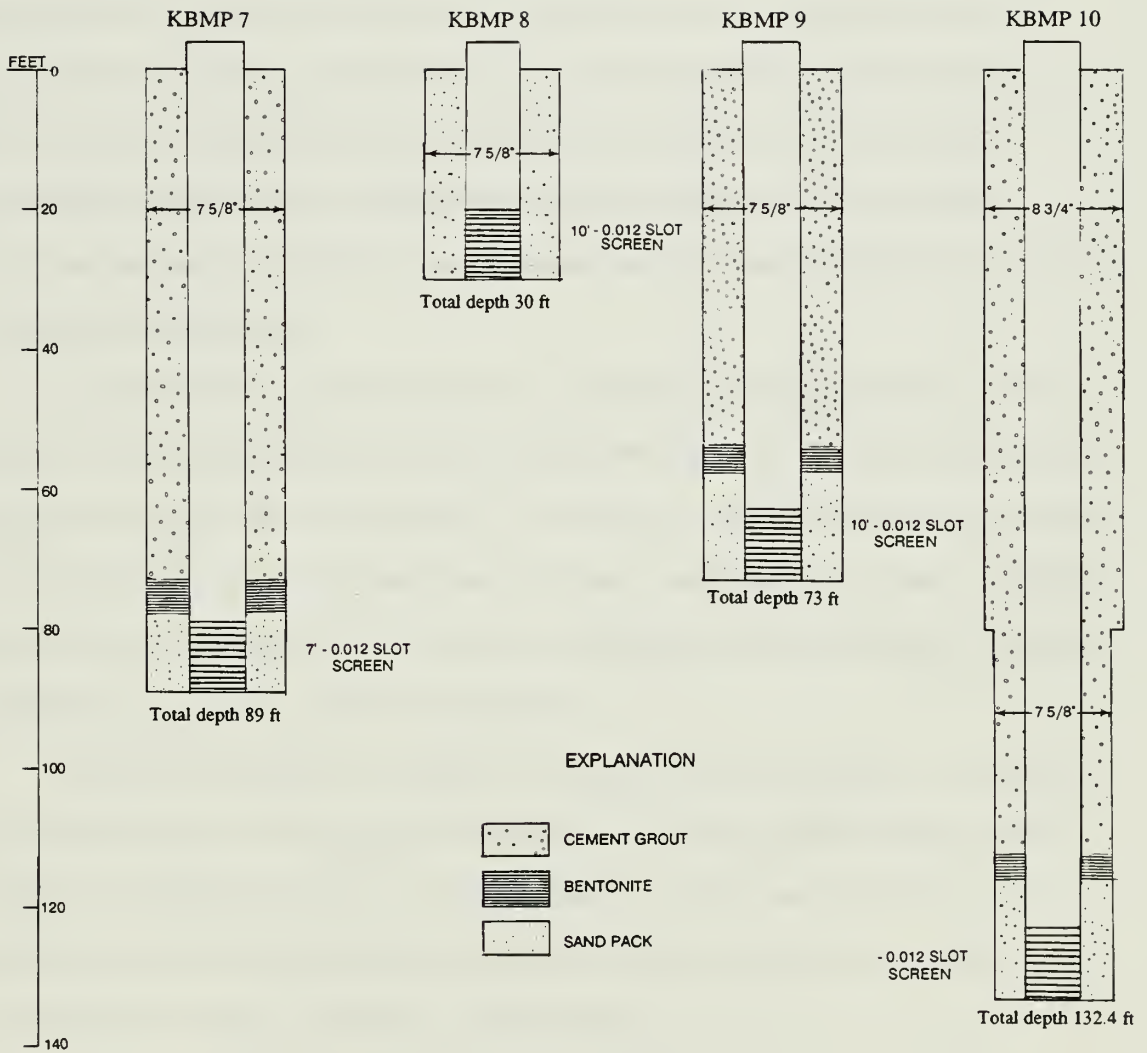


Figure 20. Well construction at well Site 3. The altitude is 15.9 feet above mean low water.

such as in well KBMP 4. Above the bentonite plug, the remaining annular space was filled with cement grout to seal the annular space and prevent leakage from overlying or underlying zones. Table 1 summarizes the construction of each well.

A grain-size analysis was conducted for the sandy aquifers to determine suitable screen slot sizes. The screen slot size chosen for each well was selected to retain 40 percent of the sediment and permit 60 percent to pass through the screen (see Figure 21). This will promote grading around the screened area and increase the porosity and permeability of the near bore formation during well development. As a result, the drawdown around the well will be reduced during pumping and the well efficiency will be increased (Driscoll, 1984).

Appropriate slot sizes for each well were selected by permitting 60 percent of the aquifer medium to pass through the screen during development. However, an exception to this procedure was made for well KBMP 9. According to the grain-size analysis, a 50-slot screen (width of the slot is in thousandths of an inch) would have been appropriate for this zone. Because a screen size this large was not available at the time of drilling, the largest available screen slot size, 12 slot, was installed.

The slot size selected for monitor wells tapping limestone aquifers was based on the percentage and size of sand present in the aquifer. The saturated zones tapped by well KBMP 3 and KBMP 7 contained a significant amount of fine sand, therefore 12-slot screens were installed. Wells KBMP 4 and KBMP 10 were installed in an argillaceous limestone and 10 and 12 slot screens were installed.

Well Development

All wells installed on Cumberland Island as a part of this investigation were developed to reduce compaction of the formations caused during drilling, remove drilling

Table 1. Well construction summary.

Well number	Latitude/ Longitude	Total depth, in ft.	Screened interval below LSD ^a , in ft.	Screened formation	Land surface elevation, in ft.	Measuring point, in ft. above LSD	Casing material	Casing diameter, in in.	Completion date
KBMP 1	30°43'11" 81°28'13"	146	136-146	Charlton	4.6	0.46	PVC	4	6/14/89
KBMP 2	30°43'11" 81°28'13"	23	13-23	Satilla	4.6	1.78	PVC	4	6/14/89
KBMP 3	30°43'11" 81°28'13"	94	79-94	Charlton	4.6	0.65	PVC	4	6/27/89
KBMP 4	30°43'10" 80°27'26"	94	79-94	Charlton	6.86	1.25	PVC	4	6/15/89
KBMP 5	30°43'10" 80°27'26"	44	34-44	Satilla	6.86	0.92	PVC	4	6/17/89
KBMP 6 ^b	30°43'10" 80°27'26"	71	61-71	Charlton	6.86	1.4	PVC	4	6/21/89
KBMP 7	30°44'50" 84°28'00"	89	82-89	Charlton	15.93	1.63	PVC	4	6/22/89
KBMP 8	30°44'50" 84°28'00"	30	20-30	Satilla	15.93	0.92	PVC	4	6/23/89
KBMP 9	30°44'50" 84°28'00"	72	62-72	Duplin	15.93	1.62	PVC	4	6/23/89
KBMP 10	30°44'50" 84°28'00"	132.4	122.4-132.4	Charlton	15.93	1.19	PVC	4	6/25/89

^a Land Surface Elevation

^b Originally well KBMP 6 was drilled to a total depth of 170 ft. below land surface. Because of partial borehole collapse, the borehole was filled, abandoned, and a new well was drilled to a total depth of 71 ft. below land surface.

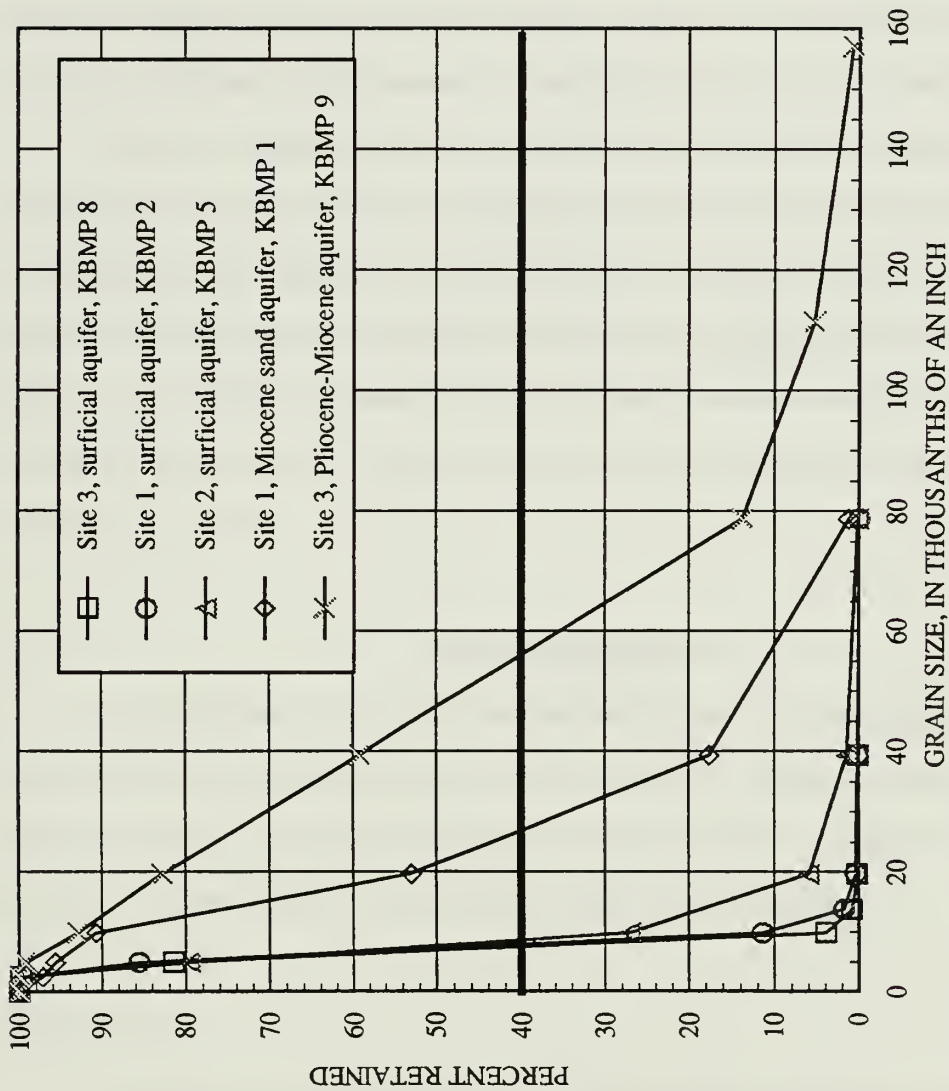


Figure 21. Grain size distribution curves, in thousandths of an inch. The ideal screen size for a zone retains 40 percent of the sediment and allows 60 percent to pass through the screen.

fluid from the formation, and increase the permeability and effective porosity around the well, which in turn increases the yield and specific capacity. The wells were developed by overpumping with a 4-inch submersible, 0.5 horsepower pump for varying times ranging from 45 minutes to 2.5 hours at approximately 20 gal/min. Well KBMP 10 could only be pumped at 5 minute intervals because the zone tapped by this well produced little water.

During overpumping, the pump was periodically shut off and restarted to create a surging effect. One drawback of overpumping is that water moves only toward the well, so backwashing is not possible. The unidirectional movement of water may cause sediment to bridge outside the screen. If the formation is agitated during normal pumping, sediment may collapse and enter the well. However, if unstable bridging occurred, the sand pack placed around the screen will prevent most of the sediment from entering the well (Driscoll, 1986).

Borehole Geophysics

At each drilling site, borehole geophysical logs were derived using an EG&G Mount Sopris logger from the deepest well of the cluster. Natural gamma, single-point resistance, and spontaneous potential logs were run at each site. Figures 13, 15, and 17 in the geology section contain the geophysical data collected at each site.

Natural Gamma

The natural gamma log measures the natural radioactive emissions from the geologic material. The gamma probe consists of a scintillation receiver and counter circuit. Gamma kick intensity in a geologic medium is proportional to the number of pulses detected by the probe per unit time. The intensity is expressed as the average number of counts per second (Driscoll, 1986). In sedimentary rocks, clay and shale usually emit

higher counts of gamma rays, due to their high potassium content, than do limestone and sand, which are characterized by low levels of potassium, thorium, and uranium.

However, micaceous sand emits high levels of radiation as do dolomite and phosphorite (Hilchie, 1982). Much of the radiation emitted from carbonates and phosphates originate from thorium and uranium particles. Some phosphate pebbles may contain up to 150 parts per million (ppm) of uranium, and therefore are gamma active zones (Kwader, 1982). At Site 1, the high intensity kicks recorded by the gamma probe did not match zones in the core that were high in phosphate. The difference between the depth read by the probe and the actual depth of the phosphatic zone appeared to be 5 feet (a kick at 75 feet below land surface on the log compared to the lithology at 70 feet).

Electric Logs

The single-point resistance (SPR) and spontaneous potential (SP) logs were run simultaneously. Instead of using the conventional system in which the probe contains a down-hole lead electrode and a ground electrode placed at the surface, the differential SPR and SP log system was used. In this system both electrodes are included in the probe and are separated by an insulator. The current flows around the insulator from the lead electrode to the probe shell. This system provides higher resolution than the conventional system (Keys, 1988).

Spontaneous Potential

The SP log measures changes in natural electrochemical potential between the borehole fluid, formation fluid, and geologic material (Kwader, 1982). To interpret the SP log, a clean clay or shale should be present in the strata so that a clay baseline can be established. Without a defined clay baseline, interpretation of the log is almost impossible.

The SP deflections are to the left of the baseline where the formation water is more saline than the drilling mud and are to the right if the formation water is fresher than borehole water (Hilchie, 1982). If the formation and borehole water are both fresh, insignificant deflection occurs and the log will be practically a straight line.

The SP logs run in the wells on Cumberland Island tended to drift with deflection that yielded little information. The geologic sequence logged was mostly calcareous sand, sandy clay, and argillaceous limestone. Clean clays were not present in these sections. Although a comparatively pure clay layer did exist at two locations logged, temporary metal casing was in place during logging and extended below these zones. Therefore, these cased zones could not be logged with the electric log, and a clay baseline could not be established.

SP drifting also occurred because the formation water alternated from saline to fresh. The direction of deflection is dependent on the relation of formation and borehole water chemistry, and an informative curve could not be generated due to the changing formation water chemistry. As a result, the SP logs taken on Cumberland Island yielded little hydrogeological information.

Single-Point Resistance

The SPR log measures the electrical resistance of the geologic formation and borehole water between two electrodes. The ability of a rock to conduct a current depends on the effective porosity and conductivity of the water in the pore spaces. Resistivity increases as porosity, water content, and hydraulic conductivity decrease (Driscoll, 1986). The SPR log was useful in providing information such as location of contacts between formations, relative water quality, and the distinction of sandy zones and sandy limestones from argillaceous limestones and dolostones.

Grain Size Analysis

A grain size analysis of samples representing each sandy zone (the Pliocene sand, Miocene sand aquifer, and the surficial aquifer at well Sites 1, 2, and 3) was performed to determine the appropriate screen sizes for the new wells, and estimate the hydraulic conductivity of these zones (Figure 21). The sandy zones were well sorted quartz sand and contained little to no clay deposits. Table A1 in Appendix A shows the interval sampled in each zone and the raw data from the analysis.

Each sample (35-45 grams) was oven dried for 2 hours and weighed to the nearest 0.01 gram. The 'nest' of sieves ranged from -2 to 4 ϕ ($\phi = -\log_2 d$, where d is the particle diameter in millimeters). The samples were vibrated for 10 minutes on 80 percent of the power setting. The fraction retained on each mesh was weighed and recorded. Finally the measurement error in recovery percent of the initial sample weight was determined (Table A1). The grain size distribution from wells KBMP 1, 2, 5, 8, and 9 are given in Figure 21.

Aquifer Test

A 48-hour aquifer test was performed at Site 3 in the Pliocene-Miocene aquifer near Dungeness. This aquifer was chosen for testing because it may be susceptible to seawater intrusion due to channel dredging. Prior to the aquifer test, a step-drawdown test was performed to determine the well efficiency and the optimum pumping rate for the aquifer test.

Step Drawdown Test

The step-drawdown test was conducted by selecting five pumping rates or steps each lasting 1.5 hours, and measuring drawdown in the pumped well. The data provided from the test can be used to determine the specific capacity of the well and the optimum pumping rate (Jacob, 1947). During the step-drawdown test, a centrifugal pump having 25 feet of intake hose and 200 feet of discharge hose was used. The discharge hose was connected to an orifice bucket that measured the discharge rate. The orifice bucket was frequently monitored to ensure a constant pumping rate. Each successively higher pumping rate was implemented by increasing the throttle 20 percent.

Multi-well Aquifer Test

The aquifer test was conducted December 9-11, 1989, at Site 3 on Cumberland Island (Figure 3). The pumping well (KBMP 7) penetrated the limestone part of the Pliocene-Miocene aquifer so that the transmissivity of this zone could be determined. During the aquifer test, six wells were monitored, three of which penetrated the limestone part of the aquifer. The pumping well was pumped for 48 hours using a 4-inch submersible pump powered by a generator. The pump discharge hose was 5/8 of an inch in diameter and 200 feet long. This distance for discharge prevented direct local recharge of the surficial aquifer during the test. The discharge was monitored for the pumping duration by an orifice bucket.

The pumping and observation wells were monitored for the duration of the test by continuous water-level recorders, pressure transducers, and/or the wetted-tape method. The water-level recorders were installed on 4 of the monitoring wells. During the test, the recorders were set to collect data for 12 hour time periods. The cylindrical drum of the recorder is connected to a pulley with a steel tape threaded through it. The steel tape has a float attached to one end and a counter weight on the other. As the water level fluctuates in

the well, the tape causes the drum to rotate. A pen, controlled by a clock, moves across the rotating drum with time, thus producing a hydrograph.

The transducer is a variable reluctance device operated in conjunction with a data logger-120. Deflection of the transducer diaphragm changed the reluctance of the transducer and produced a voltage proportional to the pressure difference, or the water level difference, across the transducer. The voltage was digitally displayed on the data logger in feet. Hollow tubing from the port of the transducers to the data logger allowed the diaphragm to be exposed to atmospheric pressure changes and hence negated these effects. A transducer was used in the pumping well and three of the monitoring wells. Periodic water-level measurements were made using the wetted-tape method for verification.

During the aquifer test, two monitoring wells were located where the pressure transducers could not reach. These wells were measured solely by the wetted-tape method. Water levels measured for the potentiometric surface maps on June 28, 1990 also were measured by this method.

Barometric pressure data were collected from the National Oceanic and Atmospheric Administration at Jacksonville, Fla., and St. Simons Island, Ga., to evaluate the effects of changes in barometric pressure on water levels during the aquifer test. The data were used to correct water-level fluctuations due to barometric pressure changes.

ANALYSIS OF SURFACE GEOPHYSICS AND WELL SITE LOCATION

EM conductivity surveys were conducted to determine the most appropriate well site locations. Areas with low specific conductivity (around 25 millimhos/meter) were optimal locations for new wells. Low specific conductivity values indicate clean, highly resistive strata, saturated with freshwater, such as sand or limestone. These zones were ideal for monitoring water quality changes. At each location of EM conductivity measurement, a reading for the 33, 66, and 132 foot intercoil spacing for each dipole configuration (horizontal and vertical) was taken so that data acquisition ranged from theoretical depths of 25 to 197 feet below land surface (see Figures 22 through 27).

The conductivity values changed depending on the intercoil spacing (or depth) for a given location. However, these differences were slight and it is suspected that the theoretical depth of reading and the actual depth may not be the same, especially in the salt marsh areas where much of the shallow sediment is clay. This lithology, combined with the high water salinity, may have prevented the current from propagating to lower zones. In the marsh areas, it is likely that only the shallow zones were explored even at the maximum coil spacing.

Although changes in conductivity were observed at a given location for varying intercoil spacings or depth of exploration, the differences in conductivity were much more dramatic for changes in geomorphology, geology, and water chemistry. Low conductivity values were observed in sandy, freshwater zones such as along the dunes; high values were observed in saline-saturated clay deposits such as in marsh areas. Therefore, similar trends of conductivity occur as a function of location rather than varying depths at a single location.

Readings taken around Dungeness were low for each intercoil spacing and

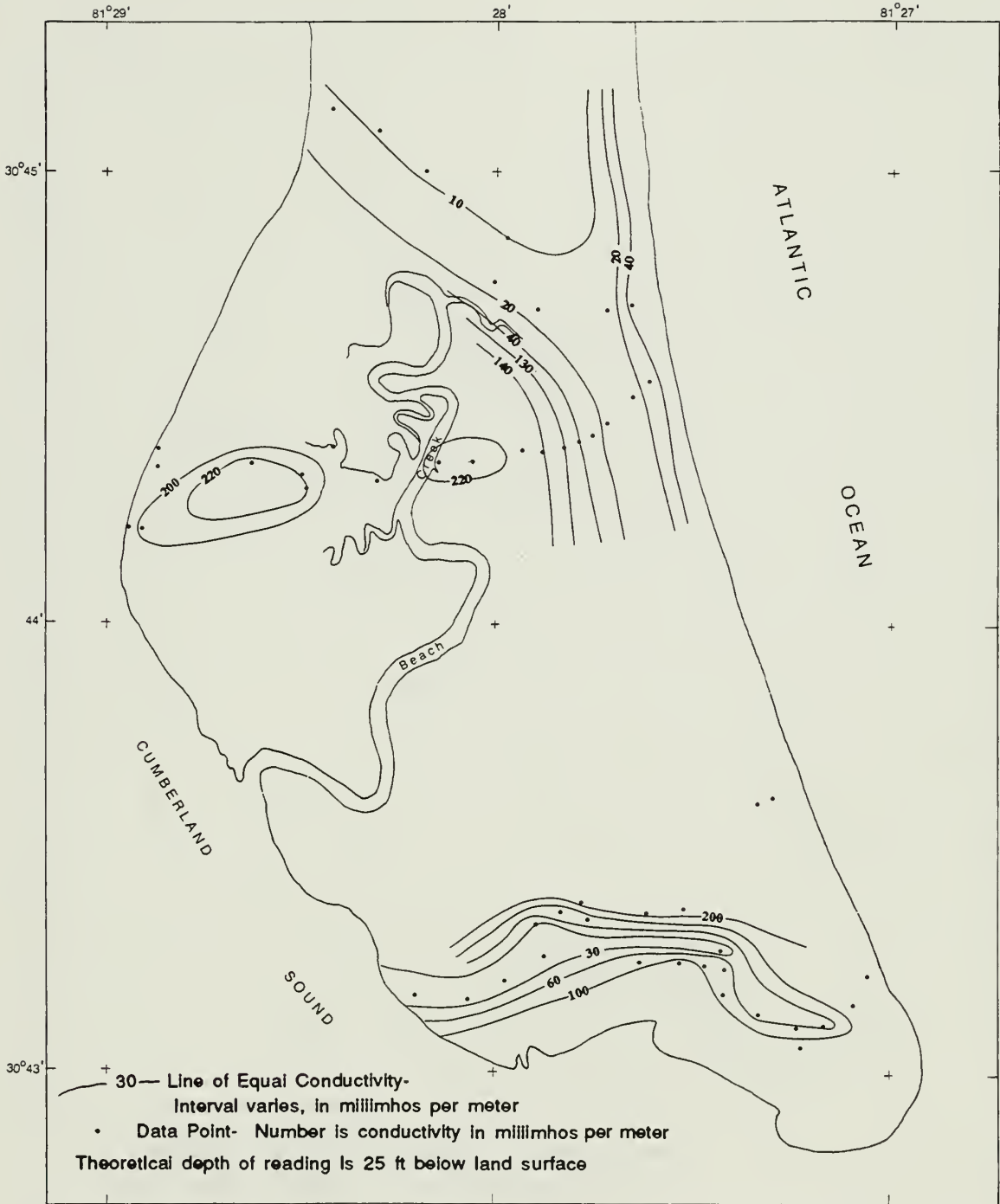


Figure 22. EM conductivity surface where the coil spacing is 33 feet and the coil configuration is horizontal.

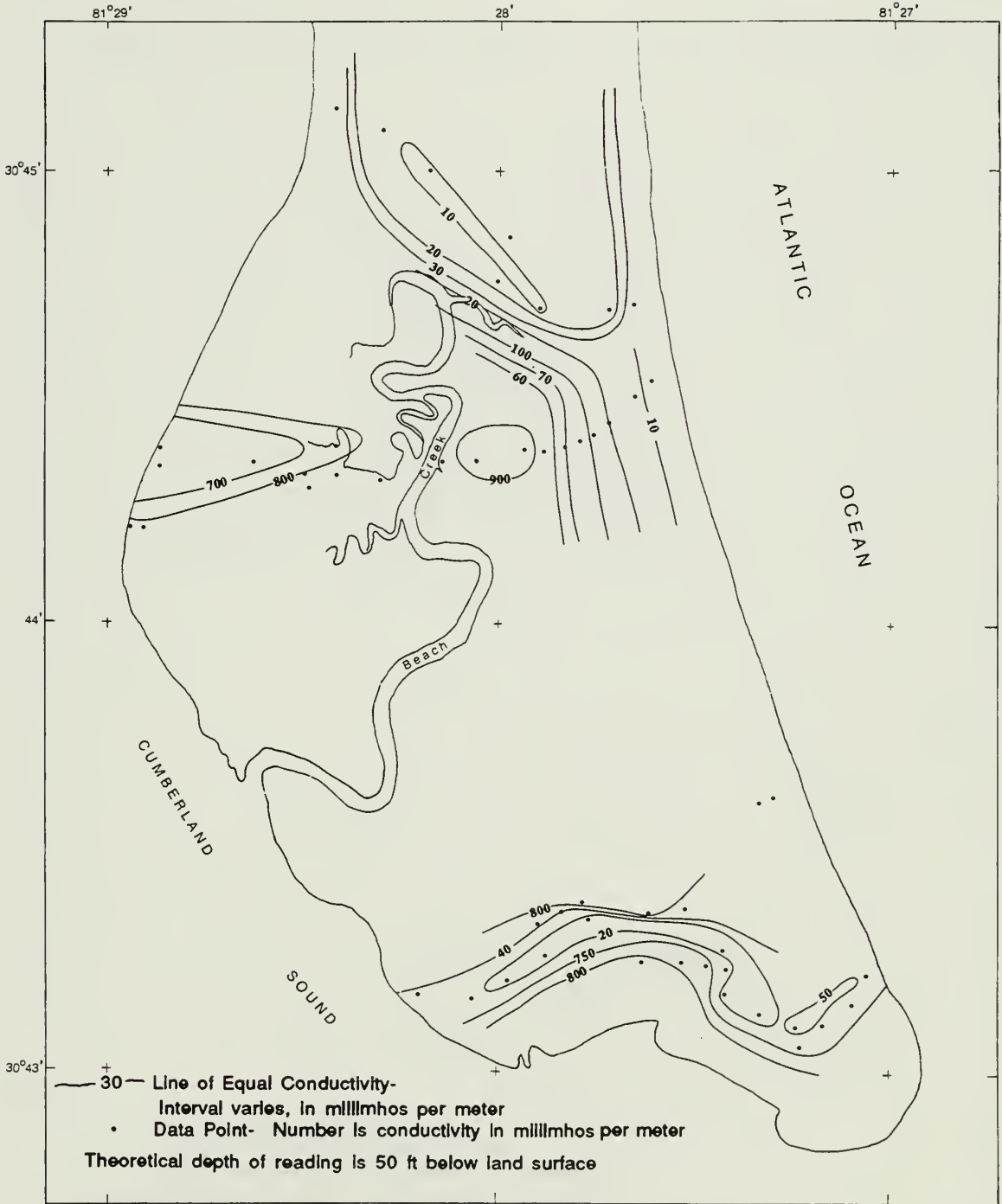
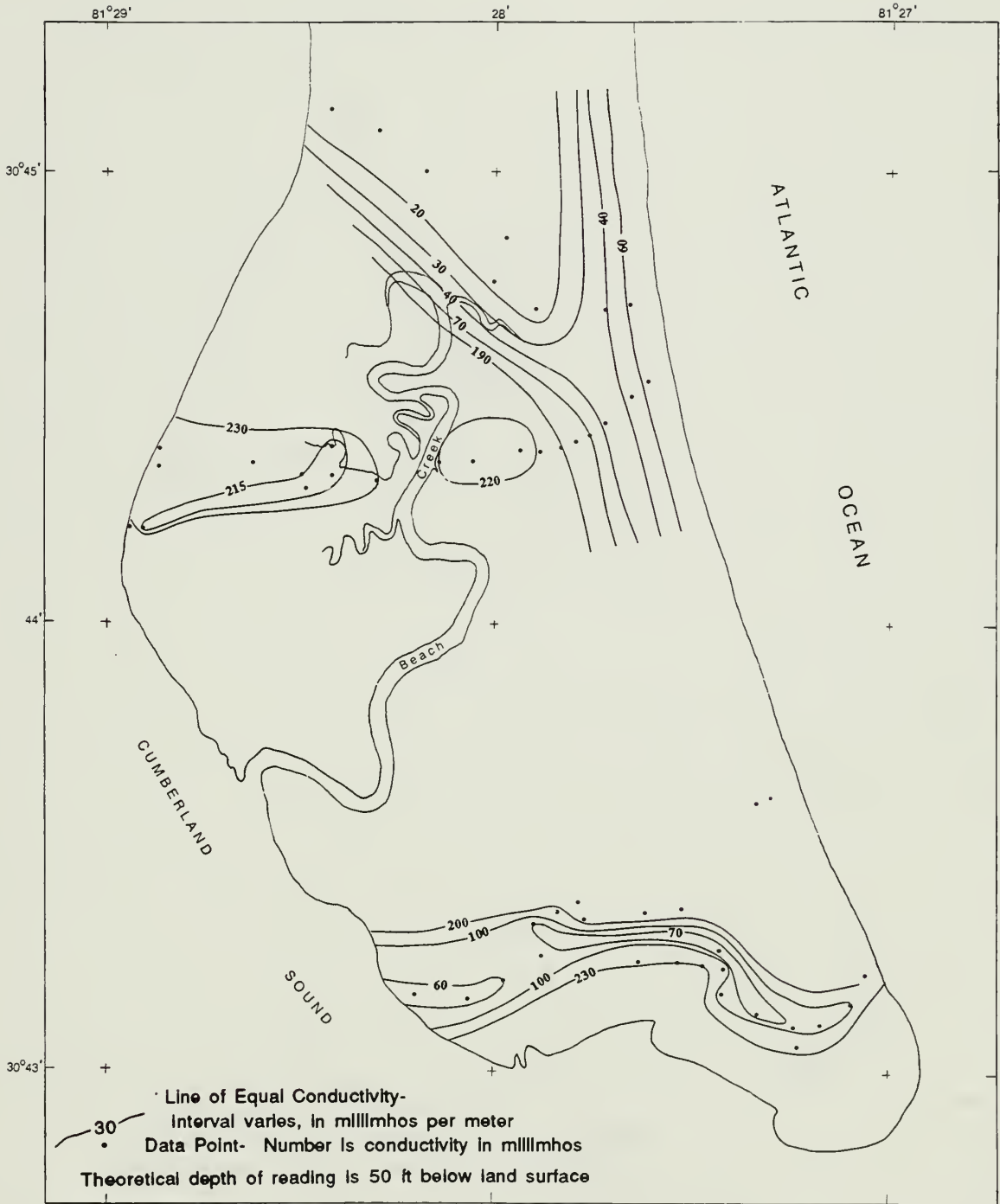


Figure 23. EM conductivity surface where the coil spacing is 33 feet and the coil configuration is vertical.



Base from U.S. Geological Survey
 Fernandina Beach, Fla.-Ga. 1:24,000, 1958 and
 Cumberland Island South, 1:24,000, 1958

Figure 24. EM conductivity surface where the coil spacing is 66 feet and the coil configuration is horizontal.

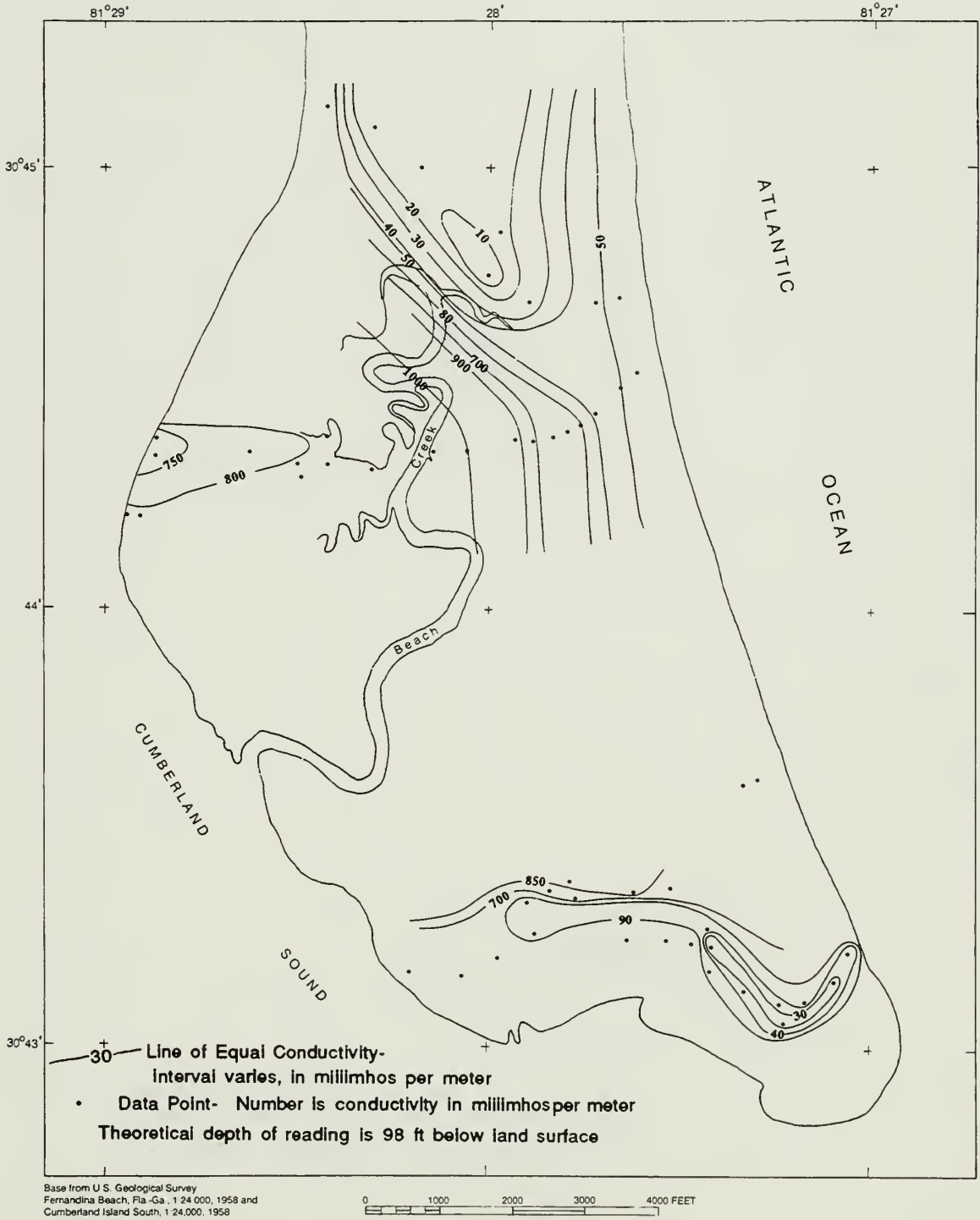


Figure 25. EM conductivity surface where the coil spacing is 66 feet and the coil configuration is vertical.

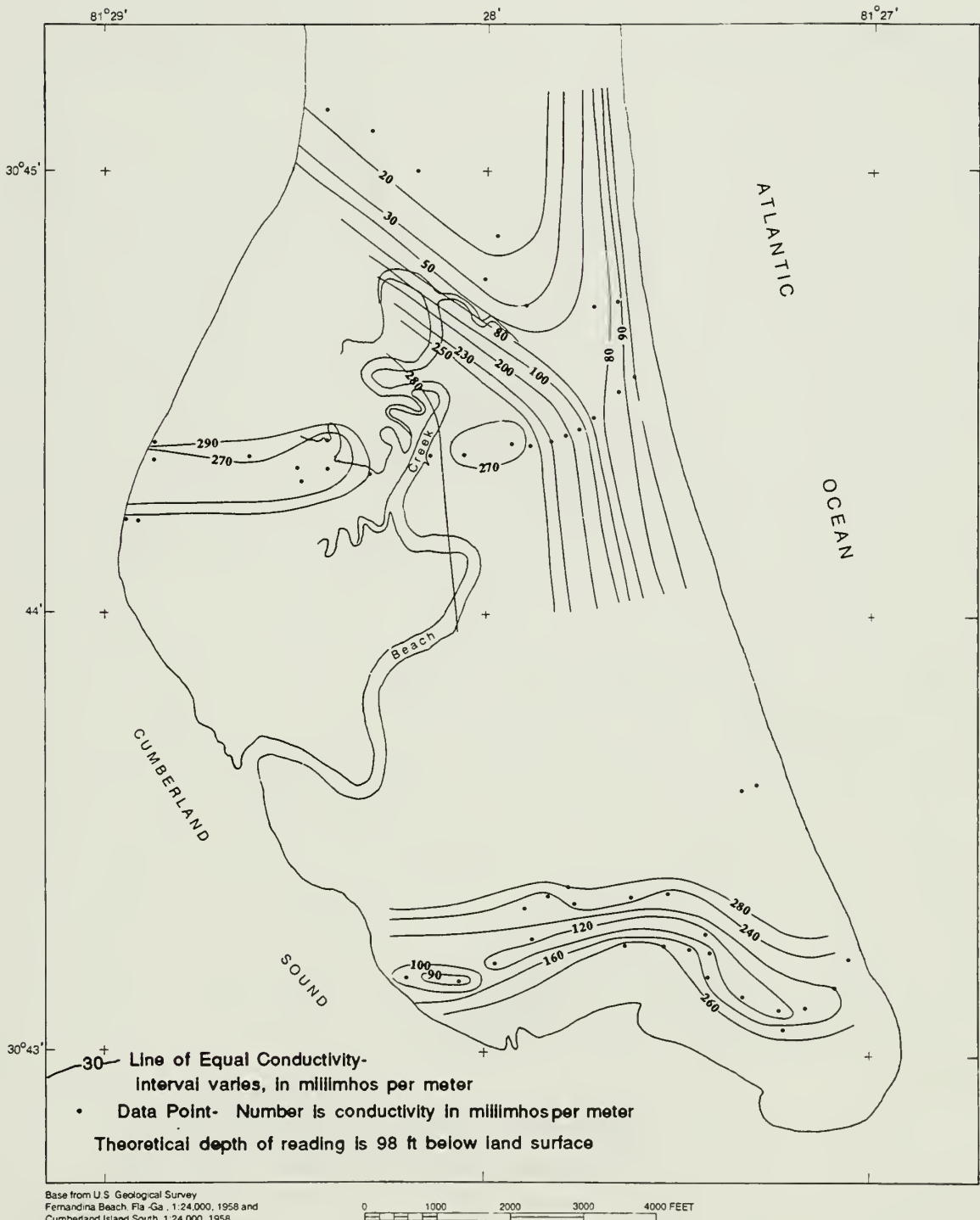


Figure 26. EM conductivity surface where the coil spacing is 132 feet and the coil configuration is horizontal.

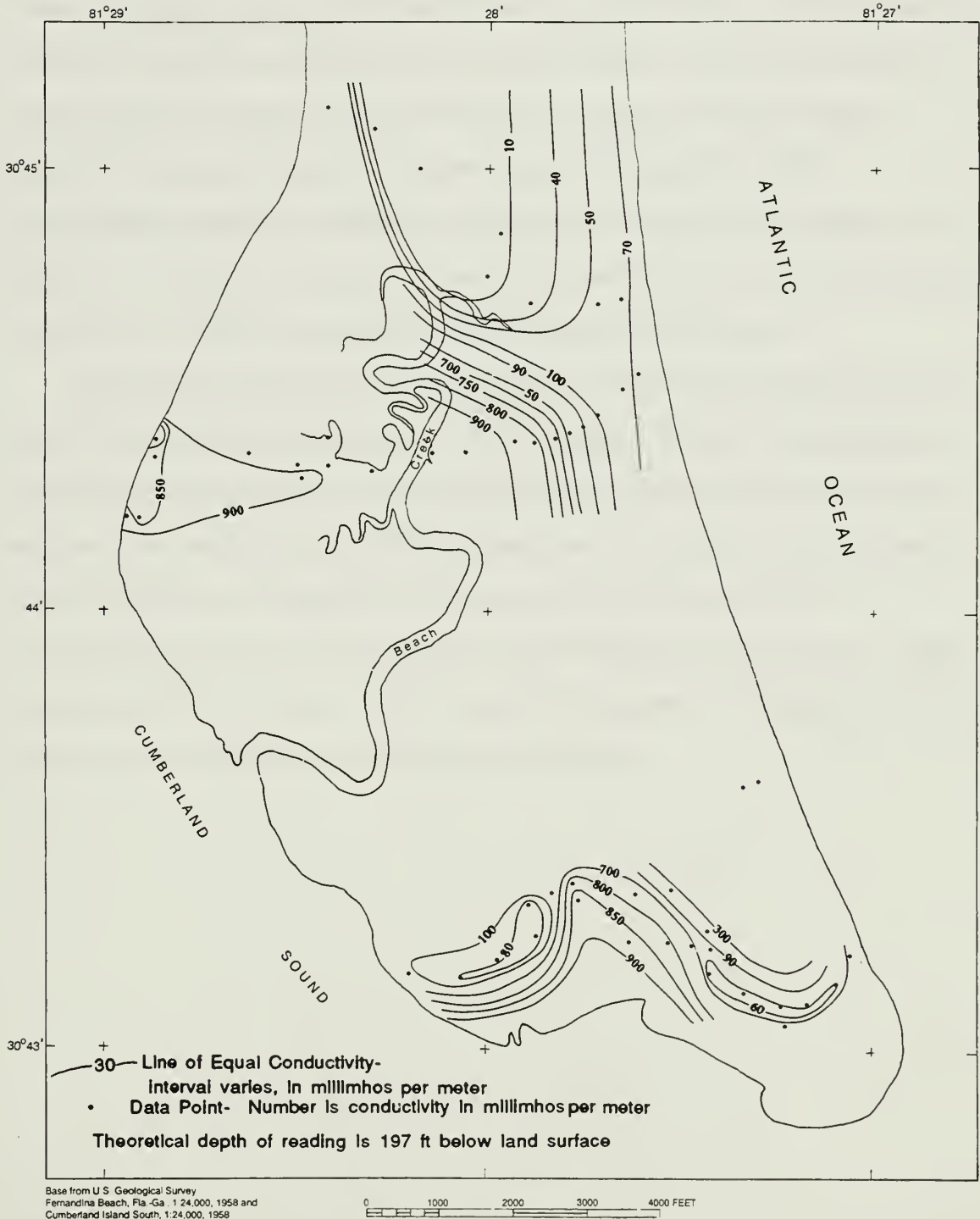


Figure 27. EM conductivity surface where the coil spacing is 132 feet and the coil configuration is vertical.

configuration. The 132 foot horizontal and 66 foot vertical readings (89 feet below land surface) were slightly higher which probably indicates the top of rock. Along the dunes the conductivity readings were also low becoming slightly higher in the interdune meadows, along the beach, and along the west side of the dunes adjacent to the marsh. High conductivity values were observed in the low-lying marsh areas (150 to 1000 millimhos/meter) which were attributable to the presence of clay sediment saturated with saline water. The only low readings measured in the marsh were on a hammock composed of silty sand. A shallow freshwater lens probably exists on the hammock.

The locations selected for the well sites in the study area were in fresh water zones. Areas with low electric conductivity were selected, such as well Site 3 at Dungeness (see Figure 3 for well site locations). On the southern part of the island the conductivity was inconsistent and ranged from 21 to 890 millimhos/meter. Here the geomorphology varies from low-lying dunes to marsh areas. The lower values were observed in the topographically higher areas where freshwater accumulates in silty-sand deposits, such as the areas selected for well Sites 1 and 2. Conductivity increased at these sites below depths of 50 feet, but not significantly (see Figures 22 through 27).

HYDROGEOLOGIC FRAMEWORK

The sediments underlying Cumberland Island comprise both local and areally extensive aquifers. For the purpose and scope of this report, the Miocene sand aquifer, Pliocene-Miocene aquifer, and surficial aquifer were investigated. The Floridan aquifer was beyond the scope of this study.

Miocene Sand Aquifer

In the study area, aquifers of Miocene age are present from 110 to 400 feet below land surface and range in thickness from 10 to 40 feet (see Figure 4). Sand zones in the Hawthorn Formation have been named the upper and lower Brunswick aquifers (Clark and others, 1990). Only the aquifers above these in the Charlton Formation were investigated during this study, and only the uppermost Miocene sand aquifer is discussed in detail.

The Miocene sand aquifer is confined above by alternating layers of argillaceous dolomite and clay and below by argillaceous dolomitic limestone. It is 10 feet thick, the top of which is located 136 feet below land surface at Site 1 (see Figure 28). The aquifer is recharged by precipitation in the Charlton Formation outcrop areas outside the study area. The areal extent of the Miocene sand aquifer is unknown because it was not penetrated by other wells.

The horizontal direction of groundwater flow in the Miocene sand aquifer is not known because only one well penetrates this zone in the study area. The potential vertical direction of groundwater flow is from the Miocene sand aquifer to the overlying Pliocene-Miocene aquifer based on water level measurements. At Site 1, the head of the Miocene sand aquifer is 0.13 feet higher than that of the overlying Pliocene-Miocene aquifer based on water-level measurements on June 28, 1990.

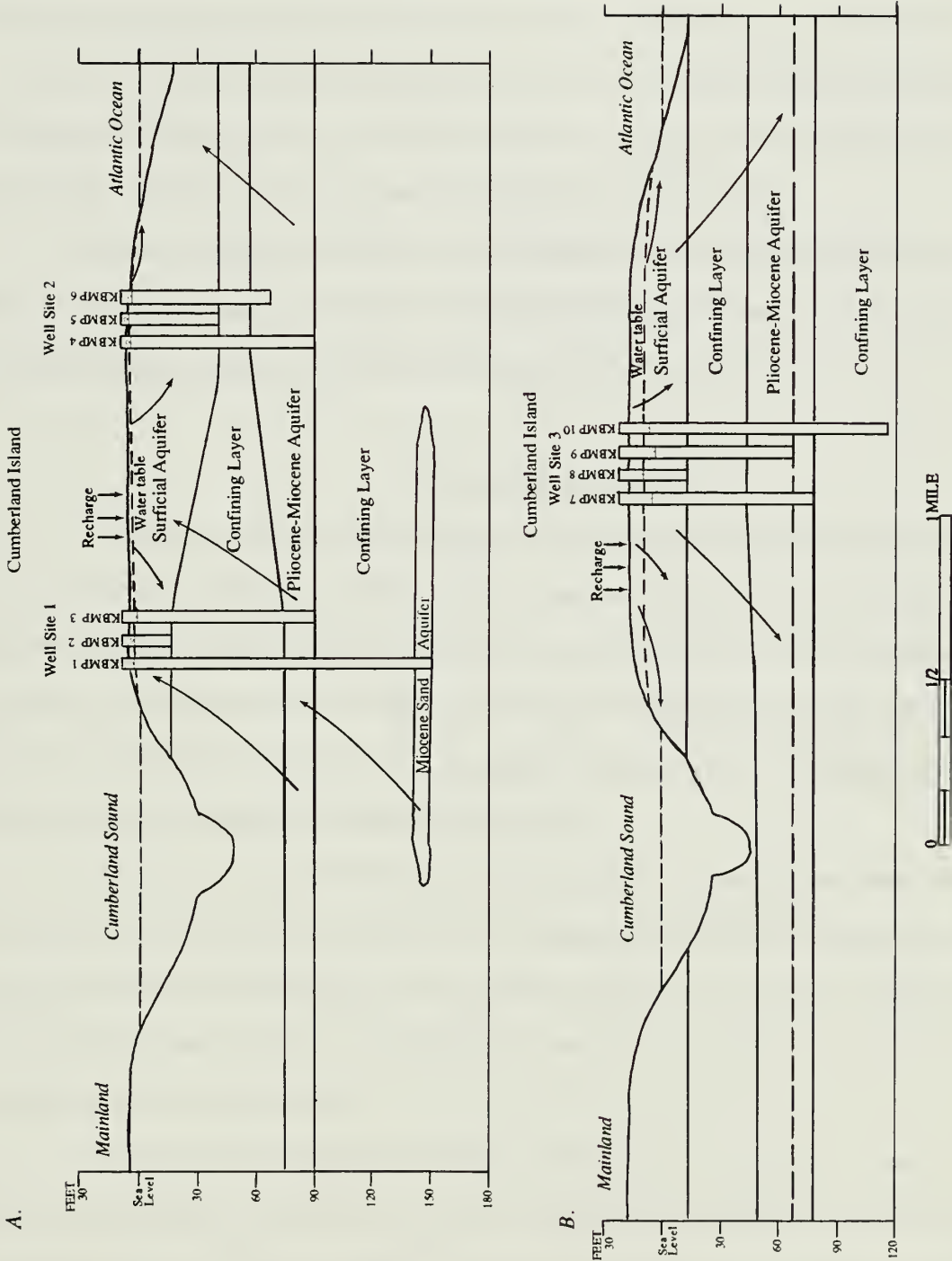


Figure 28. A. Hydrogeology at well sites 1 and 2. B. Hydrogeology at well site 3. Arrows indicate potential direction of groundwater flow. Water levels measured June 28, 1990.

Clarke and others (1990) determined that the hydraulic conductivity of the lower Brunswick aquifer ranged from 20 to 57 ft/d based on aquifer testing. The hydraulic conductivity of the Miocene sand aquifer as derived by the method of grain size distribution described by Masch and Denny (1966) is 53 ft/d. See Appendix C for the Masch and Denny method of determining hydraulic conductivity and calculations.

The water quality of the Miocene sand aquifer is unsuitable for most uses. The dissolved solids content in the aquifer exceed State drinking standards. The chloride content is 6,200 mg/L having 32 percent seawater (Wilson, 1990).

Pliocene-Miocene Aquifer

The Pliocene-Miocene aquifer consists of Miocene-age limestone and Pliocene-age sand. At Site 1, the Duplin Formation is clayey sand resulting in low permeability. The aquifer consists of vuggy, fractured dolomite that is enhanced by well-developed secondary porosity. The Pliocene-Miocene aquifer is present at a depth of 79 feet below land surface, and it is 15 feet thick (see Figure 28). The aquifer is confined above by dense dolomite and clay and below by argillaceous dolomitic limestone.

At Site 2, the top of the Pliocene-Miocene aquifer is located 61 feet below land surface and is 33 feet thick (see Figure 28). The aquifer has low permeability due to the high clay content and poorly developed secondary porosity. At this site the aquifer consists of dolomitic limestone and is confined above by sandy clay and clayey sand and below by argillaceous dolomitic limestone.

At Site 3 and northward on the island, the Pliocene-Miocene aquifer consists of two zones having different lithologies and different hydraulic properties. The upper zone of the aquifer consists of sand of the Duplin Formation ranging from 2 to 42 feet thick. The lower zone consists of about 10 feet of fractured limestone of the Charlton Formation.

These two zones are separated by 8 feet of sandy clay and clayey sand. The aquifer is confined above by about 30 feet of clay sediments of Pleistocene age and below by alternating layers of argillaceous dolomite and clay (see Figure 28).

The Duplin Formation consists of sandy clay, clayey sand lenses, based on core and cutting samples. The formation increased in clay content at Sites 1 and 2 causing lower hydraulic conductivity values at these sites. Variation in the lithology of the Pliocene age deposits indicates that this zone is anisotropic and heterogeneous. The weathered and fractured Charlton limestone also was anisotropic and heterogeneous based on aquifer testing results. The heterogeneities were due to thickness or facies changes in the limestone.

The horizontal groundwater flow gradient is low in the Pliocene-Miocene aquifer as shown by the aquifer's potentiometric surface map of June 28, 1990 (see Figure 29). The direction of groundwater flow was solved for by applying the three point method where the exact location of an equipotential line is solved for by determining the gradient between the highest and lowest head values. Table 2 summarizes the ground-water levels for June 28, 1990 made during high tide midway between spring and neap tides. Table 3 summarizes the groundwater densities at each well (see Appendix D for density corrections). Potential horizontal and vertical groundwater flow directions are based on June 28, 1990 data. For wells tapping the Pliocene-Miocene aquifer near Dungeness, the Nightingale well, and the Sea Camp well, the water levels vary areally 0.4 feet per mile. The horizontal gradient in this area is so small that the gradient direction could easily change if water-level and/or land surface altitude measurement errors are made. Because the horizontal gradient in this area is nearly zero, horizontal groundwater flow probably is influenced more by tidal fluctuations and storm surges than by regional recharge.

It seems logical that the regional horizontal groundwater flow direction in the

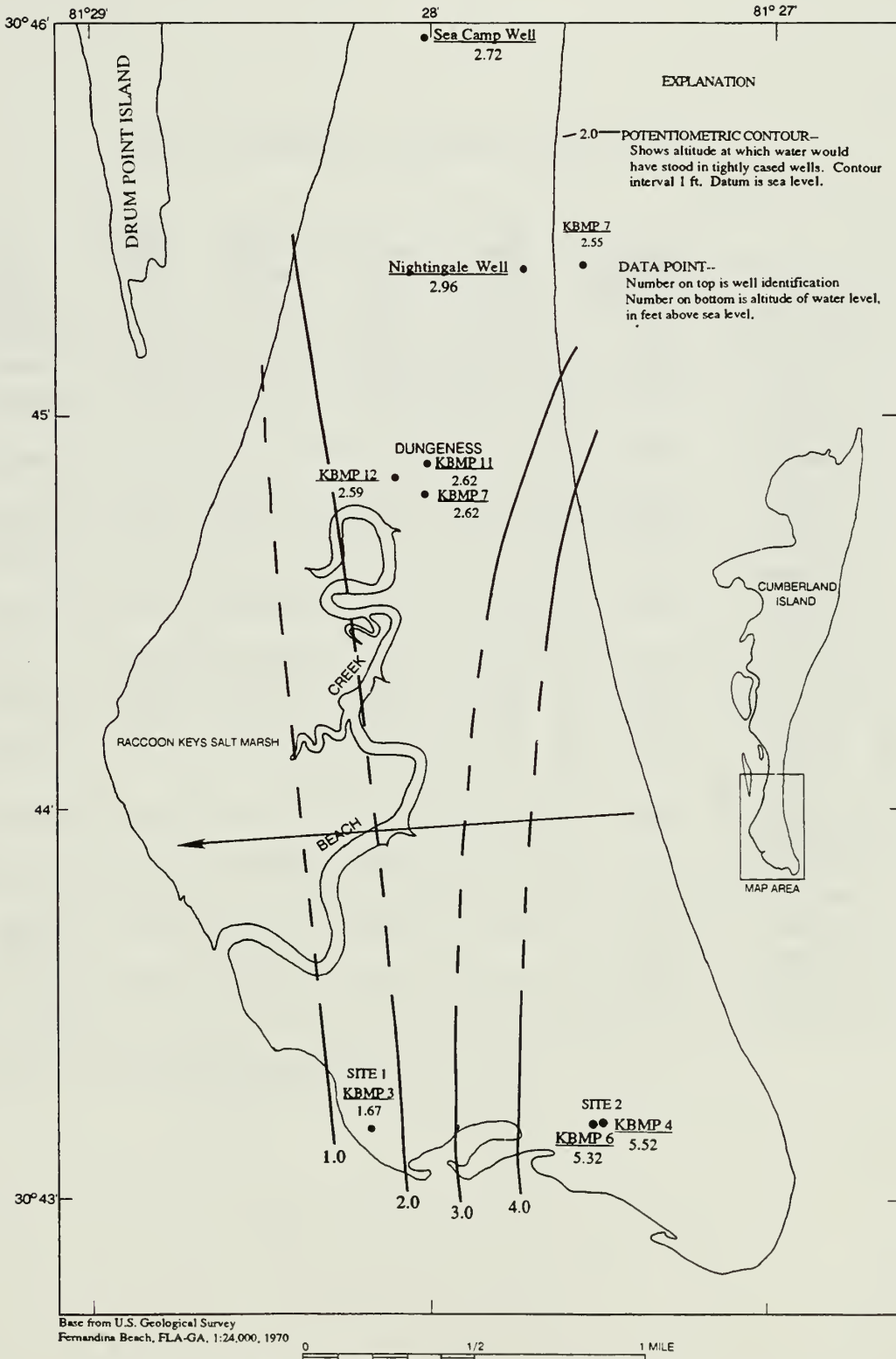


Figure 29. Potentiometric surface map of the Pliocene-Miocene aquifer for June 28, 1990. Arrow indicates potential direction of groundwater flow.

Table 2. Groundwater level summary for June 28, 1990.

Well identification	Depth to water level, in ft.	Land surface elevation, in ft.	Measuring point, in ft.	Water level elevation, in ft.	Corrected* water level elevation, in ft.	Hydrogeologic zone
KBMP 1	4.4	4.6	0.46	0.66	1.8	Miocene sand
KBMP 2	5.8	4.6	1.78	0.5	0.5	Surficial
KBMP 3	5.1	4.6	0.65	0.15	1.67	Pliocene-Miocene age
KBMP 4	4.24	6.86	1.25	3.87	5.52	Pliocene-Miocene age
KBMP 5	3.37	6.86	0.92	4.41	4.44	Surficial
KBMP 6	4.43	6.86	1.4	3.83	5.32	Pliocene-Miocene age
KBMP 7	15.01	15.93	1.63	2.55	2.62	Pliocene-Miocene age
KBMP 8	11.92	15.93	0.92	4.93	4.93	Surficial
KBMP 9	15.06	15.93	1.62	2.48	2.48	Pliocene sand
KBMP 10	14.54	15.93	1.19	2.58	2.58	Miocene confining layer
KBMP 11	16.32	16.73	2.14	2.55	2.62	Pliocene-Miocene age
KBMP 12	14.55	16.42	0.72	2.59	2.59	Pliocene-Miocene age
Nightingale well	15.15	17.86	0.25	2.96	2.96	Pliocene-Miocene age
Sea Camp well	16.73	18.98	0.47	2.72	2.72	Pliocene-Miocene age

*Refer to Table 3 for percent seawater in each well.

Table 3. Percent seawater and water density at each well*.

Well number	Percent seawater	Density (gm/cc)	Density (lb/ft3)
KBMP 1	32	1.008	62.93
KBMP 2	0.2	1.000.	62.43
KBMP 3	68	1.017	63.49
KBMP 4	73	1.018	63.55
KBMP 5	3.0.	1.001	62.49
KBMP 6	89	1.022	63.80.
KBMP 7	4.2	1.001	62.49
KBMP 8	0.7	1.000.	62.43
KBMP 9	0.2	1.000.	62.43
KBMP 10	0.2	1.000.	62.43
KBMP 11	5.2	1.017	62.49

*Refer to Appendix D for freshwater head calculations corrected for density.

Pliocene-Miocene aquifer should be to the southeast, because the aquifer is recharged in outcrop areas in the northwest. However, this direction of horizontal groundwater flow was not observed in the field. The direction observed may represent a local flow system in the aquifer. The water level at well Site 2 is almost 3 feet higher than at Sites 1 and 3. The high water level at Site 2 may be due to the high clay content in the aquifer compared to the lithology of the aquifer at Sites 1 and 3. A higher water level occurs in a zone with low hydraulic conductivity than in a zone under the same conditions with a high hydraulic conductivity. The high water level at Site 2 contributes to the westward direction of horizontal groundwater flow (see Figure 29). The westward direction of groundwater flow indicates that recharge is occurring from offshore. Adequate data is not available to determine if recharge is occurring from the ocean to the Pliocene-Miocene aquifer or if the high water level at Site 2 is an anomaly and represents local flow in the aquifer.

The vertical groundwater flow gradient for the Pliocene-Miocene aquifer varies with time and space. At Site 3, the surficial aquifer water level is 2.45 feet higher than that of the Pliocene-Miocene aquifer. Therefore, the vertical gradient flow potential is from the surficial aquifer downward to the Pliocene-Miocene aquifer. At Sites 1 and 2 the Pliocene-Miocene aquifer water level is slightly higher than that of the surficial aquifer ranging from 0.88 to 1.17 feet. Here the vertical direction of groundwater flow is the reverse of Site 3, and the vertical groundwater flow potential is from the Pliocene-Miocene aquifer upward to the surficial aquifer. The water level measurements were made June 28, 1990 during high tide. It is possible that during low tide the potential groundwater flow direction reverses and groundwater flows from the surficial aquifer to the Pliocene-Miocene aquifer.

The Pliocene-Miocene aquifer receives recharge in the outcrop areas outside the study area in western Camden and eastern Charlton counties. The aquifer also receives recharge by leakage from along the St Marys River, from the Cumberland Sound, and from

the overlying surficial aquifer and the underlying Miocene sand aquifer depending on the hydraulic gradient between the aquifers (see Figure 28).

Regional recharge to the Pliocene-Miocene aquifer is from the Georgia Coastal Plain. The area of regional discharge is likely off the east coast of Cumberland Island. However, the observed horizontal flow direction is toward the west and possibly represents local groundwater flow as previously discussed. The aquifer is intermittently pumped by wells on the island, but total withdrawal is negligible.

The transmissivity of the Pliocene-Miocene aquifer ranges from 235 to 650 square feet per day (ft^2/d), and the storage coefficient from 1.05×10^{-5} to 5.6×10^{-5} based on aquifer testing conducted during the investigation. Only the limestone part of the aquifer was stressed during the aquifer test; the well screen did not extend into the sand of the Duplin Formation. The hydraulic conductivity for the Miocene limestone ranges from 34 ft/d to 94 ft/d based on aquifer testing. The hydraulic conductivity of the Pliocene sand is 100 ft/d based on the method of deriving this value from grain size analysis as described by Masch and Denny (1966).

The quality of water from the Pliocene-Miocene aquifer is suitable for drinking. However, near Dungeness, salinity has increased in the past 2 years apparently due to saltwater intrusion. In December 1988, KBMP 11 began producing salty water (David Hines, oral comm., 1989) and now contains 5.2 percent seawater. Well KBMP 12, located 200 feet away, penetrates the same aquifer zone and yields freshwater. Well KBMP 7, located 247 feet from KBMP 11, yields water that contains 4.2 percent seawater (Wilson, 1990). For most of the extent of the island the water meets all state drinking water standards and has low dissolved solids content (Brown, 1984). However, near the coast, the water chemistry approaches that of seawater as was observed at Sites 1 and 2, which produced water having 68 and 89 percent seawater content, respectively (Wilson,

1990).

The clay deposits that overlie the Pliocene-Miocene aquifer consist of sediments of Pleistocene age and are approximately 30 feet thick. The zone varies from a clean clay on the south end of the island to a sandy clay on the north end. This confining layer extends the length and width of the island and is present below the mainland, but is not continuous across the Kings Bay channel as a result of dredging, channel scour, or both.

Surficial Aquifer

The surficial aquifer is bound by the Cumberland River on the west, the Atlantic Ocean on the east, St Andrew Sound on the north, and Cumberland Sound on the south. It is confined below by 5 to 40 feet of clay and sandy clay. The aquifer extends the length and width of the island and ranges from 15 to 35 feet in saturated thickness.

The surficial aquifer primarily consists of well-sorted fine sand that was deposited by long shore wind and wave processes (Hoyt, 1967). These processes deposit sediment in a directional configuration that parallels the shore. This results in an anisotropic aquifer medium with a higher hydraulic conductivity in the lateral direction parallel to shore. The aquifer is homogeneous based on the lithology.

A freshwater lens occurs in the topographically higher areas and generally beneath the interior forest and back dunes based on surface geophysical surveys. However, the freshwater dimensions are not as extensive as the aquifer dimensions, as indicated by surface geophysical data. Little freshwater exists in the marshes except at higher elevations such as on hammocks.

The water table ranges from 4 to 20 feet above sea level on the island's interior and drops to near sea level along the coast (Brown, 1984). Based on June 28, 1990 data, the

direction of horizontal groundwater flow is toward the southwest in the study area (see Figure 30). This direction was solved for by applying the 3 point method. Horizontal groundwater flow in the surficial aquifer tends to mimic the topography, and it is therefore possible that the dunes along the east coast of the island act as a groundwater divide. If this is assumed, the direction of flow on the west side of the dunes is toward the west and on the east side of the dunes, toward the east. All water levels in the surficial aquifer were measured on the west side of the dunes and the direction of groundwater flow is toward the southwest. If water level data were available east of the dunes, these data may indicate an eastward direction of groundwater flow.

The potential vertical groundwater flow gradient at Site 3 was from the surficial aquifer to the Pliocene-Miocene aquifer based on June 28, 1990 data. The surficial aquifer water level was 2.45 feet higher than the head of the Pliocene-Miocene aquifer. At Sites 1 and 2 the potential vertical gradient is reverse; the water level of the Pliocene-Miocene aquifer is 1.17 feet higher than the surficial aquifer at Site 1 and 0.88 feet higher at Site 2.

The vertical groundwater flow direction of the surficial aquifer may change with the wet and dry seasons. During wet seasons, the aquifer has a higher water level and may be a source of recharge for the Pliocene-Miocene aquifer. During dry seasons, the water level is lower and may receive leakage from the Pliocene-Miocene aquifer. Also, on the south end of the island where the water level of the Pliocene-Miocene aquifer is approximately 0.88 feet higher than the surficial aquifer, the vertical direction of groundwater flow may reverse daily due to tides. Although the Pliocene-Miocene aquifer fluctuates from 0.5 to 0.8 feet during tide cycles, the surficial aquifer is not affected by the tides because of its high storage coefficient value.

The surficial aquifer is recharged primarily by rainfall and occasional storm washover. The average annual rainfall for the area is 52 inches. Approximately 40 inches

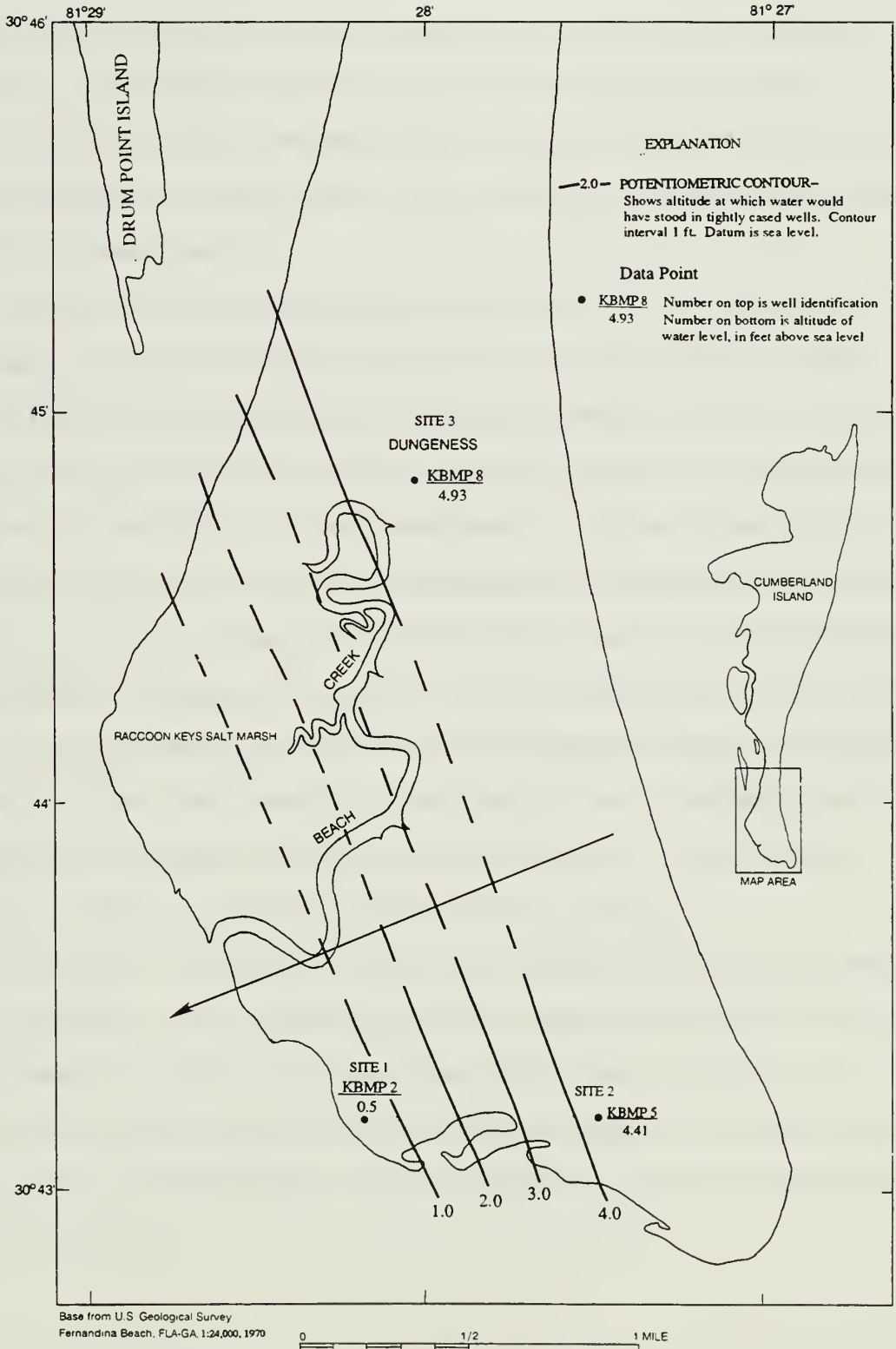


Figure 30. Potentiometric surface map of the surficial aquifer for June 28, 1990. Arrow indicates potential direction of groundwater flow.

are lost to evapotranspiration, 6 inches to surface run off, and 6 inches are available to recharge the aquifer (Brown, 1984). The topsoil does not impede the downward groundwater flow of rainfall to the surficial aquifer because it is only 2 to 3 inches thick, relatively immature, and highly permeable. Surface runoff is low as indicated by the lack of interior freshwater streams.

The water level in the surficial aquifer changed little from June 1989 to June 1990. The greatest water-level fluctuation observed was a rise of 1.73 feet from June 1989 to December 1989 due to recharge from precipitation during the fall. Assuming a porosity of 30 percent for silty sand (Freeze and Cherry, 1979), similar to that of the surficial aquifer in the area, then the 6 inches of recharge should produce a 1.67 foot rise in water-level. This value was somewhat lower than the observed water-level fluctuation. The amount of recharge was an estimated value and may be higher for the year. Also, the actual volume of water available as recharge may be higher as a result of an antecedent soil-moisture surplus.

The surficial aquifer hydraulic conductivity values derived by the method described by Masch and Denny (1966) varied little between each well site. The values obtained from samples from wells KBMP 2, KBMP 5, and KBMP 8 were 22.7, 19.4 and 22 ft/d, respectively. The relevant calculations are described in Appendix C.

The quality of water from the surficial aquifer is suitable for drinking and domestic use, but could easily become contaminated because the water table is near land surface and has little overburden to filter the recharge (Brown, 1984). The total dissolved solids of water from wells tapping the surficial aquifer in the area averages 398 mg/L. However, on the south end of the island the total dissolved solids have been reported as high as 1,318 mg/L (Wilson, 1990).

Aquifer Interaction

The Miocene sand, Pliocene-Miocene, and surficial aquifers in the study area interact by leakage through confining layers. If a difference in head exists between two aquifers, groundwater has the potential to move vertically from one aquifer to another in the direction of the aquifer having the lower potential head. Appendix E provides the leakage equation and calculations.

Based on water levels of June 28, 1990, at Sites 1 and 2 the groundwater head of the Pliocene-Miocene aquifer was 0.88 to 1.17 feet higher than that of the surficial aquifer. The potential groundwater flow direction is from the Pliocene-Miocene to the surficial aquifer. Because the water-levels in the Pliocene-Miocene aquifer fluctuate from 0.5 to 0.8 feet during a tide cycle, the direction of vertical leakage may reverse during low tide (see Figure 31). Therefore, during high tide, the Pliocene-Miocene aquifer is likely a potential source for the surficial aquifer, and during low tide it is a potential sink for the surficial aquifer. The calculated leakage rate values between the surficial and Pliocene-Miocene aquifer at Sites 1 and 2 were 2.09×10^{-5} ft/d and 3.17×10^{-4} ft/d, respectively.

At Site 3 the head in the surficial aquifer was 2.31 feet higher than that of the Pliocene-Miocene aquifer. The aquifers are separated by about 30 feet of clay. Here the calculated leakage rate from the surficial aquifer to the Pliocene-Miocene aquifer was 4.08×10^{-4} ft/d.

At Site 1 the head in the Miocene sand aquifer was only 0.13 feet higher than the head in the Pliocene-Miocene aquifer. These aquifers are separated by 42 feet of argillaceous dolomite. The leakage rate from the Miocene sand aquifer to the Pliocene-Miocene aquifer was 3.1×10^{-6} ft/d (see Appendix E for calculations).

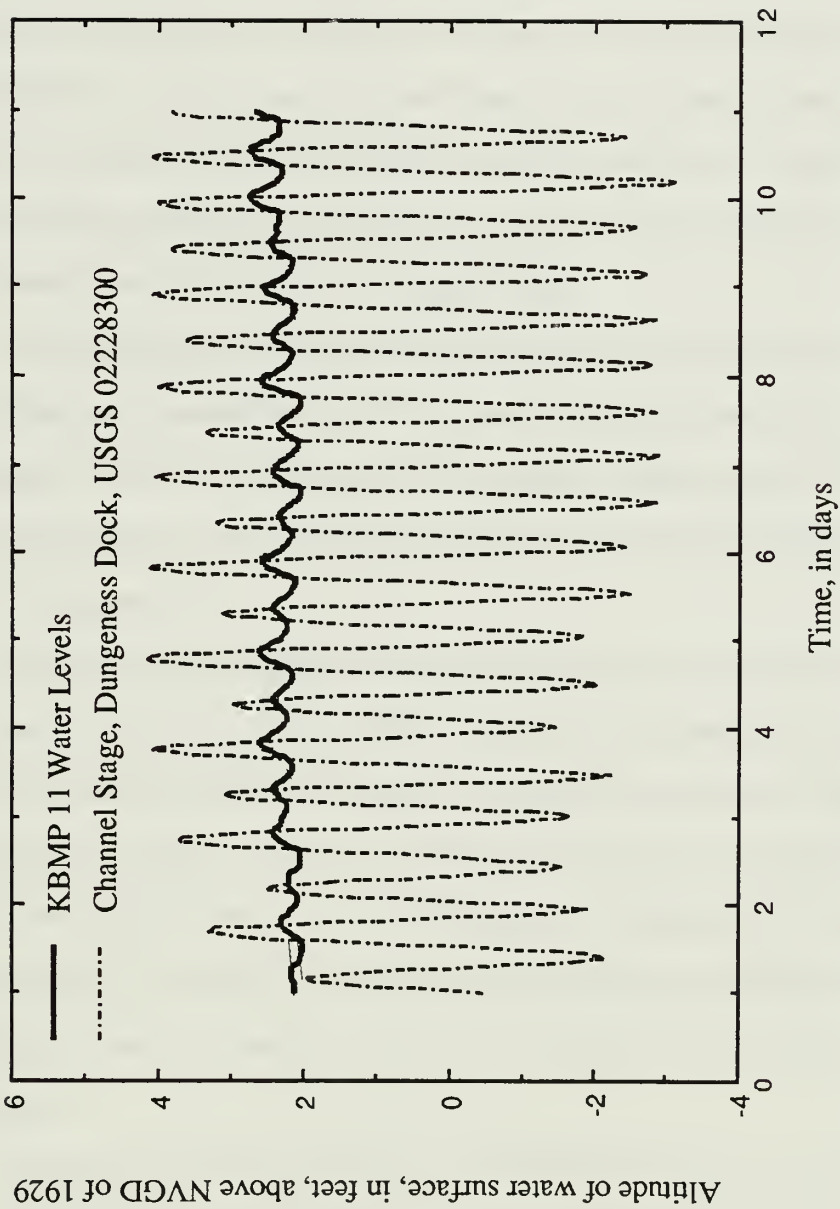


Figure 31. Comparison of Pliocene-Miocene aquifer water levels to the channel stage, August, 1990.

Analytical Model

An analytical model was developed to mathematically describe the hydrogeologic groundwater flow regime of the surficial and Pliocene-Miocene aquifers. A dynamic groundwater flow system exists in the study area due to fluctuating tides which cause change in the vertical and horizontal groundwater flow directions. The equations and schematic diagram (Figure 32) represent the groundwater flow system at a time-average mean where the water levels are at a constant altitude.

For this study the analytical model describes the groundwater flow system in the area of Dungeness because here the geology and hydrogeology are typical for a large part of the island. The recharge, discharge, and volumetric leakage rates for a 1 square mile area were calculated as part of the analytical model. The calculations for the model are provided in Appendix E.

The surficial aquifer is in a steady-state condition with constant long-term recharge, equivalent discharge, and no appreciable withdrawals due to pumping. Approximately 6 inches are available to recharge the aquifer each year (104 million gallons of precipitation per square mile per year). About 2.85×10^5 gallons per square mile recharge the aquifer each day and nearly the same amount is discharged to a combination of the low lying wetlands (1.92×10^5 gal/d), the underlying Pliocene-Miocene aquifer (8.5×10^4 gal/d), and along the coast at the seepage face (7.58×10^3 gal/d). See Appendix E for calculations.

The equation governing surficial aquifer discharge along the seepage face is derived from the Dupuit theory of free surface flow (Raudkivi and Callander, 1976) and is expressed as:

$$q = [K \frac{(h_1^2 - h_2^2)}{2L}] \quad (1)$$

where

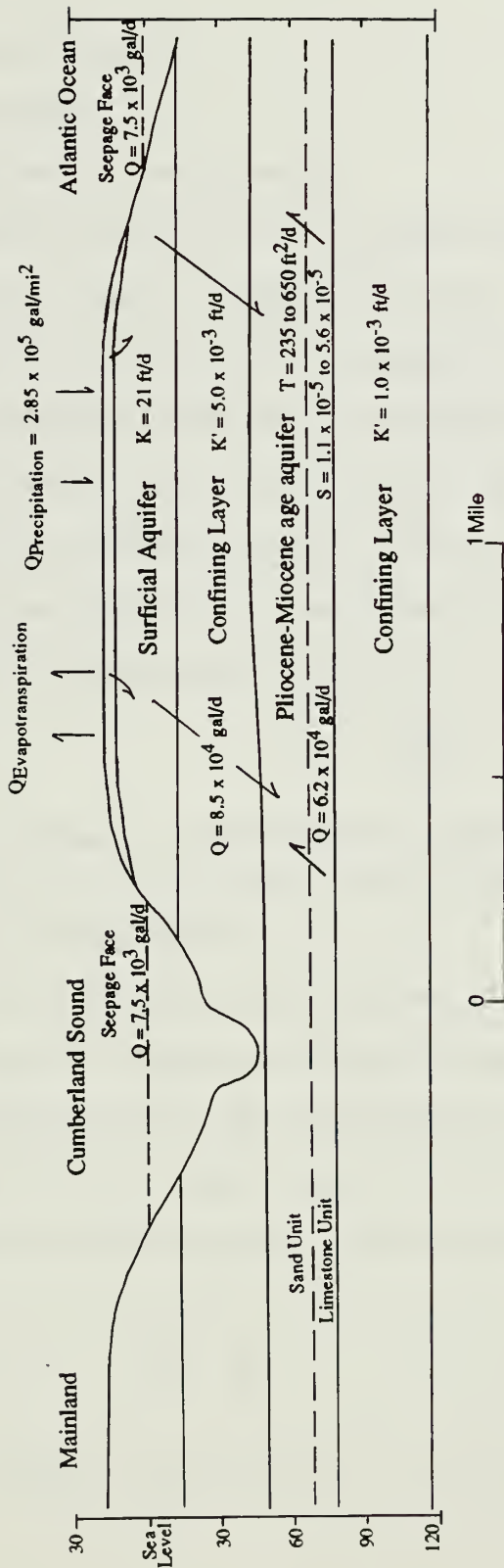


Figure 32. Conceptual model of the aquifer system, site 3. Values are for a 1 square mile area. Arrows indicate direction of flow.

q = specific discharge [ft/d]

h_1 = water level [ft],

h_2 = water level at the seepage face [ft],

K = hydraulic conductivity of the surficial aquifer [ft/d],

L = length from center of the island to the coast [ft],

The assumptions for discharge along a seepage face are that, 1) the flow lines are horizontal and equipotentials are vertical, and 2) the hydraulic gradient is assumed to be equal to the slope of the phreatic surface (Freeze and Cherry, 1979). The total discharge along the seepage face was calculated by assuming a phreatic surface of zero at the seepage face and subtracting this value from the measured water level at Site 3. Leakage to or from an overlying or underlying aquifer is expressed as:

$$q = \frac{K' \Delta h}{b'} \quad (2)$$

where

K' = vertical hydraulic conductivity of confining layer [ft/d],

Δh = difference in potentiometric head between aquifers [ft], and

b' = confining bed thickness [ft].

The surficial aquifer is a potential source of recharge for the underlying aquifer, and is under steady state conditions, unconfined, homogeneous, anisotropic, and receives areal recharge from precipitation. The partial differential equation that describes the three-dimensional flow in the surficial aquifer as modified for aquifer assumptions and boundary conditions from Freeze and Cherry (1979) is expressed as:

$$\begin{aligned} \frac{\partial}{\partial x} (K_x (h - z_b) \frac{\partial h}{\partial x}) + \frac{\partial}{\partial y} (K_y (h - z_b) \frac{\partial h}{\partial y}) + \frac{\partial}{\partial z} (K_z (h - z_b) \frac{\partial h}{\partial z}) + Q_{\text{precipitation}} \\ - \frac{(K'_b \Delta h)}{b} - Q_{\text{evapotranspiration}} - [K \frac{(h_1^2 - h_2^2)}{2L}] = 0 \end{aligned} \quad (3)$$

where

z_b = altitude of the base of the surficial aquifer [ft],

Q = volumetric inflow, outflow rate [ft³/d].

The altitude of the bottom of the aquifer (z_b) was subtracted from the head in the aquifer to account for saturated thickness changes from the center of the island to the coast.

The Pliocene-Miocene aquifer consists of two zones hydraulically connected but geologically distinct. At Site 3, the sand layer is separated from the limestone layer by approximately 8 feet of sandy clay. A difference in potentiometric head of 0.14 feet exists between the sand and limestone water bearing zones. However, if the two water-bearing zones are considered as one aquifer, then an average or effective transmissivity for both zones may be assumed. The Pliocene-Miocene aquifer receives approximately 8.5×10^4 gal/d/mi² recharge from the overlying surficial aquifer. Based on water levels and the hydraulic conductivity of the zones, approximately 6.2×10^4 gal/d/mi² leak from the Pliocene sand to the Miocene limestone.

The Pliocene-Miocene aquifer is a potential sink for discharge from the overlying surficial aquifer, under steady state conditions, confined, heterogeneous, and anisotropic. The equation governing the flow in the Pliocene-Miocene aquifer as modified for aquifer assumptions and boundary conditions from Freeze and Cherry (1979) is expressed as:

$$\frac{\partial}{\partial x} (T_x \frac{\partial h}{\partial x}) + \frac{\partial}{\partial y} (T_y \frac{\partial h}{\partial y}) + \frac{\partial}{\partial z} (T_z \frac{\partial h}{\partial z}) + \frac{(K'_a \Delta h)}{b} = 0 \quad (4)$$

where

h = water level [ft],

K'_a = vertical hydraulic conductivity of confining layer above the aquifer [ft/d],

b = thickness of aquifer [ft],

T = transmissivity [ft²/d].

As defined in the equation, the aquifer receives leakage from the overlying surficial aquifer. The schematic diagram (Figure 32) portrays the Pliocene-Miocene aquifer flow as described by equation (4).

Aquifer test

The 48-hour aquifer test was conducted December 9-11, 1989, at Site 3 on Cumberland Island. Well KBMP 7 was used as the pumping well; and KBMP 11 and KBMP 12 were used as observation wells (see Figure 33 for location of wells). In addition to these wells, KBMP 8, KBMP 9, and KBMP 10 were used as observation wells in the overlying and underlying zones to monitor leakage during the test. Figure 34 schematically shows the hydrogeology at the test site and well construction of the pumping and observation wells.

Prior to the aquifer test, a step-drawdown test was performed to determine the well efficiency and the optimum pumping rate for the aquifer test. Based on data analysis, the optimum pumping rate was 1.47 ft³/min (11 gal/min). The pumping rate used during the test was 1.54 ft³/min (11.5 gal/min). (See Appendix F for the step drawdown procedure and calculations of the well efficiency and optimum pumping rate.)

The aquifer test methods of analysis were selected based on the similarity between the theoretical assumptions of the methods and the real system flow. If the method chosen involved a type curve, the plot of the data matched the type curve shape fairly well. Often the flow in an aquifer involves parameters that are not assumed by the method, such as heterogeneities or boundaries. In these cases, the shape of the plotted data curve indicated the type of boundary present in the system, such as a recharge or impermeable boundary. By evaluating the hydrogeological system, the assumptions of the method, and the curve shape of the data, the direction of the boundary or heterogeneity (lateral or vertical) was determined.

The following section discusses the methods applied for aquifer test analysis. The Hantush-Jacob method and the Streltsova method evaluate for vertical heterogeneities and the Bixel-Van Poolen method evaluates for lateral discontinuities in the aquifer.

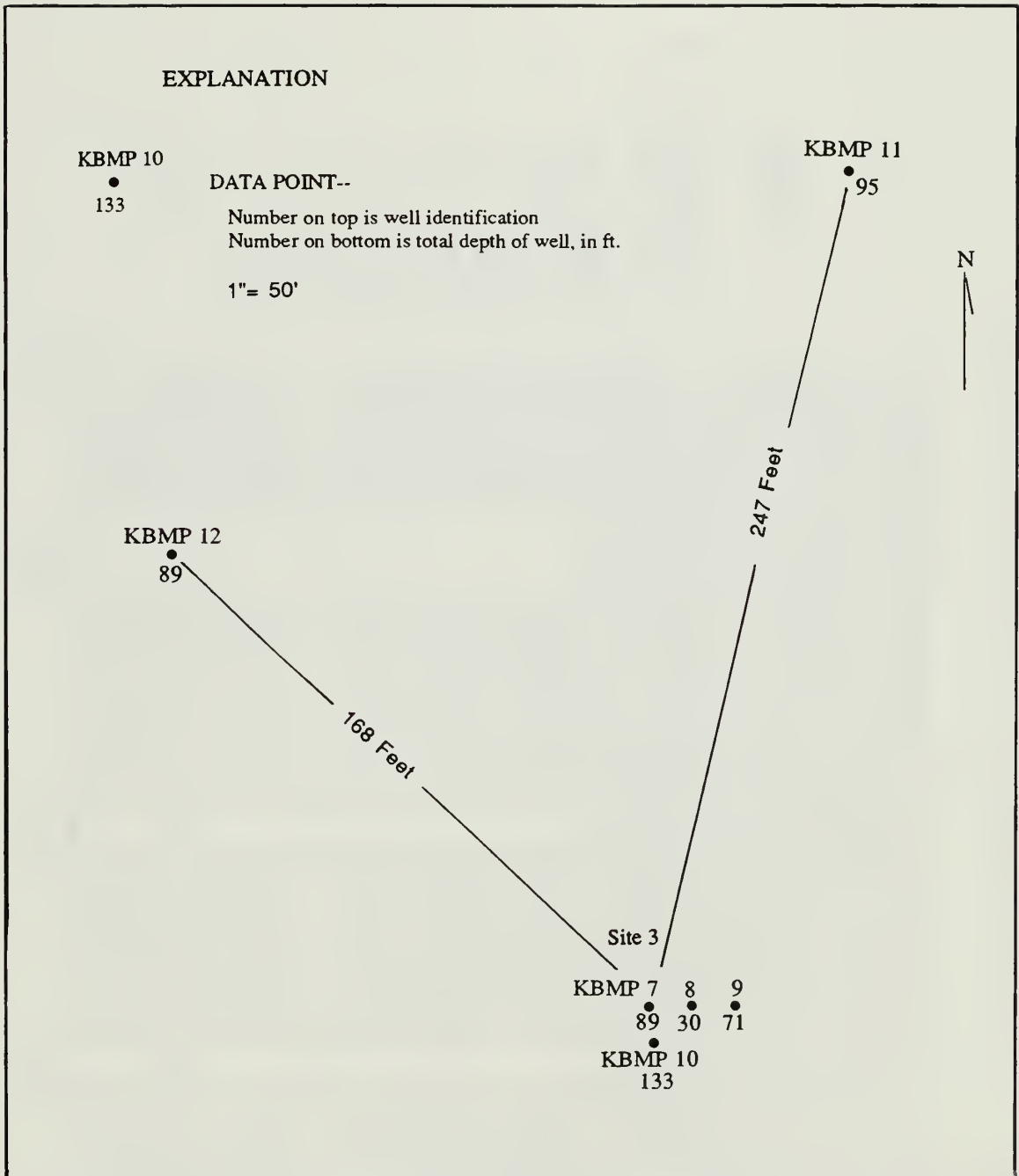


Figure 33. Location and depth of pumping and observation wells for aquifer test, site 3.

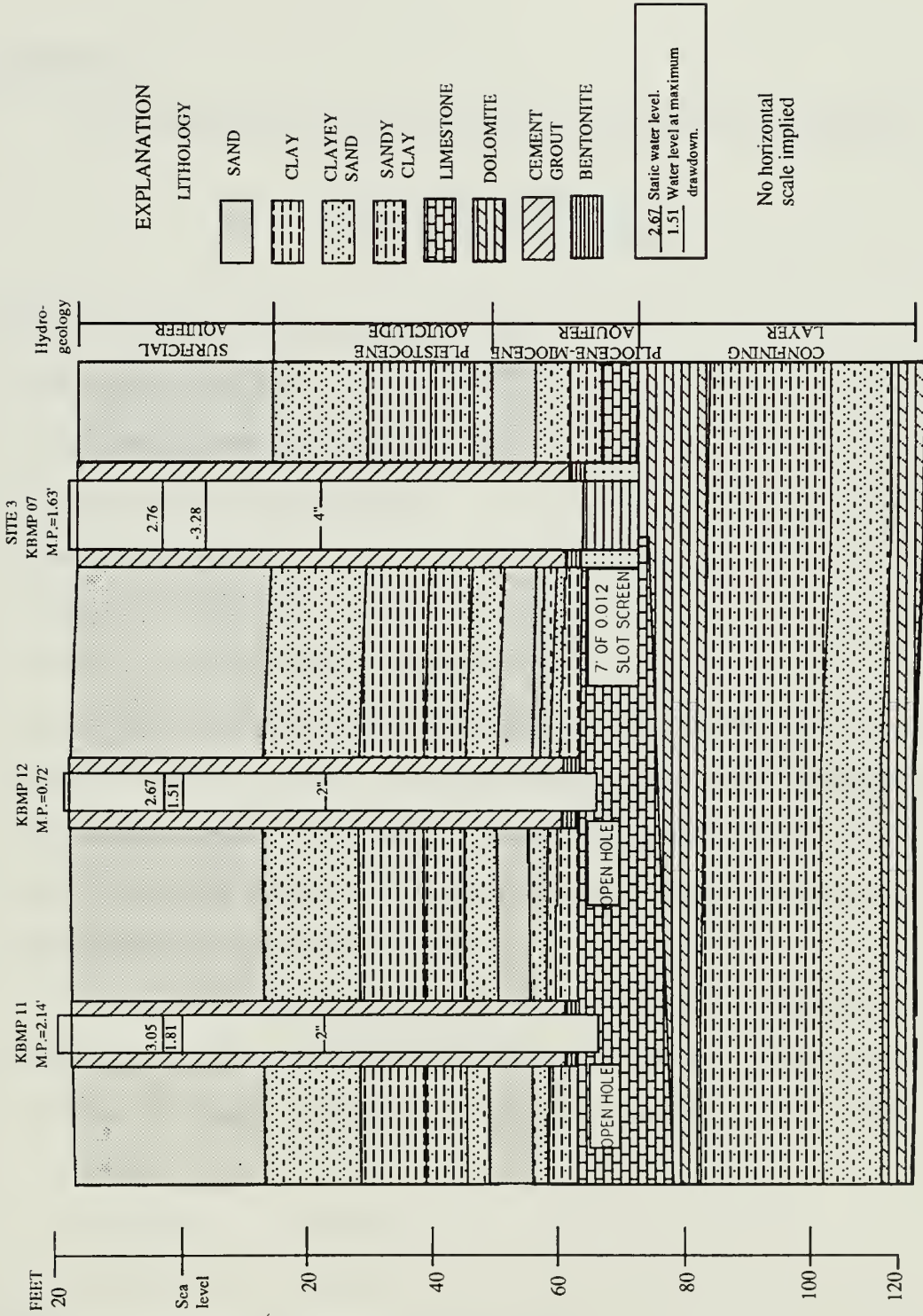


Figure 34. Schematic diagram of the hydrogeology and well construction at the aquifer test site.

Interpretation

Nonsteady radial flow in a confined aquifer is expressed mathematically as:

$$\frac{\partial^2 h}{\partial r^2} + \frac{1}{r} \frac{\partial h}{\partial r} = \frac{S}{T} \frac{\partial h}{\partial t} = \frac{1}{\eta} \frac{\partial h}{\partial t} \quad (5)$$

which is known as the diffusion equation, where

h = head in the aquifer [ft]

r = radial distance from the pumping well [ft]

S = storage coefficient [dimensionless]

T = transmissivity [ft²/d]

t = time [d]

η = diffusivity coefficient [ft²/d] (Lohman, 1972).

Appendix G provides derivation of the diffusion equation based on Darcy's law and the principle of continuity equation. The diffusion equation has a number of solutions based on the boundary conditions of the aquifer. The hydraulic properties of the Pliocene-Miocene aquifer were determined by methods which solve the diffusion equation by applying boundary conditions to the equation.

Theis (1935) applied the theory of heat flow to arrive at an analytical solution of the diffusion equation that involves initial assumptions and boundary conditions for the flow in the aquifer. The boundary conditions to be satisfied are as follows (Theis, 1935):

$h(r,t)$

$h(r,0) = h_0$ for $r \geq 0$

$h(\infty,t) = h_0$ for $t \geq 0$

The Theis equation is written in terms of drawdown:

$$s = \frac{Q}{4\pi T} \int_u^{\infty} \frac{e^{-u}}{u} du \quad (6)$$

where

Q = discharge rate [ft³/d]
and

$$u = \frac{r^2 S}{4 T t} \quad (7)$$

See Figure 35 for assumptions.

The exponential integral of equation (6) is known as the well function $W(u)$ for a nonleaky aquifer where:

$$W(u) = \int_u^{\infty} \frac{e^{-u}}{u} du \quad (8)$$

Values of $W(u)$ for values of u are provided in tables in Lohman (1972) and Freeze and Cherry (1979). By substituting $W(u)$ in equation (6) drawdown may be expressed as:

$$s = \frac{Q}{4 \pi T} W(u) \quad (9)$$

or

$$\log_{10} s = \left[\log_{10} \frac{Q}{4 \pi T} \right] + \log_{10} W(u) \quad (10)$$

and

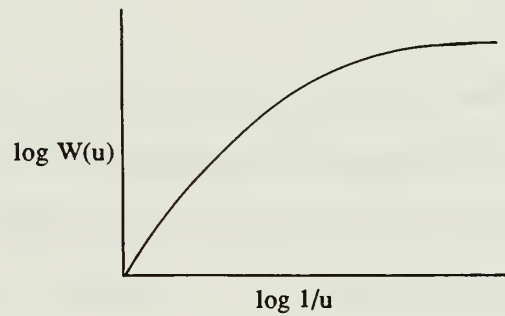
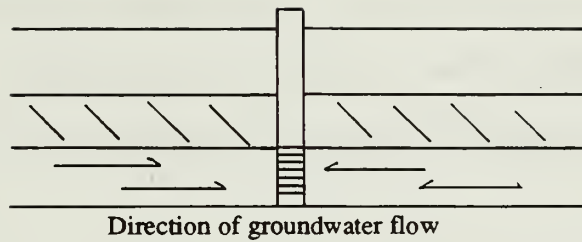
$$t = \frac{r^2 S}{4 T u} \quad (11)$$

or

$$\log_{10} t = \left[\log_{10} \frac{r^2 S}{4 T} \right] + \log_{10} 1/u \quad (12)$$

(Lohman, 1972).

The bracketed parts of equations (10) and (12) are constant if the discharge rate is constant during the aquifer test. If values of drawdown versus time are plotted on logarithmic paper and superimposed to the type curve ($W(u)$ versus $1/u$), a fit between the data curve and type curve are made. By selecting a common match point from the fit,



The governing equations are:

$$T = \frac{Q}{4\pi s} W(u) \quad S = \frac{4 T t u}{r^2}$$

The Theis assumptions are:

1. The aquifer is confined;
2. nonsteady flow occurs;
3. the aquifer is horizontal having an infinite aerial extent;
4. the pumped well fully penetrates the aquifer and is infinitesimal in diameter;
5. the aquifer is homogeneous and isotropic;
6. flow is horizontal; and
7. discharge is derived exclusively from aquifer storage.

Figure 35. The Theis governing equations and assumptions.

values of $W(u)$, $1/u$, s , and t are determined. Solution of equation (9) is possible for most instances where the storage capacity of the producing well is negligible and the distance to the observation well is equal to or greater than 200 times the pumping well radius (Streltsova, 1988).

Hantush-Jacob Method

The data curve from the aquifer test was not similar to the Theis type curve and a match could not be made. The assumptions of the Hantush-Jacob Leaky method (1955) match closely to the real system and the shape of the type curve matched the data curve (see Figure 36 for assumptions). Therefore, this analytical method was used to analyze the test data.

The Hantush-Jacob solution of the diffusion equation is as follows:

$$\frac{\partial^2 h}{\partial r^2} + \frac{1}{r} \frac{\partial h}{\partial r} - \frac{h}{T b'} K' = \frac{S}{T} \frac{\partial h}{\partial t} = \frac{1}{\eta} \frac{\partial h}{\partial t} \quad (13)$$

where

K' = vertical hydraulic conductivity of the confining layer [ft/d]

b' = confining layer thickness [ft] (Hantush and Jacob, 1955).

The governing boundary conditions are:

$h(r, t)$

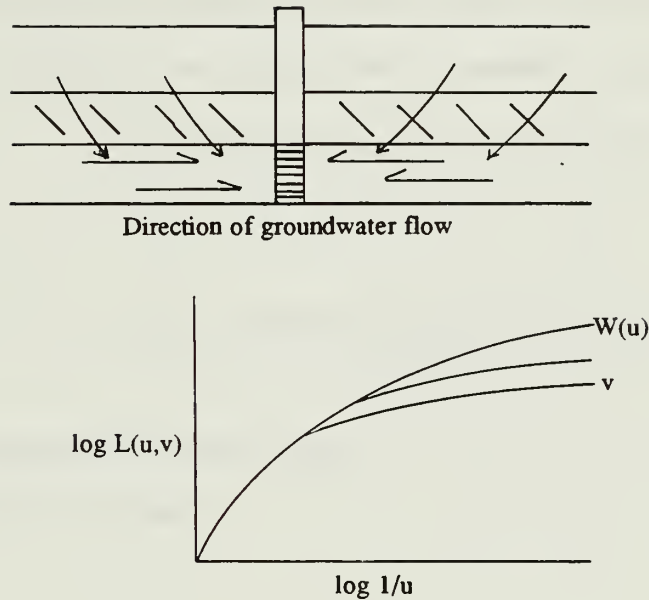
$h(r, 0) = h_0$ for $r \geq 0$

$h(\infty, t) = h_0$ for $t \geq 0$

$Q = 0$ for $t < 0$

Q is constant at values > 0 for $t \geq 0$.

$\lim_{r \rightarrow 0} r \frac{\partial h}{\partial r} = -\frac{Q}{2\pi T}$ for $t > 0$



The governing equations are:

$$T = \frac{Q}{4\pi s} L(u,v) \quad S = \frac{4 T t u}{r^2} \quad K' = 4T \frac{v^2}{r^2} \frac{b'}{b}$$

The Hantush-Jacob leaky assumptions are:

1. The aquifer is a leaky confined aquifer;
2. the aquifer is overlain or underlain by a leaky confining bed having uniform hydraulic conductivity and thickness;
3. the pumping well maintains a constant discharge;
4. the aquifer is horizontal having infinite aerial extent;
5. flow in the confined aquifer is two dimensional and radial in the horizontal plane; flow from the confining bed is vertical;
6. water is not released from storage in the confining bed during pumping; and
7. the pumping well has an infinitesimal diameter and fully penetrates the aquifer
8. water level in the overlying permeable zone remains constant (Bedinger and Reed, 1988).

Figure 36. The Hantush-Jacob Leaky governing equations and assumptions.

The Hantush-Jacob solution of the diffusion equation is similar to the Theis solution, but the second part of the equation is more complicated. The equation is expressed as:

$$s = \frac{Q}{4\pi T} \left[2K_0(2v) - \int_{\frac{v^2}{u}}^{\infty} \frac{1}{y} \exp\left(\frac{-y-v^2}{y}\right) dy \right] \quad (14)$$

where

$$L(u,v) = \left[2K_0(2v) - \int_{\frac{v^2}{u}}^{\infty} \frac{1}{y} \exp\left(\frac{-y-v^2}{y}\right) dy \right] \quad (15)$$

$L(u,v)$ = well function for a leaky aquifer

y = the variable of integration

$$u = r^2 S / 4 T t$$

$$v = \frac{r}{2} \sqrt{\frac{K'}{b' T}}$$

If the right side of equation (14) is represented as the leakance function of u and v , $L(u,v)$, the equation may be written as:

$$s = \frac{Q}{4 \pi T} L(u,v) \quad (16)$$

and

$$\frac{K'}{b'} = 4 T \frac{v^2}{r^2} \quad (17)$$

(Hantush and Jacob, 1955).

Again, values of drawdown versus time are plotted on logarithmic paper and superimposed to the type curve ($L(u,v)$ versus $1/u$), and a fit between the data curve and type curve is made. By selecting a common match point from the fit, values of $L(u,v)$, $1/u$, s , and t are determined.

After about 100 minutes from the starting time of drawdown and recovery, tidal fluctuations had a greater impact on the water levels in each well than the magnitude of pumping or recharge. The data were corrected for the influencing tidal and barometric

pressure fluctuations before they were matched to the theoretical curves. (See Appendix I for well tidal efficiency and the method applied to correct for tidal fluctuations)

Drawdown and recovery data from wells KBMP 11 and KBMP 12 provided a good fit with the Hantush-Jacob theoretical curve (see Figures 37 to 40). The transmissivity values calculated by the Hantush-Jacob method ranged from 235 to 504 ft²/d (Table 4). (Aquifer test calculations and data tables are provided in Appendix H.) The storage coefficient may be solved for by rearranging equation (7). The storage coefficient values ranged from 1.4×10^{-5} to 5.6×10^{-5} . Once the transmissivity and storage coefficient are known the diffusivity may be calculated by:

$$\eta = \frac{T}{S} \quad (18)$$

η = diffusivity of the aquifer [ft²/d]

(Freeze and Cherry, 1979). The diffusivity values ranged from 4.5×10^6 to 3.5×10^7 ft²/d (see Table 4).

The delayed drawdown and recovery response in KBMP 12 for the first 3 minutes after pumping began may be due to poor lateral fracture interconnection or facies changes between KBMP 12 and the pumping well. In addition to delayed drawdown and recovery, the total drawdown in well KBMP 12 was less than in well KBMP 11 which is located further from the producing well. This indicates that less interconnected fractures exist between KBMP 12 and the pumping well.

The Hantush-Jacob method was designed for hydraulic analysis of leaky aquifers. The calculated storage values indicate that the aquifer is well confined, and no leakage was observed from the overlying and underlying zone during the test. The aquifer responds as if it were a leaky aquifer because it is composed of two lithologic zones with the overlying zone having a much greater transmissivity than the underlying zone. As water is

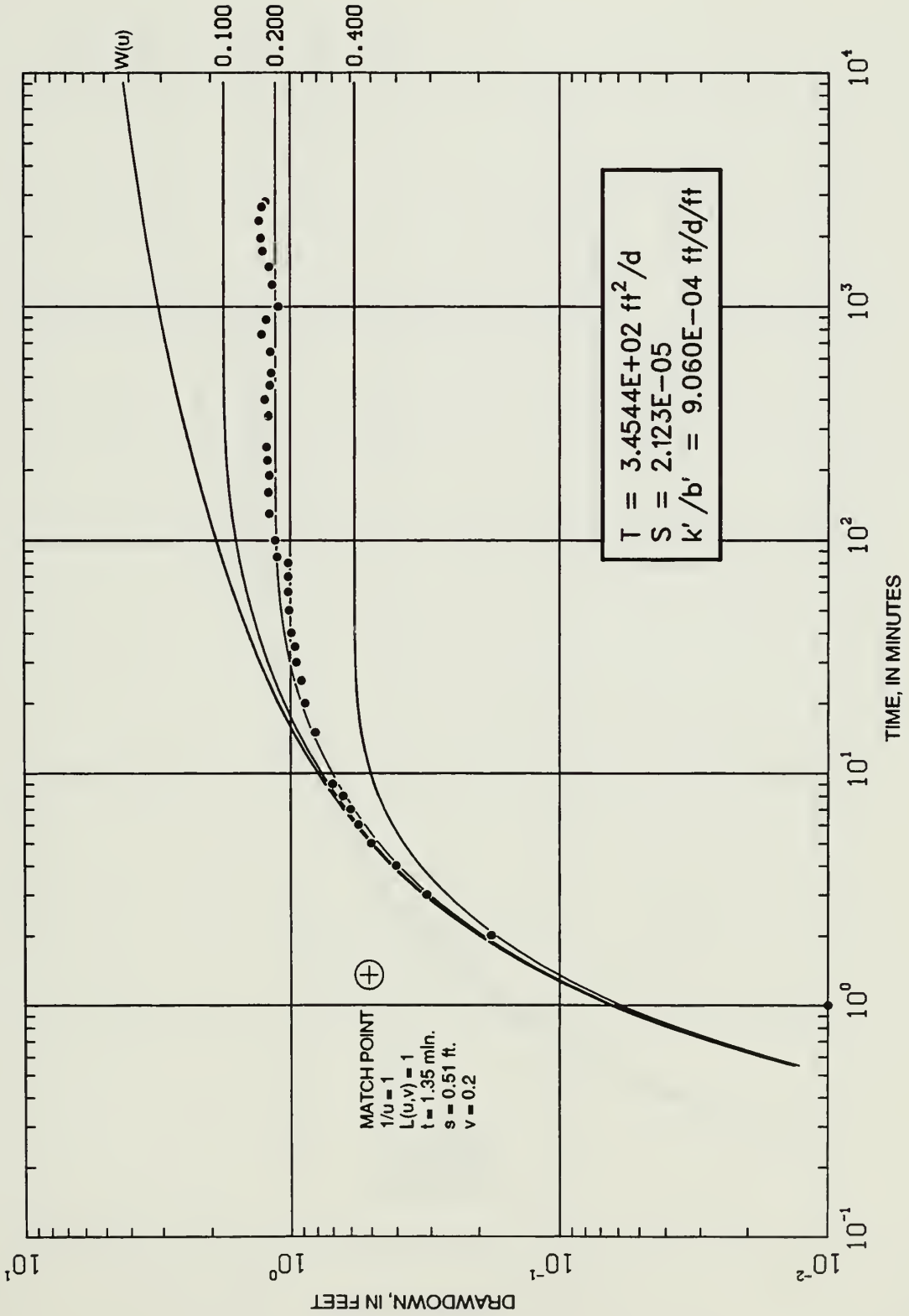


Figure 37. Comparison of well KBMP 11 drawdown data to the Hantush-Jacob leaky curve.

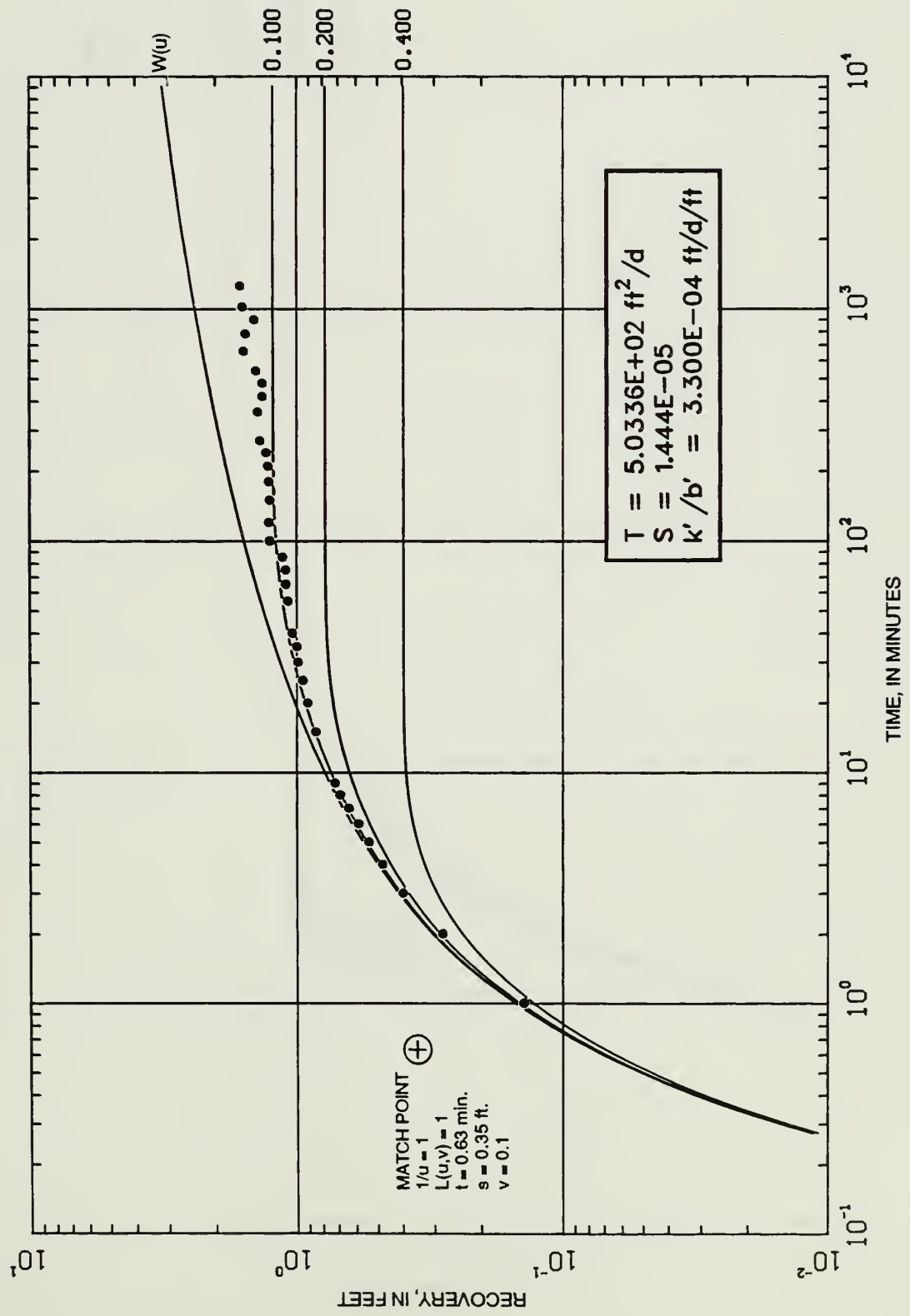


Figure 38. Comparison of well KBMP 11 recovery data to the Hantush-Jacob leaky curve.

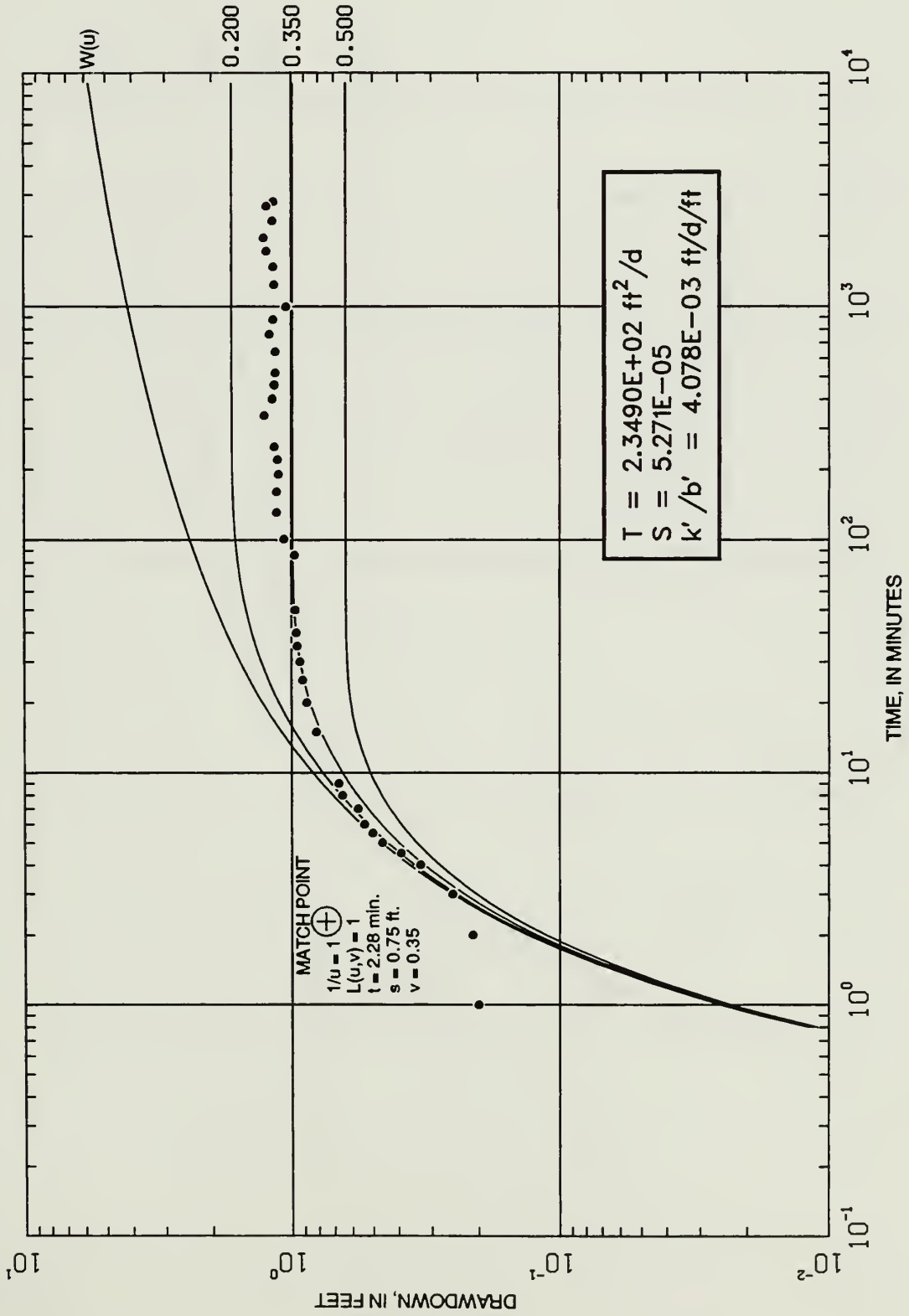


Figure 39. Comparison of well KBMP 12 drawdown data to the Hantush-Jacob leaky curve.

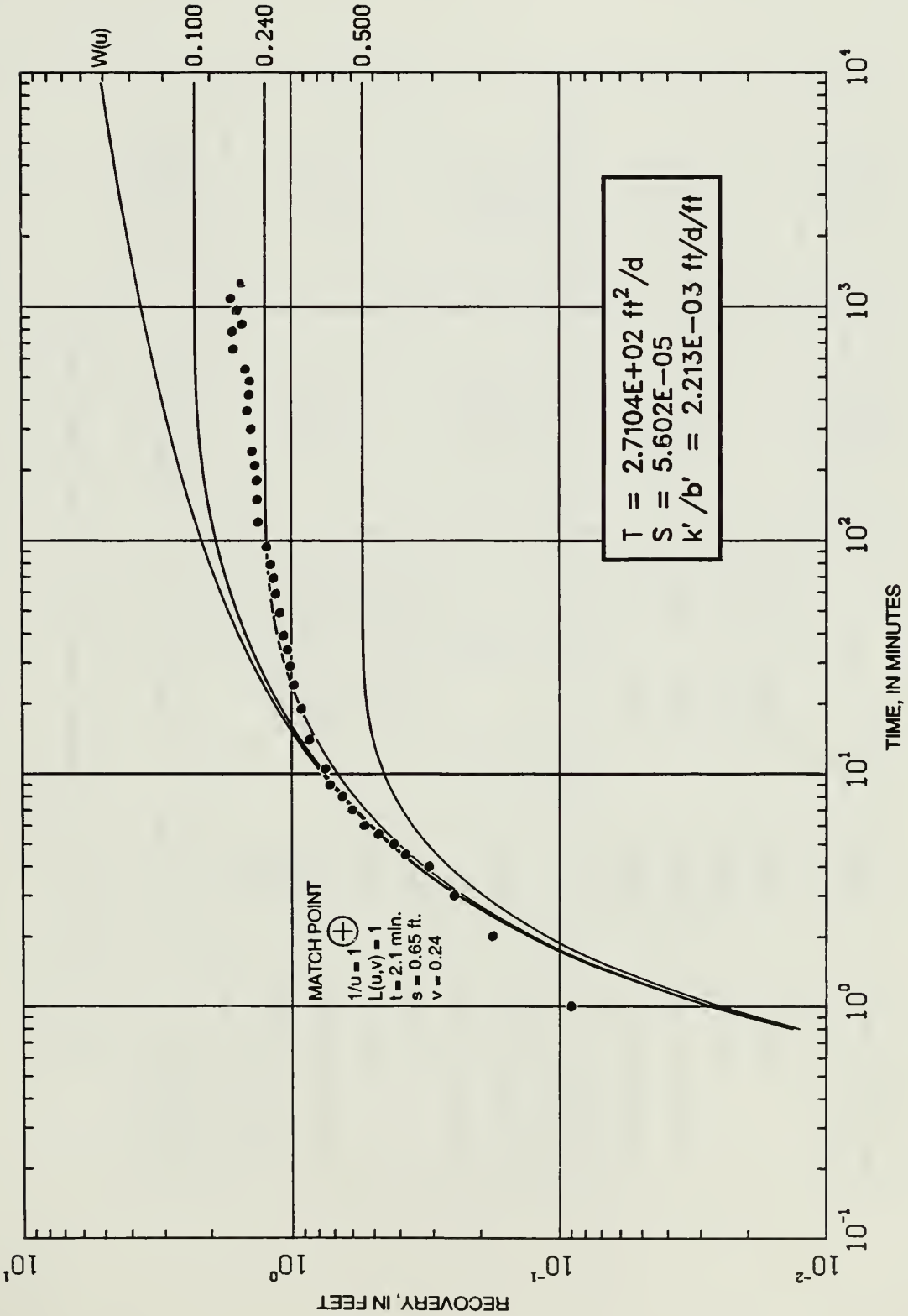


Figure 40. Comparison of well KBMP 12 recovery data to the Hantush-Jacob leaky curve.

Table 4. Transmissivity and storage values of the Pliocene-Miocene aquifer

Method of analysis	Well number	Transmissivity (ft ² /d)	Storage coefficient	Diffusivity (ft ² /d)
DRAWDOWN				
Bixel-Van Poolen	KBMP 7	644		
Bixel-Van Poolen	KBMP 11	507 (T ₁) 1951 (T ₂)	1.6 x 10 ⁻⁵	2.17 x 10 ⁴
Bixel-Van Poolen	KBMP 12	436 (T ₁) 2021 (T ₂)	4.2 x 10 ⁻⁵	7.18 X 10 ³
Strelsova	KBMP 11	507 (T ₁) 722 (T ₂)		
Strelsova	KBMP 12	436 (T ₁) 792 (T ₂)		
Hantush-Jacob Leaky	KBMP 11	346	2.1 x 10 ⁻⁵	1.6 x 10 ⁷
Hantush-Jacob Leaky	KBMP 12	235	5.27 x 10 ⁻⁵	4.5 x 10 ⁶
RECOVERY				
Bixel-Van Poolen	KBMP 7	654		
Bixel-Van Poolen	KBMP 11	653 (T ₁) 1477 (T ₂)	1.05 x 10 ⁻⁵	4.31 x 10 ⁴
Bixel-Van Poolen	KBMP 12	380 (T ₁) 1425 (T ₂)	4.4 x 10 ⁻⁵	5.98 x 10 ³
Strelsova	KBMP 11	653 (T ₁) 412 (T ₂)		
Strelsova	KBMP 12	380 (T ₁) 522 (T ₂)		
Hantush-Jacob Leaky	KBMP 11	504	1.44 x 10 ⁻⁵	3.5 x 10 ⁷
Hantush-Jacob Leaky	KBMP 12	271	5.6 x 10 ⁻⁵	4.8 x 10 ⁶

discharged from the underlying limestone unit, the overlying sand provides recharge to the limestone. This is reflected in the plotted data as the curve flattens late in the test.

Straight line method

Streltsova Method

Streltsova (1988) presented a method that numerically solves for the transmissivity in a stratified aquifer during transient groundwater flow. The model evaluates for the effect that a permeable layer separated by an impervious zone has on the underlying producing zone. (Figure 41 illustrates the direction of groundwater flow in a stratified aquifer during discharge.) Change in drawdown with time for a well producing at a constant rate from a stratified aquifer results in multiple slopes on a semilog graph. Early drawdown data on a semilog graph plots a straight line slope that represents the transmissivity of the producing layer. The transmissivity of this zone is calculated by:

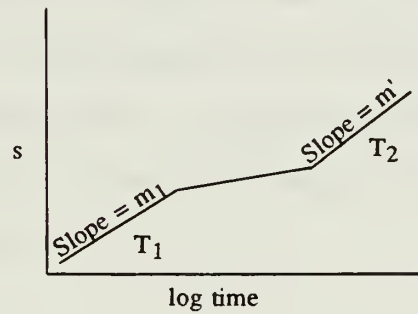
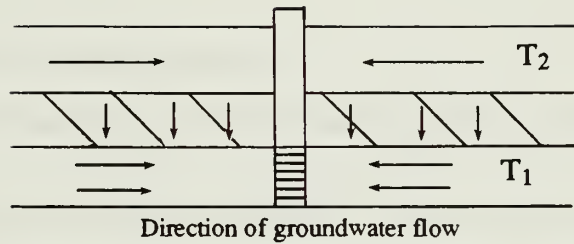
$$T_1 = \frac{2.3 Q}{4 \pi m_1} \quad (19)$$

where

T_1 = transmissivity of the producing zone [ft²/d]

m_1 = slope of the initial segment [ft/min] (see Figure 41 for assumptions).

When the semipervious layer begins to influence system flow, the curve grades into a transitional slope, the shape and duration of which depend on the storage ratio of the two regions (S'/S where S' is the storage of the overlying permeable zone). When the second permeable layer begins to contribute to the groundwater flow, the slope of the final curve (m') is dependent upon the transmissivity of both permeable layers (T_1 and T_2). The final segment slope is related to the initial slope by the relationship:



The governing equations are:

$$T_1 = \frac{2.3 Q}{4\pi m} \quad T_2 = \frac{T_1 (m_1 - m')}{m'}$$

The Streltsova assumptions are:

1. stratified aquifer
2. vertical flow in the semipervious layer
3. horizontal flow in the highly transmissive layers

Each layer is:

4. homogeneous, isotropic
5. compressible
6. of infinite radial extent

Figure 41. Streltsova (1988) governing equations and assumptions.

$$m' = \frac{m_1 T_1}{T_1 + T_2} \quad (20)$$

where

m' = slope value of the final segment [ft/min]

T_2 = transmissivity of the permeable zone overlying the producing zone [ft²/d].

The transmissivity of each layer is provided in Table 4. As the data indicate, the transmissivity is usually one and one-half times greater when the overlying sand zone contributes to the groundwater flow. The transmissivity values calculated by the Streltsova straight line method range from 380 to 792 ft²/d. A transition curve does not exist in the test data (Figures 42 through 45). This indicates that the storage of the producing and overlying permeable zones are similar.

Bixel-Van Poolen

The change in drawdown with time for a well producing at a constant rate from a formation with radial discontinuity is represented by multiple slopes on a semilog plot. A numerical evaluation of transient drawdown for a well centered in an aquifer with radial discontinuities was made by Bixel and Van Poolen (1967). See Figure 46 for assumptions and schematic diagram of an aquifer with radial discontinuities. Early drawdown data on a semilog graph plots a straight line of a slope that represents the transmissivity of the aquifer region from the producing well to the radial discontinuity. The transmissivity of this region in the aquifer is calculated by equation (19). When the region outside the discontinuity begins to influence the drawdown, the straight line grades into a transitional curve, the shape and duration of which depend on the storage ratio of the two regions. Finally, when the groundwater is produced from the region outside the discontinuity, the drawdown

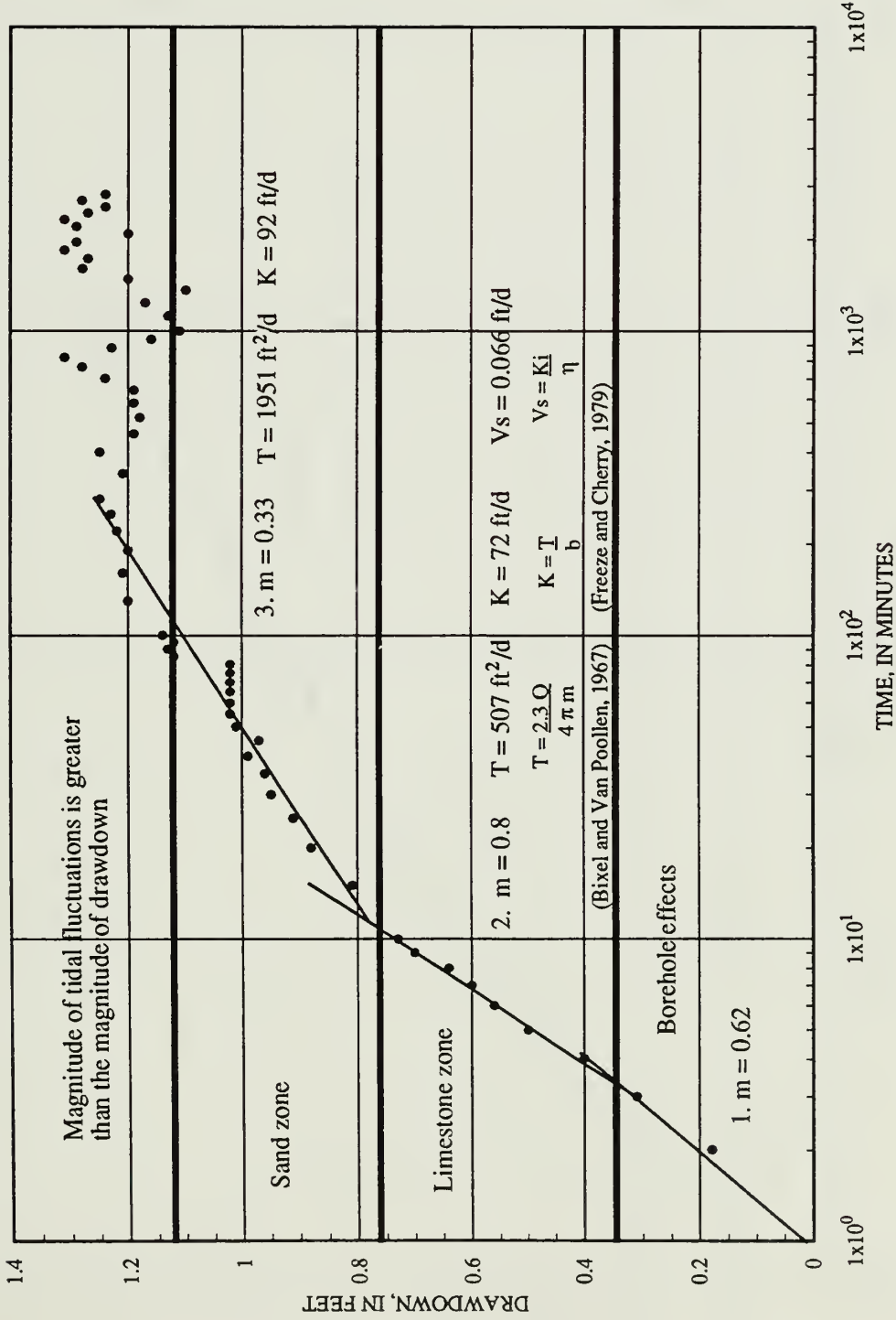


Figure 42. KBMP 11 drawdown. Transmissivity solved for by the straight line method.

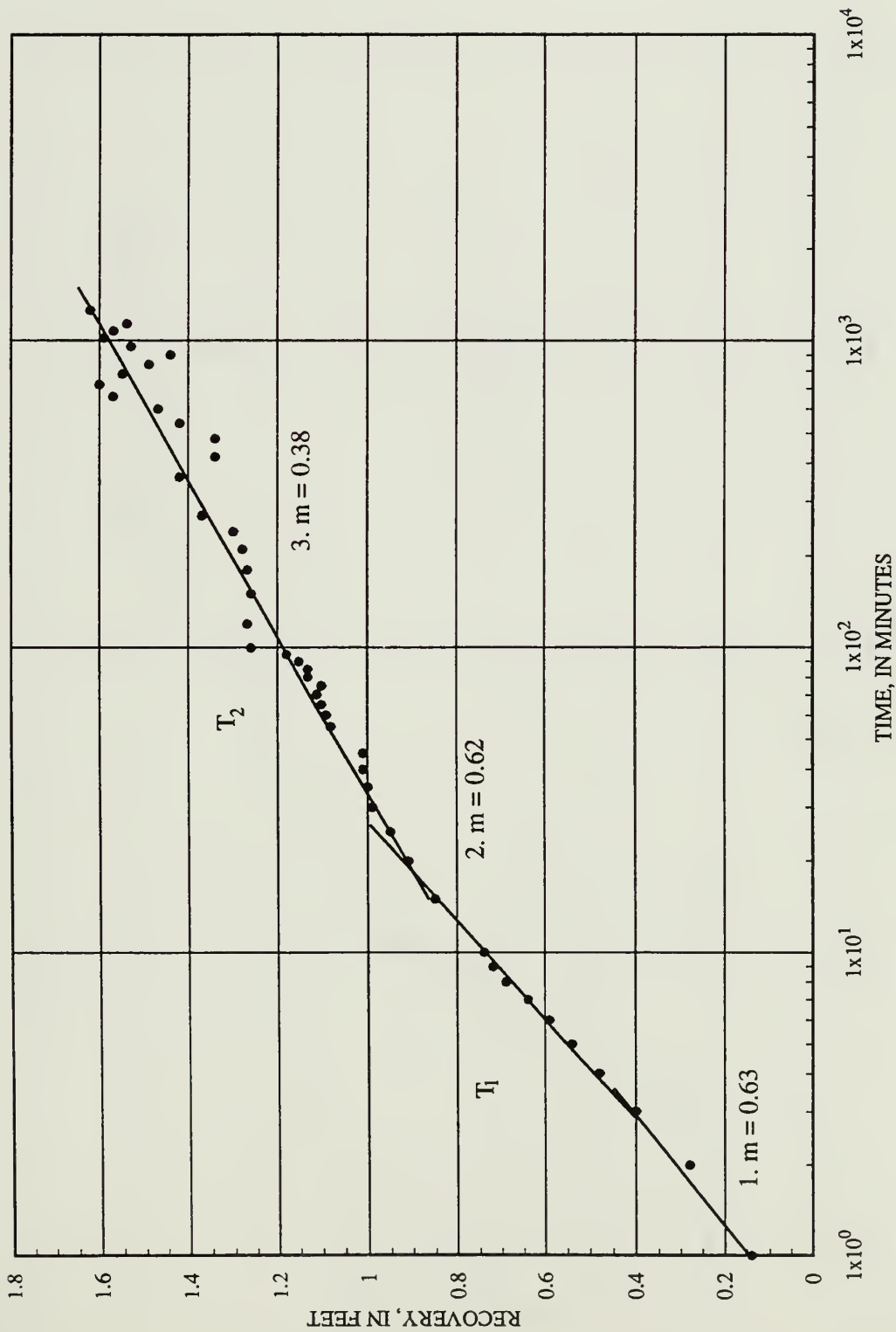


Figure 43. KBMP 11 recovery data. Transmissivity solved for by the straight line method.

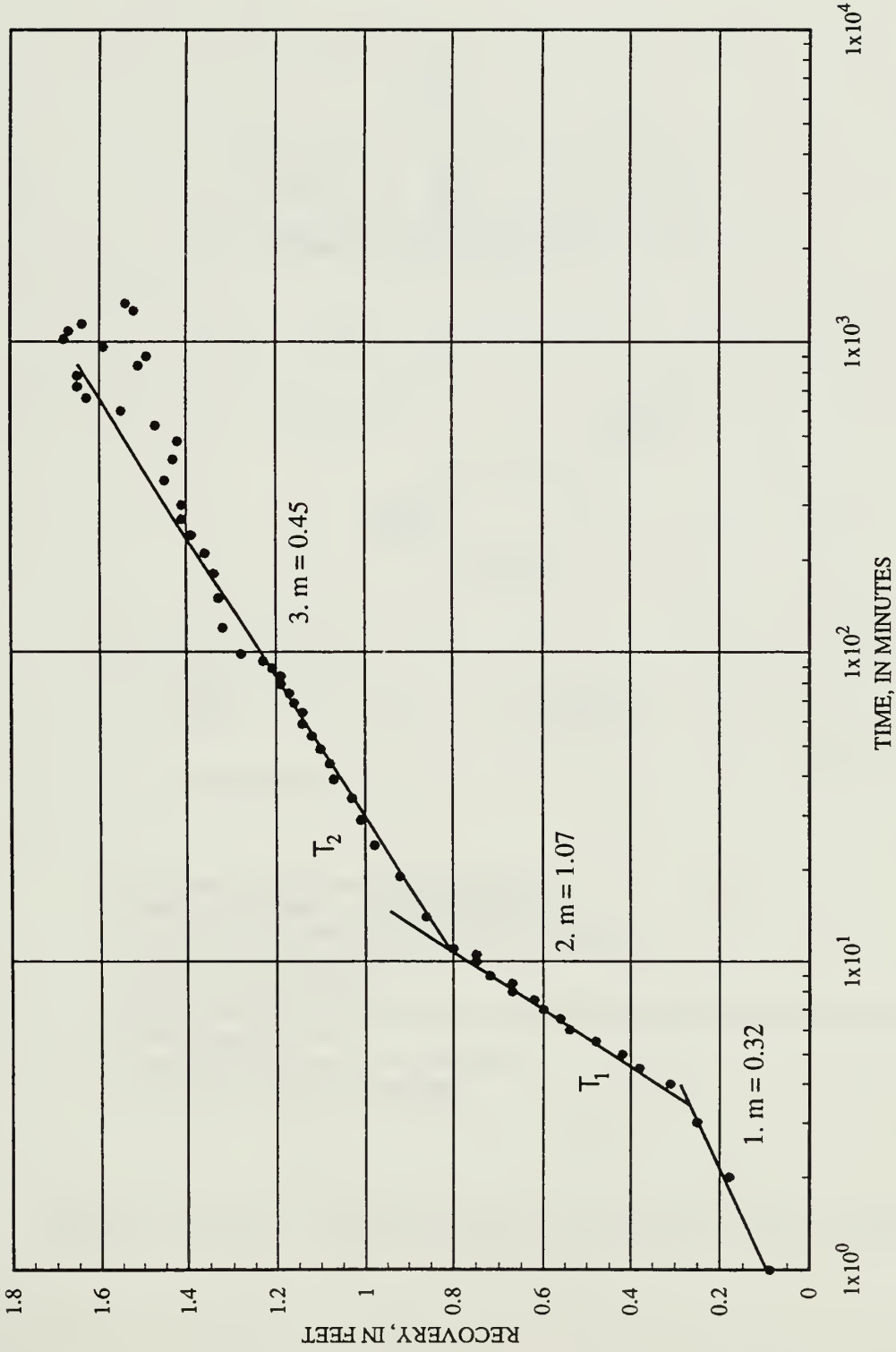
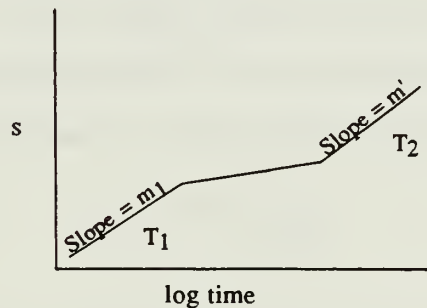
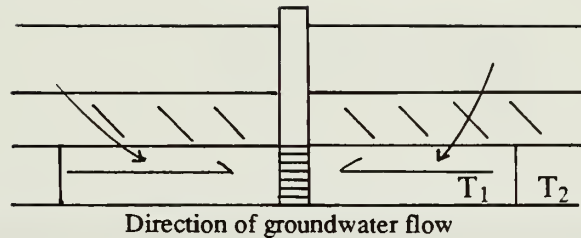


Figure 45. KBMP 12 recovery data. Transmissivity solved for by the straight line method.



The governing equations are:

$$T_1 = \frac{2.3 Q}{4\pi m_1} \quad S = \frac{T}{\eta} \quad \eta = \frac{r^2}{2.246 (t_0)}$$

$$T_2 = \frac{T_1 (2m_1 - m')}{m'}$$

The Bixel and Van Poolen assumptions are:

1. Fluids in the aquifer are slightly compressible;
 2. permeability and porosity are independent of pressure;
 3. homogeneous, isotropic medium;
 4. constant aquifer thickness;
- These parameters are constant but may be different on opposite sides of the discontinuity
5. constant pumping rate;
 6. continuous flow across the discontinuity;
 7. the aquifer is of infinite areal extent.

Figure 46. Bixel and Van Poolen (1967) governing equations and assumptions.

curve exhibits a final straight line (m'). The final slope that represents the outside region, m' , is related to the initial slope, m_1 , by the relationship of:

$$m' = m_1 \left\langle \frac{n}{1 + (n-1) \frac{T_2}{T_1}} \right\rangle \quad (21)$$

where

T_2 = transmissivity of the aquifer outside the radial discontinuity [ft²/d].

$(n-1)$ is the number of image wells. An image well is equivalent to a fictitious recharge or discharge straight line boundary (Bear, 1979). If a linear recharge boundary is assumed, then $(n-1) = 1$ or $n = 2$. Substituting $(n = 2)$ into equation (21) results in:

$$m' = m_1 \left\langle \frac{2}{1 + \frac{T_2}{T_1}} \right\rangle \quad (22)$$

The transmissivity values calculated by the Bixel-Van Poolen straight line method range from 380 to 2,021 ft²/d (Table 5). Once the transmissivity and diffusivity of the aquifer are known, the storage coefficient may be determined by rearranging equation (7). The diffusivity of the aquifer may be calculated by an equation derived by Streltsova (1988) that is expressed as:

$$\eta = \frac{r^2}{2.246 (t_0)} \quad (23)$$

where

t_0 = intercept of straight line at zero drawdown [min.]. The diffusivity values calculated by equation (23) range from 5.98×10^3 to 4.31×10^4 ft²/d. The storage values range from 1.1×10^{-5} to 4.4×10^{-5} . Based on aquifer testing, the hydraulic conductivity for the Miocene limestone ranges from 34 to 101 ft/d. The hydraulic conductivity of the Pliocene sand is 100 ft/d based on the method of deriving this value from grain size analysis as described by Masch and Denny (1966).

Table 5. Transmissivity, hydraulic conductivity, and seepage velocity values of the limestone and sand zones of the Pliocene-Miocene aquifer calculated by the Bixel-Van Poolen straight line method.

	Limestone transmissivity (ft ² /d)	Limestone hydraulic conductivity (ft/d)	Seepage velocity (ft/d)	Sand transmissivity (ft ² /d)	Sand hydraulic conductivity (ft/d)
KBMP 11 drawdown	507	72	0.066	1951.2	91.5
KBMP 11 recovery	653	93	0.085	1477.8	73.9
KBMP 12 drawdown	436	62.3	0.057	2021	101.1
KBMP 12 recovery	380	54.2	0.049	1425	71.5

Transmissivity values calculated for well KBMP 7 were slightly higher than those values obtained from the observation wells (see Figures 47 and 48). These values were calculated from equation (19). Data recorded after 100 minutes were not included in the straight-line fit because the water level began to fluctuate with changing tides. The first 4 minutes of drawdown were also excluded in the analysis because of the casing storage effect.

Discussion

The transmissivity of an aquifer is directly related to the hydraulic conductivity and the saturated thickness of the aquifer medium; the thicker the saturated zone and more interconnected the pore spaces, the greater the transmissivity of the aquifer. The storage coefficient of an aquifer is directly related to the porosity of the medium, and the compressibility of the rock matrix and fluid. The greater these values, the greater the storage coefficient.

For a homogeneous, isotropic aquifer, aquifer test data should plot a straight line on a semilog graph. Breaks in the straight line graph reflect vertical heterogeneities or lateral discontinuities in the aquifer medium. A three segment curve, excluding early borehole effects, indicates variations of transmissivity and storage values in the aquifer (see Figure 49). The first segment represents the transmissivity inside the discontinuity in an aquifer with lateral discontinuities. In a stratified aquifer, this segment represents the transmissivity of the producing zone. The second segment represents the transition of transmissivity in the medium from the region inside the discontinuity to the region outside the discontinuity, or in a stratified aquifer, the transition from the producing zone to the overlying permeable zone. The shape and duration of the second segment depends on the storage ratio between the two regions. If $S_1 = S_2 = S$ then a transient curve will not exist on a semilog plot. The third segment represents the transmissivity of the region outside the

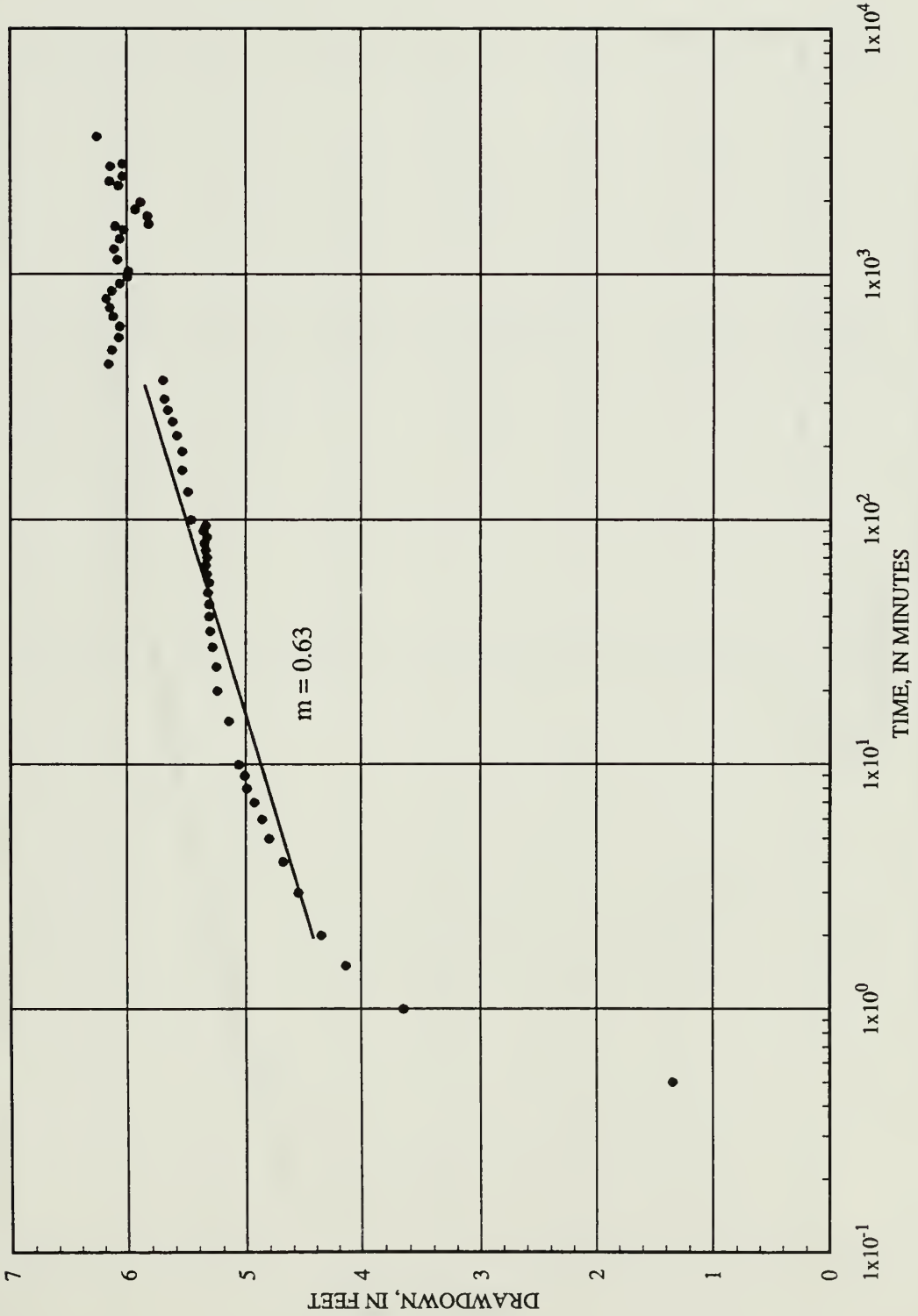


Figure 47. KBMP 7 drawdown. Transmissivity solved for by the straight line method.

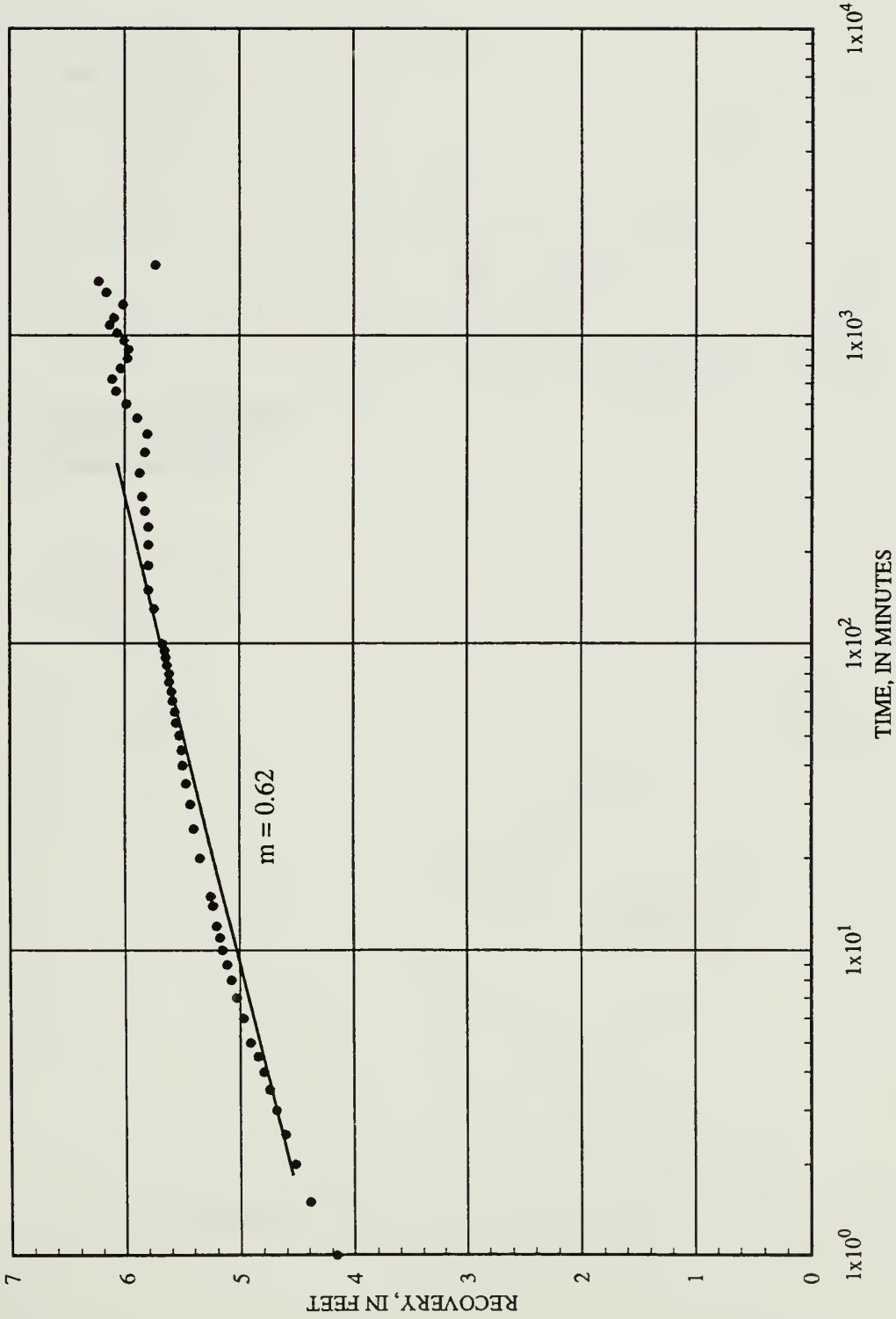
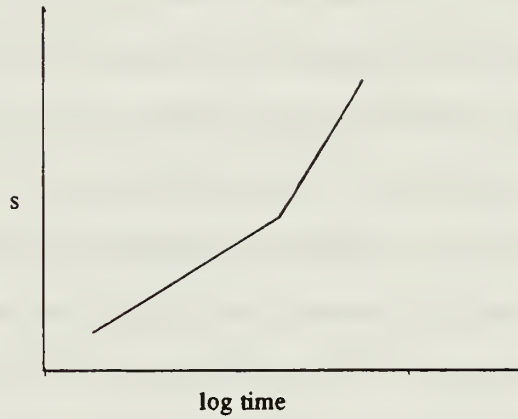
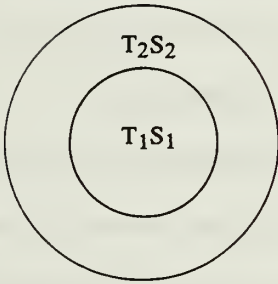


Figure 48. KBMP 7 recovery data. Transmissivity solved for by the straight line method.

If $S_1 = S_2$
and $T_1 \neq 10 \times T_2$



T = transmissivity [ft^2/d]
 S = storage coefficient
 s = drawdown [ft]

If $S_1 \neq 10 \times S_2$
and $T_1 \neq 10 \times T_2$

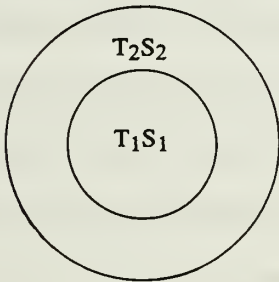


Figure 49. Configuration of aquifer test plots with varying transmissivity and storage values.

lateral or vertical discontinuity. In a stratified aquifer, the third segment represents the transmissivity of a combination of the overlying permeable zone and the producing zone. In a stratified aquifer, a three segment curve indicates that the transmissivity and storage of the producing zone and the overlying permeable zone are not equal (Streltsova, 1988).

A single break in the straight line or a two segment curve on a semilog plot, excluding early borehole effects, indicates that the aquifer permeability and/or thickness vary across the discontinuity. The transmissivity inside the discontinuity (T_1) and the transmissivity outside the discontinuity (T_2) are not equal (Figure 49). It may be assumed that the storage value is uniform in the aquifer because a transition curve does not exist (the storage ratio equals one).

Aquifer test data from the Pliocene-Miocene aquifer yields a 3 segment curve on a semilog graph (see Figures 42 to 45). The first slope represents borehole and near borehole effects. The second segment represents the transmissivity of the limestone part of the aquifer, and the third slope represents contribution from the sand unit of the aquifer and/or a lateral recharge boundary. A transition curve is not present which indicates that the storage coefficient is uniform in the aquifer. Based on analysis of the Streltsova and Bixel-Van Poolen methods, this curve shape indicates differences of transmissivity between the sand and limestone zones of the aquifer and across the lateral discontinuity.

The first segment of early time data represents near well bore conditions that includes factors such as well bore storage, skin effect, formation damage, and near well bore formation transmissivity. The length of time for the well storage effect to subside was about 4.3 minutes after initial pumping time (see Appendix F for calculations).

The second segment represents the transmissivity of the limestone part of the aquifer or the producing zone inside the lateral discontinuity. This is assumed because the limestone has a much lower transmissivity than the overlying sand and should therefore

have a greater slope value than a slope represented by the combination of the two water-bearing zones and the zone outside the lateral discontinuity. The transmissivity of this zone was calculated from equation (19). See Table 4 for values calculated by each straight line method.

The third segment represents vertical groundwater contribution from the overlying sand zone and/or a lateral recharge boundary. The recharge effects are represented by the low slope value of the third segment. The third segment indicates that the magnitude of recharge is greater than the magnitude of drawdown and represents contribution from both water-bearing zones. The transmissivity values calculated for the third slope were 2 to 4 times greater than the transmissivity calculated from the slope of the second segment. (See Table 5 for transmissivity values.)

Vertical heterogeneities and lateral discontinuities are present in the Pliocene-Miocene aquifer as observed in the aquifer test data. As a result of these heterogeneities, the values of transmissivity vary vertically and laterally. Vertical heterogeneity in the aquifer medium is due to the overlying Pliocene sand having a much greater transmissivity value than the Miocene limestone. As the overlying sand zone contributes to the aquifer flow, the transmissivity values increase one and one-half times (see Table 4). The lateral discontinuity could be the result of thickness or facies changes in the aquifer or possibly recharge from the ocean.

The Streltsova (1988) model solves for the transmissivity of each permeable zone of a vertical section in the stratified aquifer. Application of this method provided the transmissivity values of the limestone (T_1) and the combination of the limestone and sand units (T_2) of the Pliocene-Miocene aquifer. Values indicate that the combination of the two zones exhibits a higher transmissivity value than the limestone zone alone.

The Bixel-Van Poolen model solves for transmissivity in an aquifer having radial discontinuities. Application of this method with the assumption of one lateral recharge boundary provided the transmissivity of the zone inside the discontinuity (T_1) and the zone outside the discontinuity (T_2). Values indicated that the formation outside the discontinuity had a greater transmissivity than the formation inside the discontinuity. Sufficient data was not available to determine the lateral source of recharge in the aquifer.

The transmissivity calculated by the straight line methods ranged from 380 to 653 ft^2/d for the T_1 values. The T_1 values are considered the valid values for the aquifer because the pumping well penetrated only the limestone unit of the aquifer. Transmissivity values calculated for the Pliocene-Miocene aquifer in Kingsland, Georgia, 15 miles west of the study area, were 750 ft^2/d based on aquifer tests (Brown, 1984).

Potential for Seawater Encroachment due to Channel Dredging

An evaluation of the volume of seawater infiltration was conducted along the Cumberland Sound Channel because the confining unit overlying the Pliocene-Miocene aquifer is breached in some areas below the channel. For this discussion, it is assumed that the confining layer overlying the Pliocene-Miocene age aquifer was completely removed in the channel, and the aquifer is in direct contact with the channel bed. Following Darcy's Law (Freeze and Cherry, 1979), specific discharge is expressed as:

$$q = -K \frac{\Delta h}{\Delta L} \quad (24)$$

where

q = specific discharge [ft/hr]

K = hydraulic conductivity [ft/hr]

h = water level [ft]

L = distance [ft].

The difference in hydraulic head of the channel and the Pliocene-Miocene aquifer fluctuates with time as a result of the fluctuation of the tides (Figure 31). Therefore the equation is time dependent and can be expressed as a function of time:

$$q(t) = -K \frac{\Delta h}{\Delta L}(t) \quad (25)$$

where

t = time [hr]

The change in head difference with respect to time can be approximated by a series of straight lines as shown in Figure 50. The change in head may be expressed as:

$$\frac{dh}{dt} = m \quad (26)$$

The first slope may be expressed by the integral:

$$\int_{b_0}^h dh = \int_0^t m dt \quad (27)$$

By integrating over a 24-hour period the equation is expressed:

$$\Delta h_i = m_i t + b_i \quad (28)$$

$i = 1, 5$

m = slope of the line [ft/hr]

b = y-intercept [ft]

i = number of slope intervals

During a 24-hr period in July 1989, the head in the aquifer was higher than channel stage during two low-tide cycles and one high-tide cycle (Figure 50). However, water levels within the channel were greater than the aquifer during alternating high tides. Therefore, during 83 percent of the day (20 hrs) the potential for groundwater flow was toward the channel, and during 17 percent of the day (4 hrs), the potential for flow was from the channel into the aquifer.

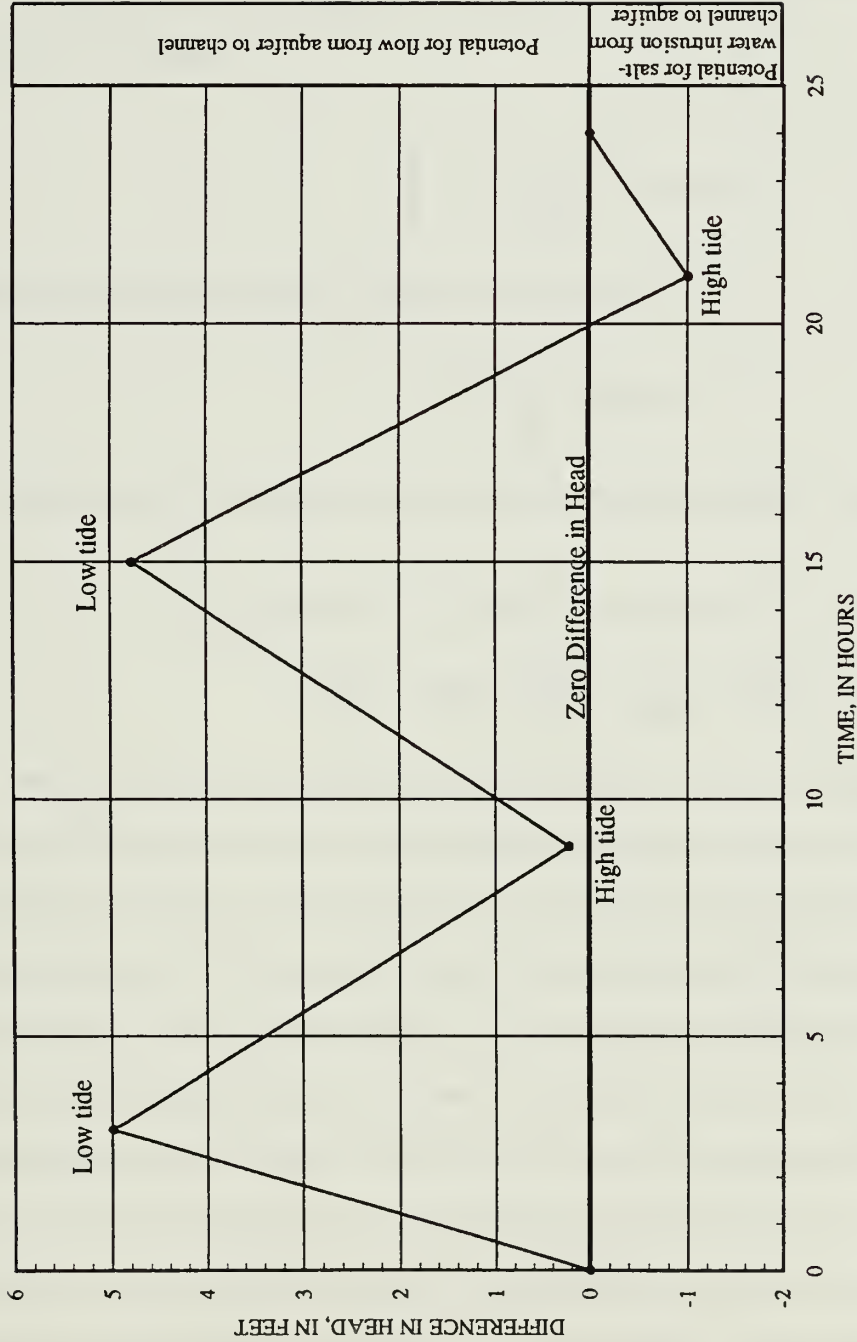


Figure 50. Difference in Pliocene-Miocene aquifer head and the channel stage during a 24 hour period. Water levels are from well KBMP 11, July 15, 1989. Head difference values greater than zero indicate that the head in the aquifer is greater than the channel stage. Values less than zero indicate the head in the aquifer is less than the channel stage.

The volume of water discharged per unit area can be calculated by substituting equation (28) into equation (25) and integrating. During a 24-hour period specific discharge can be expressed by the integral:

$$\int_0^{24} q \, dt = \frac{K}{\Delta L} \int_0^{24} (mt + b) \, dt \quad (29)$$

Integrating the equation yields the volume per unit area:

$$qt \Big|_0^{24} = \frac{K}{\Delta L} \left\langle \frac{mt^2}{2} + bt \right\rangle_0^{24} \quad (30)$$

The volume of water discharged per square foot during a 24-hr period (1 day) is expressed as:

$$\begin{aligned} \frac{V}{A} = \frac{K}{\Delta L} & \left[\left\langle \frac{m_1 t^2}{2} + b_1 t \right\rangle_0^3 + \left\langle \frac{m_2 t^2}{2} + b_2 t \right\rangle_3^9 + \left\langle \frac{m_3 t^2}{2} + b_3 t \right\rangle_9^{15} \right. \\ & \left. + \left\langle \frac{m_4 t^2}{2} + b_4 t \right\rangle_{15}^{20} + \left\langle \frac{m_4 t^2}{2} + b_4 t \right\rangle_{20}^{21} + \left\langle \frac{m_5 t^2}{2} + b_5 t \right\rangle_{21}^{24} \right] \quad (31) \end{aligned}$$

When the hydraulic gradient was sloped from the Pliocene-Miocene aquifer toward the channel (20 hrs), the volume of water discharged from the aquifer per unit area was 0.02 ft³/ft² (0.15 gal/ft²). When the hydraulic gradient was sloped from the channel toward the Pliocene-Miocene aquifer (4 hrs), the volume of seawater infiltrating the aquifer was 0.001 ft³/ft² (0.007 gal/ft²). The net volume of freshwater discharged from the Pliocene-Miocene aquifer per unit area was 0.019 ft³/ft² d (0.142 gal/ft² d). These values are small and indicate that little movement occurs between the aquifer and the channel. Seawater intrusion from the channel was insignificant near Site 3 because the total volume of freshwater discharging from the aquifer was an order of magnitude greater than the total volume of seawater entering the aquifer. The seepage velocity in the aquifer is 0.064 ft/d

which indicates groundwater movement in the aquifer is slow. Any seawater that intrudes the aquifer will not travel far.

The volume of water, inflow and outflow, could not be estimated at Sites 1 and 2 due to lack of water-level data. However, the high chloride concentrations reported in the aquifer at the sites (ranging from 13,000 to 17,000 mg/L) indicate that seawater encroachment has occurred at the southern end of the island (Wilson, 1990). Because there was no water-quality data for the Pliocene-Miocene aquifer prior to dredging, it may not be possible to conclude that channel dredging promoted seawater intrusion.

CONCLUSIONS

The geology of the study area consists of alternating layers of sand, clay, limestone, and dolomite. The upper Charlton Formation consists of consolidated to semi-consolidated calcareous sediment. An open marine environment existed during deposition as indicated by the abundant marine fossils and burrowing found in the core. The overlying Duplin Formation, ranging from 2 to 42 feet thick, consists of coarse sand, shell fragments and clay lenses. The formation increases in clay content at the southern most well sites. The Holocene-Pleistocene undifferentiated deposits consist of a basal clay layer, 5 to 40 feet thick, overlain by silty sand ranging from 22 to 62 feet thick.

The Miocene sand aquifer consists of coarse to very coarse calcareous sand, poorly sorted with lenses of argillaceous dolomite. The aquifer is recharged by precipitation in outcrop areas outside the study area. The leakage rate from the Miocene sand aquifer to the Pliocene-Miocene aquifer was 3.1×10^{-6} ft/d. The hydraulic conductivity derived from grain size analysis from well KBMP 1 was 53 ft/d.

At sites 1 and 2, the Pliocene-Miocene aquifer consists of fractured dolomitic limestone. At site 3 the aquifer consists of two hydraulically connected zones that are geologically distinct: 20 to 30 feet of Pliocene-age sand underlain by about 10 feet of Miocene-age fractured limestone. These two zones are separated by 8 feet of sandy clay.

The horizontal gradient of the Pliocene-Miocene aquifer on the south end of Cumberland Island was toward the west based on June 28, 1990 water levels. The seepage velocity ranged from 0.049 to 0.085 ft/d and changed with fluctuating tides and storm surges. The vertical gradient varied with time and space. At well sites 1 and 2 the direction of groundwater flow was from the Pliocene-Miocene aquifer to the surficial aquifer; at well site 3 the direction of flow was reverse from the surficial aquifer to the Pliocene-Miocene aquifer. The magnitude and direction of the vertical gradient changed

with fluctuating tides and storm surges.

Based on aquifer testing, the transmissivity of the Pliocene-Miocene aquifer ranged from 235 to 650 ft²/d and the storage coefficient from 1.05×10^{-5} to 5.6×10^{-5} . Transmissivity values calculated for the Pliocene-Miocene aquifer in Kingsland, Georgia, 15 miles west of the study area, were 750 ft²/d based on aquifer tests (Brown, 1984). Transmissivity values, storage values, and the straight line plots, indicate that the porosity of the aquifer medium is uniform but the hydraulic conductivity varies throughout the medium. Variation of the hydraulic conductivity is the result of lateral and vertical heterogeneities in the medium. Lateral heterogeneities may include facies changes, changes in the aquifer thickness, and possibly recharge from the ocean. Vertical heterogeneities are due to the sand unit of the aquifer having a much higher transmissivity than the limestone unit.

The surficial aquifer is composed of sands and clays of the Holocene and Pleistocene ages. The aquifer ranged from 15 to 35 feet of saturated thickness and was confined below by 5 to 40 feet of clay. The horizontal direction of groundwater flow was toward the southwest based on June 28, 1990 water levels. The vertical leakage rate from the surficial aquifer to the Pliocene-Miocene aquifer at site 3 was 4.08×10^{-4} ft/d. At sites 1 and 2 the vertical gradient between these aquifers was the reverse. The calculated leakage values from the Pliocene-Miocene aquifer to the surficial aquifer was 2.09×10^{-5} ft/d at site 1, and 3.17×10^{-4} ft/d at site 2. The hydraulic conductivity of the surficial aquifer was about 21 ft/d based on grain size analysis of samples from three sites.

The surficial aquifer was in a steady-state condition with constant long-term recharge, equivalent discharge and no appreciable withdrawals due to pumping. Approximately 2.85×10^5 gallons per square mile recharged the aquifer each day and nearly the same amount was discharged to the low lying wetlands (1.92×10^5 gal/d), the

underlying Pliocene-Miocene aquifer (8.5×10^4 gal/d), and along the coast at the seepage face (7.58×10^3 gal/d).

In the channel adjacent to site 3, the volume of water discharged from the Pliocene-Miocene aquifer into the channel was an order of magnitude greater than the total volume of seawater that entered the aquifer during a 24-hour period in July 1989. The net volume of freshwater discharged from the aquifer per unit area was $0.019 \text{ ft}^3/\text{ft}^2 \text{ d}$ ($0.142 \text{ gal}/\text{ft}^2$). Therefore, seawater encroachment from the channel was insignificant near site 3. Near sites 1 and 2, however, high chloride concentrations in the aquifer, ranging from 13,000 to 17,000 mg/L, indicated that seawater encroachment has occurred. Because water-chemistry data does not exist for the Pliocene-Miocene aquifer prior to dredging, it is not possible to conclude that channel dredging promoted seawater encroachment into the aquifer.

FUTURE WORK

Much work could be done to enhance the hydrogeologic description of Cumberland Island. The feasible possibilities are discussed below.

1. Install continuous water-level recorders on surficial-aquifer wells and on ponds on the island's south end to determine the extent of surface and ground water interaction. Continuous water-level recorder data along with data from weather stations (to be installed) will yield information that can be used to determine an annual surficial-aquifer water budget.
2. Install continuous water-level recorders on the Pliocene-Miocene aquifer wells and the Miocene sand aquifer well to determine vertical and horizontal gradients of the shallow aquifers during tidal fluctuations and storm surges.
3. Conduct aquifer tests at sites 1 and 2 for the Pliocene-Miocene aquifer. If pumping is not feasible, slug tests could be preformed. Slug tests could also be conducted at each well site for the surficial aquifer. Shallow piezometers or well points could be installed near the control well to monitor water-level changes during the test.
4. Install 3 or more monitoring wells/piezometers in the Pliocene-age sand to determine the horizontal groundwater flow gradient and seepage velocity of this zone.

References

- Aral, M. M., 1989, *Ground Water Modeling in Multilayer Aquifers, Steady Flow*, Lewis Publishers, Inc., Chelsea, Michigan.
- Bear, Jacob, 1979, *Hydraulics of Groundwater*, McGraw-Hill Inc., N.Y., N.Y., pp. 34-60.
- Bedinger, M.S. and Reed, J.E., 1988, *Practical Guide to Aquifer-Test Analysis*, U.S. Environmental Protection Agency, Las Vegas, Nevada, 78 p.
- Bixel, H.C. and Van Poolen, H.K., 1967, Pressure Drawdown and Buildup in the Presence of Radial Discontinuities, *Society of Petroleum Engineering Journal*, v. 7, pp. 301-309.
- Boylan, D.M., 1986, *The Hydrogeologic Resources of North Padre Island; Coastal South Texas*, unpublished master thesis, Baylor University, Waco, Texas, 143 p.
- Brown, David P., 1984, Impact of Development on Availability and Quality of Ground Water in Eastern Nassau County, Florida, and Southeastern Camden County, Georgia, *USGS Water Resources Investigations Report 83-4190*, 113 p.
- Bush, P.W. and Johnston, R.H., 1988, Ground-Water Hydraulics, Regional Flow, and Ground-Water Development of the Floridan Aquifer System in Florida and in Parts of Georgia, South Carolina, and Alabama, *USGS Professional Paper 1403-C*, 80 p.
- Clarke, J.S., C.M. Hacke, and M.F. Peck, 1990, Geology and Ground-Water Resources of the Coastal Area of Georgia, *Georgia Geologic Survey Bulletin*, 113, 106 p.
- Cobb, W.M., H.J. Ramey, Jr., and F.G. Miller, 1972, Well-test Analysis for Wells Producing Commingled Zones, *Journal of Petroleum Technology*, v. 24, pp. 407-418.

- Cooper, H.H., Jr. and Jacob, C.E., 1946, A generalized graphical method for evaluating formation constants and summarizing well-field history, *American Geophysical Union Transactions*, v. 27, no. 4, pp. 526-534.
- Dillon, W.P., 1970, Submergence effects on a Rhode Island barrier and lagoon and inferences on migration of barriers, *Journal of Geology*, v. 78, pp. 94-106.
- Driscoll, Fletcher G. 1986, *Groundwater and Wells*, Johnson Division, St Paul, Minnesota, 1089 p.
- Dupuit, J., 1848, Etudes theoriques et pratiques sur le mouvement des eaux courantes: Paris, Carilian-Goeury et V. Dalmont, 275 p.
- Dunne, T. and Leopold, L.B., 1978, *Water in Environmental Planning*, W.H. Freeman and Company, San Francisco, 818 p.
- Duran, P.B., 1984, The Effects of Cultural and Natural Interference on Electromagnetic Conductivity Data, NWWA/EPA Conference on Surface and Borehole Geophysical Methods in Ground Water Investigations, Worthington, Ohio, 20 p.
- Ferris, J.G., Knowles, D.B., Brown, R.H., and Stallman, R.W., 1962, Theory of Aquifer Test, *USGS Water-Supply Paper 1536-E*, 174 p.
- Fisher, J.J., 1968, Barrier Island Formation: Discussion, *Geological Society of America Bulletin*, v. 79, pp. 1421-1425.
- Freeze, R.A., and Cherry, J.A., 1979, *Groundwater*, Prentice-Hall, Inc., Englewood Cliffs, New Jersey, 604 p.
- Gardner, J., 1926, The Molluscan Fauna Alum Bluff Group of Florida, *U.S. Geological Survey Professional Paper 142 A-E*.
- Gregg, D.O., 1966, An Analysis of Ground-Water Fluctuations Caused by Ocean Tides in

Glynn County, Georgia, *Ground Water*, v.4, no. 3, 9 p.

Griffin, M.M., 1982, *Geologic Guide to Cumberland Island National Seashore*, 36 pp.,
United States Department of the Interior, Atlanta, GA, 36 p.

Hantush, M.S., and C.E. Jacob, 1955, Nonsteady Radial Flow in an Infinite Leaky
Aquifer, *American Geophysical Union Transactions*, v 36, pp. 95-100.

Henry, V.J., and Kellam, J.A., 1988, Seismic Investigation of the Phosphate-Bearing,
Miocene-Age Strata of the Continental Shelf of Georgia, *Georgia Geologic Survey
Bulletin 109*, 43 p.

Hilchie, Douglas W., 1982, *Applied Openhole Log Interpretation*, Douglas W. Hilchie
Inc., Golden, Colorado, 340 p.

Huddleston, P.F., 1988, A Revision of the Lithostratigraphic Units of the Coastal Plain of
Georgia, The Miocene through Holocene, *Georgia Geologic Survey Bulletin 104*,
162 p.

Jacob, C.E., 1947, Drawdown Test to Determine Effective Radius of Artesian Well,
Transactions, American Society of Civil Engineers, v. 112, pp. 1047-1070.

Keys, W.S., 1988, Borehole Geophysics Applied to Ground-Water Investigations, *USGS
Open-File Report 87-539*, 305 p.

Kohout, F.A., 1964, The Flow of Fresh Water and Salt Water in the Biscayne Aquifer of
the Miami Area, Florida, *USGS Water Supply Paper 1613-C*, 30 p.

Krause, R.E. and Randolph, R.B., 1989, Hydrology of the Floridan Aquifer System in
Southeast Georgia and Adjacent Parts of Florida and South Carolina, *USGS
Professional Paper 1403-D*, 65 p.

Kwader, Thomas, 1982, *Interpretation of Borehole Geophysical Logs and Their
Application to Water Resources Investigations*, 201 p.

- Lohman, S.W., 1972, Ground-Water Hydraulics, *USGS Professional Paper 708*, 70 p.
- Luszczynski, N.J., 1961, Head and Flow of Ground Water of Variable Density, *Journal of Geophysical Research*, v. 66, no. 12, pp. 4247-4256.
- Martinez, J.O., 1980, *Neogene Stratigraphy and Sedimentary Environments of Cumberland Island, GA*, p. 103, unpublished master thesis, Univ, of Ga., Athens, Ga.
- Masch, F.D., and Denny, K.J., 1966, Grain Size Distribution and Its Effect on the Permeability of Unconsolidated Sands, *Water Resources Research*, v. 2, pp. 665-677.
- Matthews, C.S., and Russell, D.G., 1967, Pressure Buildup and Flow Tests in Wells, *Society of Petroleum Engineers of AIME*, v. 1.
- McKinley, R.M. and Streltsova, T.D., 1984, Early-Time Pressure Buildup Analysis for Prudhoe Bay Wells, *Society of Petroleum Engineers of AIME*, v. 36, pp. 311-319.
- McLemore, W.H., C.E. Swann, P.B. Wigley, M.C. Turlington, V.J. Henry, J. Martinez, R.E. Carver, and J.T. Thurmond, 1981, *Geology as Applied to Land-Use Management on Cumberland Island, Georgia*, Georgia Geologic Survey, Atlanta, GA, 227 p.
- McNeill, J.D., 1980, Electromagnetic Terrain Conductivity Measurement at Low Induction Numbers, Geonics Limited, Technical Note 6 & 8, Ontario, Canada, 15 p.
- Miller, J.A., 1986, Hydrogeologic Framework of the Floridan Aquifer System in Florida and in Parts of Georgia, Alabama, and South Carolina, *USGS Professional Paper 1403-B*, 91 p.
- Milton, Charles, and Hurst, Vernon, 1965, Subsurface 'Basement' Rocks of Georgia, *USGS Bulletin 76*.

- Raudkivi, A.J., and Callander, R.A., 1976, *Analysis of Groundwater Flow*, Edward Arnold Ltd., 214 p.
- Stewart, Mark T., 1982, Evaluation of Electromagnetic Methods for Rapid Mapping of Salt-Water Interfaces in Coastal Aquifers, *Ground Water*, v. 20, no. 5, pp. 538-545.
- Streltsova, T.D., 1988, *Well Testing in Heteogeneous Formations*, John Wiley and Sons, Ind., NY,NY, 213 p.
- Theis, C.V., 1935, The relation between the lowering of the piezometric surface and the rate and duration of discharge of a well using ground-water storage, *American Geophysical Union Transactions*, v. 16, pp.519-524.
- Wilson, S.K., 1990, *The hydrogeochemistry of Southern Cumberland Island, Georgia*, unpublished master thesis, Georgia State University, Atlanta, Georgia.
- Zohdy, A.A.R., Eaton G.P., and Mabey, D.R., 1974, *Application of Surface Geophysics to Ground-Water Investigations*, USGS TWRI Book 2, chapter D1, 116 p.

APPENDIX A

Grain Size Analysis Data

Table A1. Raw grain size analysis data

	Sieve diameter (ø)	Beaker weight (g)	Beaker and sample weight (g)	Sample weight (g)	Corrected weight (g)	Cumulative percent
Site 1, 136-146 ft. interval		47.64	83.31	35.61		
	-1		48.07	0.43	1.21	1.21
	0		53.45	5.81	16.36	17.57
	1		60.2	12.56	35.36	52.93
	2		61.06	13.42	37.78	90.71
	3		49.41	1.77	4.98	95.69
	4		48.19	0.55	1.54	97.23
	pan		48.62	0.98	2.76	99.99
Percent error = 0.25%						
Site 2, 20-30 ft. interval		50.1	85.61	35.51		
	-1		50.14	0.04	0.113	0.113
	0		50.57	0.47	1.33	1.44
	1		51.69	1.59	4.49	5.93
	2		57.59	7.49	21.16	27.09
	3		68.68	18.58	52.49	79.58
	4		57.2	7.1	20.06	99.64
	pan		50.23	0.13	0.367	100
Percent error = 0.31%						
Site 3, 10-20 ft. interval		64.38	108.65	44.27		
	0		64.42	0.04	0.09	0.09
	1		64.41	0.068	0.068	0.158
	1.5		64.66	0.633	0.633	0.791
	2		65.75	3.1	3.1	3.89
	3		98.69	77.54	77.54	81.43
	4		72.52	18.4	18.4	99.83
	pan		64.46	0.181	0.181	100
Percent error = 0.05%						
Site 3, 60-70 ft. interval		50.2	93.89	43.69		
	-2		50.54	0.34	0.78	0.78
	-1.5		52.17	1.97	4.53	5.31
	-1		53.86	3.66	8.42	13.73
	0		69.99	19.79	45.55	59.28
	1		60.37	10.17	23.41	82.69
	2		54.68	4.48	10.31	93
	3		52.93	2.73	6.28	99.28
	4		50.49	0.29	0.66	99.94
	pan		50.22	0.02	0.046	99.99
Percent error = 0.5%						
Site 1, 10-11.5 ft. interval		50.11	98.11	48		
	-1		50.12	0.01	0.02	0.02
	0		50.18	0.07	0.147	0.167
	1		50.21	0.1	0.21	0.377
	1.5		50.75	0.64	1.34	1.72
	2		54.69	4.58	9.62	11.34
	3		85.44	35.33	74.21	85.55
	4		56.66	6.55	13.76	99.31
	pan		50.44	0.33	0.69	100
	Percent error = 0.81%					

APPENDIX B

Core Descriptions

Description of split spoon samples and core samples from well KBMP 1, Site 1.

Driller: Corps of Engineers, Savannah, GA
 Latitude/Longitude: 30°43'11", 81°28'13"
 Altitude: 4.59 ft. above mean low water
 Total Depth: 155.5 ft.

(Colors were wet and matched to the Rock Color Chart, GSA, 1984)

Slit spoon samples

<u>Depth in ft. below land surface</u>	<u>Description</u>
Holocene to Pleistocene Undifferentiated	
5.0-6.5	Sand: Yellowish gray (5Y7/2), v.f.g. sand, subangular, well sorted, 20% heavy minerals, 20% organics.
10-11.5	Sand: Same as previous section
15-16.5	Sand: Yellowish gray (5Y7/2), v.f.g. sand, subangular, well sorted, 20% heavy minerals, 20% organics, trace of shell fragments.
20-21.5	Sand: Olive gray (5Y4/1), v.f.g., subangular, 20% heavy minerals, 10 clay, 1% mica flakes.
23.0-23.5	Clay: Dk. gray (N3) fat, clean, trace of shell fragments, trace of mica
25-26.5	Sandy Clay: Med. gray (N5), v.f.g. sand, subangular, alt. layers of fat gray clay 2-3 inch. in thickness (30%), slightly calcareous.
30-31.5	Sandy Clay: Med. gray (N5), v.f.g. sand, subangular, alt. layers of fat gray clay 2-3 inch. in thickness (30%), 10% organic material, slightly calcareous, trace of shell fragments.
35-36.5	Same as 30-31.5 section
Pliocene Series	
40-41.5	Clayey Sand: Brown gray (5YR4/1), v.f.-f.g., subangular, 20% shell fragments, 10% clay, slightly calcareous.

- 45-46.5 Clayey Sand: Mod. olive brown (5Y4/4), f.g.-m.g. sand, subangular, 15% clay, 10% heavy minerals, trace of shell fragments, trace of mica, slightly calcareous.
- 50-51.5 Clayey Sand: Same as previous section
- 60-61.5 Clayey Sand: Same as 45-45.6 section

Core Descriptions
Middle Miocene
Upper Hawthorne Formation

- 66.2-89.15 Dolomite to dolomitic sand, very lt. to lt. gray (N7), massive, high sand content, vugs, moderate porosity, hard dense dolomite at top of section grading into softer, pitted, fossiliferous dolomitic limestone at 80 feet. Contact based on top of rock.
- 66.2-66.7 Dolomite: med. gray (N5), 7% f.g. sand, hard, dense, small vugs present, phosphate present, low effective porosity.
- 66.7-67.0 Dolomitic Sand: very lt. gray (N8), poorly indurated, argillaceous, 30% calcareous clay, 5% shell fragments, 0.5% heavy minerals, phosphate present.
- 67.0-67.8 Dolomite: very lt. gray (N8), arenaceous, 50% f.g. sand, subrounded, medium hard, low effective porosity.
- 67.8-68.92 Dolomite: very lt. gray (N8), arenaceous, 50% v.f.g. to f.g. sand, subrounded, 0.5% heavy minerals, several small vugs, low effective porosity.
- 68.92-69.72 Dolomitic Sand: yellowish gray (5Y8/1), arenaceous, 50% f.g. to m.g. sand, 0.5% heavy minerals, phosphate present, medium hard, moderate effective porosity.
- 69.72-70.6 Dolomite: lt. gray (N7), arenaceous, 45% f.g. sand, subangular, 7% calcareous clay, 0.5% heavy minerals, 2% fossils, several small vugs, low effective porosity.
- 70.6- 75.5 Cavity
- 75.5-76.1 Dolomite: lt. gray (N7), hard, 50% f.g. sand, subrounded grains, several vugs (1 inch diameter) not interconnected, poor effective porosity.
- 76.1-76.9 Dolomite: lt. gray (N7), hard, 50% f.g. sand, subrounded grains, 0.5% heavy minerals, several horizontal fractures, small vugs, moderate effective porosity.

- 76.9--77.9 Dolomite: lt. gray (N7), 50-60% f.g. sand, 0.5% heavy minerals, subrounded grains, several fractures and joints, small vugs, med. hard, moderate effective porosity.
- 77.9-79.6 Dolomite: lt. gray (N7), hard, 45% f.g. sand, 1% heavy minerals, 10% calcareous clay, fractured, jointed, vuggy, good secondary porosity.
- 79.6-80.1 Core loss
- 80.1-80.7 Limestone: white (N9), soft, 50% f.g. sand, poorly indurated, 10% calcareous clay lenses, semi-plastic, fractured, fair effective porosity.
- 80.7-81.2 Dolomitic Limestone: lt. gray (N7), 50% f.g.-m.g. sand, 30% weathered shells & molds, fossiliferous, 1% mica, 0.5% heavy minerals, highly weathered and fractured, high effective porosity.
- 81.2-81.9 Dolomite: lt. gray (N7), hard, 40% f.g. sand, 20% weathered shell fragments (pelecepods), 0.5% heavy minerals, phosphate present, many small vugs (.25mm), weathered, highly pitted, good effective porosity.
- 81.9- 82.4 Dolomite: lt. gray (N7), medium hard, 50-60% f.g. sand, 1% heavy minerals, highly pitted, many small vugs.
- 82.4-83.0 Dolomitic Sand: lt. gray (N7), 50% f.g. sand, subrounded to subangular, poorly indurated, fractured, weathered, high effective porosity.
- 83.0-83.4 Dolomite: same as 81.9-82.4 section
- 83.4-86.2 Dolomite: lt. gray (N7), hard, 50-60% f.g.-m.g sand, subrounded grains, 1% heavy minerals, 1% very coarse smokey qtz. grains, horizontal fractures, some vugs, moderate effective porosity.
- 86.2-88.0 Dolomitic Sand: lt. gray (N7), soft, poorly indurated, f.g.-m.g subrounded grains, 1% heavy minerals, 1% mica flakes, fine sand seams, fractured, weathered, high effective porosity.
- 88.0-88.4 Core loss
- 88.4-89.15 Same as 86.2-88.0 section.
- 89.15-94.0 Dolomite: lt.gray (N7), harder, tighter section, sandy, very pitted, vuggy, very fossiliferous, weathered, good effective porosity. Contact based on denser rock and rapid increase in fossil content.

- 89.15-92.3 Dolomite: lt. gray (N7), 35% f.g.-m.g. sand, subangular to subrounded, 10% very coarse smokey qtz. grains, subrounded sand, 20% weathered shell frags. (pelecepods), 1% heavy minerals, 0.5% mica flakes, fossiliferous, vuggy, fractured, pitted, good effective porosity.
- 92.3-92.6 Dolomite: lt. gray (N7), 40% f.g.-m.g. sand, subrounded to subangular, 10% v.c. smokey qtz. grains, poorly indurated, surgary, 1% heavy minerals, fair effective porosity.
- 92.6-94.0 Dolomite: lt. gray (N7), 50% f.-m.g. sand, surgary, 20 % fossils, shells, 1% heavy minerals, med. hard texture, pitted, vuggy, fossiliferous, fractured, fair effective porosity.
- 94.0-102.3 Dolomite: lt. gray (N7), argillaceous, arenaceous, highly bioturbated (*Ophiomorpha nodosa*), high phosphate content. Gradational contact based on increase in clay content, bioturbation and decrease in shell content.
- 94.0-97.3 Dolomite: lt. gray (N7-8), argillaceous, arenaceous, 35% v.f-f.g. sand, subrounded to subangular, 15% clay, 5% coarse qtz. grains and phosphatic calcite, 1% heavy minerals, 1% mica flakes, phosphate present, mottled (*Callianassa* burrows) continuous core, low permeability, good confining unit.
- 97.3-98.3 Dolomite: lt. gray (N7-8), argillaceous, arenaceous, 40% v.f.-f.g. sand, subrounded to subangular, 40% clay, 5% c.g. qtz. and phosphatic calcite, 2% heavy minerals, plastic, continuous, good confining unit.
- 98.3-102.3 Dolomite: lt. gray (N7-8), argillaceous, arenaceous, 50% v.f-f.g. sand, subrounded to subangular, 1% phosphate, many *Callianassa* burrows, med. hard, low permeability. This section contains med. gray silty calcareous clay lenses (30%), subangular silt grains, 20% v.c. qtz & phosphatic calcite grains, low permeability.
- 102.3-102.8 Core loss
- 102.8-105.8 Calcareous Clay: very lt. gray (N8), little to no burrowing, high clay and sand content, soft, plastic, continuous. Contact based on change in lithology from dolomite to a sandy calcareous clay.
- 102.8-105 Calcareous Clay: very lt. gray (N8), 20% v.f.-f.g. sand, subangular to subrounded, 1% c.g. qtz. & phosphatic calcite, plastic, soft, sparse shell fragments, sulfur smell, low permeability.

- 105-105.8 Calcareous Clay: very lt. gray (N8), argillaceous, arenaceous, 30% f.g. sand, subangular to subrounded, c.g. sand (5%), subrounded, 4% phosphate, plastic, soft, continuous, low permeability.
- 105.8-113.5 Dolomitic L.S.: lt. gray (N7), argillaceous, arenaceous, soft, mottled, fossiliferous. Contact based on lithology change, and an increase in burrowing and phosphate content.
- 105.8-109.2 Dolomitic L.S.: very lt. gray (N8) with lt. gray (N7) burrows, argillaceous, arenaceous, 30% f.-m.g. sand, subangular to subrounded, 20% clay, 10% large qtz. and phosphatized calcite grains (v.c. to 6 mm in diam.), 5% phosphate, 25% shell molds, sparse shell frags., mottled (*Callianassa* burrows), poorly indurated, plastic, fossiliferous, med. soft, low permeability.
- 109.2-112.2 Dolomitic L.S.: lt. gray (N7), argillaceous, arenaceous, 40% f-m.g. sand, subrounded to subangular, 20% clay, 15% v.c. qtz & phosphatized calcite grains, 20% shell molds & casts, 3% phosphate, fossiliferous, friable, low permeability.
- 112.2-113.5 Dolomitic L.S.: lt. gray (N7), alt. sand & clay lenses, 50% f.g. sand, subangular to subrounded, 25% clay, 10% v.c. qtz. and phosphatized calcite grains, 3% phosphate, .5% mica, sparse fossils, burrows present, friable, low permeability.
- 113.5-120.3 Dolomitic L.S.: lt. gray (N7), arenaceous, argillaceous, highly bioturbated from 117.2-119.5, high phosphate and coarse quartz grain content. Gradational contact based on increase bioturbation and phosphate content.
- 113.5-117.2 Dolomitic L.S.: lt. gray (N7) with med. lt. gray (N6) burrows, 40% v.f.-f.g. sand, 20% clay, 20% v.c. qtz. and phosphatized calcite, 3% particulate phosphate, 0.5% mica, abundant shell molds, fossiliferous (mostly pelecypods), some *Callianassa* burrows, friable, moderate hard, low permeability.
- 117.2-120.3 Dolomitic L.S.: lt. gray (N7) with med. lt. gray (N6) burrows, 35% v.f.-f.g. sand, subangular to subrounded, 20% clay, 20% v.c. qtz. and phos. calcite, subrounded, 10% weathered fossil molds & casts, highly bioturbated, poorly indurated, plastic, med. hard, continuous, low permeability. 20% of this section contains med. gray silty clay lenses w/ 20% v.c. qtz. grains.

- 120.3-127.6 Dolomitic L.S.: lt. gray (N7), arenaceous, argillaceous, fossiliferous, low permeability. Gradational contact based on decrease bioturbation, phosphate, and coarse quartz grains.
- 120.3-121.5 Dolomitic L.S.: lt. gray (N7), 35% v.f.-f.g. sand, subrounded to subangular, 20% clay, 7% v.c. qtz & phos. calcite grains, burrows present, med. hard, continuous, low permeability.
- 121.5-122.2 Core Loss
- 122.2-126.4 Dolomitic L.S.: lt. gray (N7), 35% f.g. sand, 20% clay, 30% shell molds, 5% v.c. qtz. & phos. calcite grains, .5% mica flakes, med. hard, fossiliferous (*Chesapecten* cf., and *Mercenaria prodroma* cf.), friable, tiny vugs present, low permeability.
- 126.4-126.6 Dolomitic L.S.: lt. gray (N7), argillaceous, arenaceous, 40% v.f.-f.g. sand, 15% clay, 7% v.c. qtz. & phos. calcite grains, 50% shell molds (clams & pelecypods), semiplastic, low permeability.
- 126.6-128.3 Dolomitic L.S.: lt. gray (N7), argillaceous, arenaceous, 40% f.-m.g. sand, subrounded to subangular, 30% clay, 10% v.c. qtz. & phos. calcite grains, 20% shell molds (pin shells, pelecypods), 5% phosphatic fossiliferous (brachiopod *Lingula*), continuous, bioturbated, low permeability.
- 128.3-135.9 Dolomitic L.S.: lt. gray (N7) argillaceous, arenaceous, highly bioturbated, increase in phosphate, low permeability. Gradational contact based on increase bioturbation, phosphate.
- 128.3-129.8 Dolomitic L.S.: lt. gray (N7), argillaceous, arenaceous, 45% f.-m.g. sand, subangular to subrounded, 45% clay, 7% v.c. qtz. & phos. calcite, 2% shell molds, bioturbated, low permeability.
- 129.8-130.9 Dolomitic L.S.: lt. gray (N7), argillaceous, arenaceous, 40% f.-m.g. sand, subrounded to subangular, 20% clay, 15% v.c. qtz. & phos. calcite grains, 15% shell molds, bioturbated, fossiliferous, low permeability.
- 130.9-131.6 Dolomitic L.S.: lt. gray (N7), argillaceous, arenaceous, 45% f.-m.g. sand, subrounded to subangular, 20% clay, 15% v.c. qtz. & phos. calcite grains, 10% shell molds & casts, bioturbated, poorly indurated, low permeability.
- 135.9-136.7 Core loss

- 136.7-145.7 Calcareous Sand: lt. gray (N7), poorly indurated loose quartz sand, poorly sorted, good permeability, fair effective porosity. Contact based on change in lithology.
- 136.7- 137.6 Calcareous Sand: lt. gray (N7), poorly sorted sand, 45% c.-v.c. sand, 35% m.g. sand, subangular to subrounded, 2% clay, poorly indurated, friable, good permeability, fair effective porosity.
- 137.6-139.1 Calcareous Sand: alternating layers of poorly sorted calcareous sand (lt. gray (N7)) & calcareous fat clay (very lt. gray (N8)), the clay lenses (30%) are about 1" in thickness, 35% c.g. sand, subrounded, 25% f.-m.g. sand, subangular to subrounded, 10% v.c. sand, subrounded, friable, poorly indurated, fair permeability, fair effective porosity.
- 139.1 -139.7 Calcareous Sand: lt. gray (N7), 60% c.-v.c. sand, subrounded, 30% f.-m.g. sand, subangular to subrounded, 2% clay, clean, friable, poorly sorted, poorly indurated, good permeability, fair effective porosity.
- 139.7-140 Dolomitic L.S.: very lt. gray (N8), arenaceous, argillaceous, 40% f.-m.g. sand, subrounded, 30% v.c.g. sand, subrounded, poorly sorted sand, 15% clay, med. hard, vugs present, low permeability.
- 140-141.1 Calcareous sand: lt. gray (N7), poorly sorted sand, 65% c.g. sand, subrounded, 20% f.-m.g. sand, subangular to subrounded, 10% v.c.g. sand, subrounded, 2% clay, 0.5% mica, poorly indurated to loose, friable, good permeability, fair effective porosity.
- 141.1-142 Core Loss
- 142-143.8 Calcareous Sand: lt. gray (N7), poorly sorted sand, 60% c.g. sand, subrounded, 15% f.-m.g. sand, subangular to subrounded, 5% v.c.g. sand, subrounded, 2% shell molds & casts, 5% thin tan gray fat clay lenses about 1/2 inch thick, friable, poorly indurated to loose, good permeability, fair effective porosity.
- 143.8-144.1 Dolomitic L.S.: very lt. gray (N8), alternating layers of calcareous poorly sorted sand and calcareous tan gray clay, 60% c.g. subrounded sand, 15% f.-m.g. subangular to subrounded sand, 5% c.g. subrounded sand, 10% calcareous clay, med. hard, friable, bioturbated, fair permeability, fair effective porosity.
- 144.1-145.7 Calcareous Sand: lt. gray (N7), poorly sorted sand, 60% c.g. rounded sand, 15% m.g. subangular sand, 5% v.c.g.

rounded sand, 5% calcareous tan gray clay (1/4" to 1.5" in thickness), poorly indurated to loose, good permeability, fair effective porosity.

- 145.7-155.5 Dolomitic L.S.: lt. gray (N7), arenaceous, argillaceous, bioturbated, soft, good confining unit. Contact based on lithology change.
- 145.7-148.2 Dolomitic L.S.: lt. gray (N7), 40% c.g. subrounded sand, 15% v.f.-m.g. subrounded, 5% v.c. subrounded sand, 15% clay, 3% shell molds, continuous, friable, some vugs, med. hard, low permeability
- 148.2-148.6 Dolomitic L.S.: lt. gray (N7), 40% c.g. subrounded sand, 15% v.f.-m.g. subrounded, 5% v.c. subrounded sand, 15% clay, 3% shell molds, poorly indurated to loose, low permeability.
- 148.6-150.3 Dolomitic L.S.: lt. gray (N7), 45% f.-m.g. sand, subrounded to subangular, 10% v.c.g. subrounded sand, 25% clay, 0.5% mica flakes, 0.5% large qtz. grains (8mm in diam.), 2% brachiopods, 20% shell molds, fossiliferous (*Chesapecten* cf., and brachiopod *Lingula*), bioturbated, continuous, low permeability.
- 150.3-153 Dolomitic L.S.: lt. gray (N7), 50% f.-m.g. sand, subrounded to subangular, 10% v.c.g. subrounded sand, 25% clay, 0.5% mica flakes, 0.5% large qtz. grains (8mm in diam.), 2% phosphate, 2% brachiopods, 3% shell molds, mottled, continuous, low permeability.
- 153-155.5 Dolomitic L.S.: lt. gray (N7), 40% f.-m.g. sand, subrounded to subangular, 15% v.c.g. sand, subrounded, 25% clay, 2% phosphate, 1% mica flakes, med. soft, continuous, mottled, low permeability, good confining unit.

Description of split spoon samples and core samples from well KBMP 1, Site 1.

Driller: Corps of Engineers, Savannah, GA

Latitude/Longitude: 30°43'11", 81°28'13"

Altitude: 4.59 ft. above mean low water

Total Depth: 155.5 ft.

(Colors were wet and matched to the Rock Color Chart, GSA, 1984)

Slit spoon samples

Depth in ft. below <u>land surface</u>	<u>Description</u>
Holocene to Pleistocene Undifferentiated	
5.0-6.5	Sand: Yellowish gray (5Y7/2), v.f.g. sand, subangular, well sorted, 20% heavy minerals, 20% organics.
10-11.5	Sand: Same as previous section
15-16.5	Sand: Yellowish gray (5Y7/2), v.f.g. sand, subangular, well sorted, 20% heavy minerals, 20% organics, trace of shell fragments.
20-21.5	Sand: Olive gray (5Y4/1), v.f.g., subangular, 20% heavy minerals, 10 clay, 1% mica flakes.
23.0-23.5	Clay: Dk. gray (N3) fat, clean, trace of shell fragments, trace of mica
25-26.5	Sandy Clay: Med. gray (N5), v.f.g. sand, subangular, alt. layers of fat gray clay 2-3 inch. in thickness (30%), slightly calcareous.
30-31.5	Sandy Clay: Med. gray (N5), v.f.g. sand, subangular, alt. layers of fat gray clay 2-3 inch. in thickness (30%), 10% organic material, slightly calcareous, trace of shell fragments.
35-36.5	Same as 30-31.5 section
Pliocene Series	
40-41.5	Clayey Sand: Brown gray (5YR4/1), v.f.-f.g., subangular, 20% shell fragments, 10% clay, slightly calcareous.

- 45-46.5 Clayey Sand: Mod. olive brown (5Y4/4), f.g.-m.g. sand, subangular, 15% clay, 10% heavy minerals, trace of shell fragments, trace of mica, slightly calcareous.
- 50-51.5 Clayey Sand: Same as previous section
- 60-61.5 Clayey Sand: Same as 45-45.6 section

Core Descriptions
Middle Miocene
Upper Hawthorne Formation

- 66.2-89.15 Dolomite to dolomitic sand, very lt. to lt. gray (N7), massive, high sand content, vugs, moderate porosity, hard dense dolomite at top of section grading into softer, pitted, fossiliferous dolomitic limestone at 80 feet. Contact based on top of rock.
- 66.2-66.7 Dolomite: med. gray (N5), 7% f.g. sand, hard, dense, small vugs present, phosphate present, low effective porosity.
- 66.7-67.0 Dolomitic Sand: very lt. gray (N8), poorly indurated, argillaceous, 30% calcareous clay, 5% shell fragments, 0.5% heavy minerals, phosphate present.
- 67.0-67.8 Dolomite: very lt. gray (N8), arenaceous, 50% f.g. sand, subrounded, medium hard, low effective porosity.
- 67.8-68.92 Dolomite: very lt. gray (N8), arenaceous, 50% v.f.g. to f.g. sand, subrounded, 0.5% heavy minerals, several small vugs, low effective porosity.
- 68.92-69.72 Dolomitic Sand: yellowish gray (5Y8/1), arenaceous, 50% f.g. to m.g. sand, 0.5% heavy minerals, phosphate present, medium hard, moderate effective porosity.
- 69.72-70.6 Dolomite: lt. gray (N7), arenaceous, 45% f.g. sand, subangular, 7% calcareous clay, 0.5% heavy minerals, 2% fossils, several small vugs, low effective porosity.
- 70.6- 75.5 Cavity
- 75.5-76.1 Dolomite: lt. gray (N7), hard, 50% f.g. sand, subrounded grains, several vugs (1 inch diameter) not interconnected, poor effective porosity.
- 76.1-76.9 Dolomite: lt. gray (N7), hard, 50% f.g. sand, subrounded grains, 0.5% heavy minerals, several horizontal fractures, small vugs, moderate effective porosity.

- 76.9--77.9 Dolomite: lt. gray (N7), 50-60% f.g. sand, 0.5% heavy minerals, subrounded grains, several fractures and joints, small vugs, med. hard, moderate effective porosity.
- 77.9-79.6 Dolomite: lt. gray (N7), hard, 45% f.g. sand, 1% heavy minerals, 10% calcareous clay, fractured, jointed, vuggy, good secondary porosity.
- 79.6-80.1 Core loss
- 80.1-80.7 Limestone: white (N9), soft, 50% f.g. sand, poorly indurated, 10% calcareous clay lenses, semi-plastic, fractured, fair effective porosity.
- 80.7-81.2 Dolomitic Limestone: lt. gray (N7), 50% f.g.-m.g. sand, 30% weathered shells & molds, fossiliferous, 1% mica, 0.5% heavy minerals, highly weathered and fractured, high effective porosity.
- 81.2-81.9 Dolomite: lt. gray (N7), hard, 40% f.g. sand, 20% weathered shell fragments (pelecepods), 0.5% heavy minerals, phosphate present, many small vugs (.25mm), weathered, highly pitted, good effective porosity.
- 81.9- 82.4 Dolomite: lt. gray (N7), medium hard, 50-60% f.g. sand, 1% heavy minerals, highly pitted, many small vugs.
- 82.4-83.0 Dolomitic Sand: lt. gray (N7), 50% f.g. sand, subrounded to subangular, poorly indurated, fractured, weathered, high effective porosity.
- 83.0-83.4 Dolomite: same as 81.9-82.4 section
- 83.4-86.2 Dolomite: lt. gray (N7), hard, 50-60% f.g.-m.g sand, subrounded grains, 1% heavy minerals, 1% very coarse smokey qtz. grains, horizontal fractures, some vugs, moderate effective porosity.
- 86.2-88.0 Dolomitic Sand: lt. gray (N7), soft, poorly indurated, f.g.-m.g subrounded grains, 1% heavy minerals, 1% mica flakes, fine sand seams, fractured, weathered, high effective porosity.
- 88.0-88.4 Core loss
- 88.4-89.15 Same as 86.2-88.0 section.
- 89.15-94.0 Dolomite: lt. gray (N7), harder, tighter section, sandy, very pitted, vuggy, very fossiliferous, weathered, good effective porosity. Contact based on denser rock and rapid increase in fossil content.

- 89.15-92.3 Dolomite: lt. gray (N7), 35% f.g.-m.g. sand, subangular to subrounded, 10% very coarse smokey qtz. grains, subrounded sand, 20% weathered shell frags. (pelecepods), 1% heavy minerals, 0.5% mica flakes, fossiliferous, vuggy, fractured, pitted, good effective porosity.
- 92.3-92.6 Dolomite: lt. gray (N7), 40% f.g.-m.g. sand, subrounded to subangular, 10% v.c. smokey qtz. grains, poorly indurated, surgary, 1% heavy minerals, fair effective porosity.
- 92.6-94.0 Dolomite: lt. gray (N7), 50% f.-m.g. sand, surgary, 20 % fossils, shells, 1% heavy minerals, med. hard texture, pitted, vuggy, fossiliferous, fractured, fair effective porosity.
- 94.0-102.3 Dolomite: lt. gray (N7), argillaceous, arenaceous, highly bioturbated (*Ophiomorpha nodosa*), high phosphate content. Gradational contact based on increase in clay content, bioturbation and decrease in shell content.
- 94.0-97.3 Dolomite: lt. gray (N7-8), argillaceous, arenaceous, 35% v.f-f.g. sand, subrounded to subangular, 15% clay, 5% coarse qtz. grains and phosphatic calcite, 1% heavy minerals, 1% mica flakes, phosphate present, mottled (*Callianassa* burrows) continuous core, low permeability, good confining unit.
- 97.3-98.3 Dolomite: lt. gray (N7-8), argillaceous, arenaceous, 40% v.f-f.g. sand, subrounded to subangular, 40% clay, 5% c.g. qtz. and phosphatic calcite, 2% heavy minerals, plastic, continuous, good confining unit.
- 98.3-102.3 Dolomite: lt. gray (N7-8), argillaceous, arenaceous, 50% v.f-f.g. sand, subrounded to subangular, 1% phosphate, many *Callianassa* burrows, med. hard, low permeability. This section contains med. gray silty calcareous clay lenses (30%), subangular silt grains, 20% v.c. qtz & phosphatic calcite grains, low permeability.
- 102.3-102.8 Core loss
- 102.8-105.8 Calcareous Clay: very lt. gray (N8), little to no burrowing, high clay and sand content, soft, plastic, continuous. Contact based on change in lithology from dolomite to a sandy calcareous clay.
- 102.8-105 Calcareous Clay: very lt. gray (N8), 20% v.f.-f.g. sand, subangular to subrounded, 1% c.g. qtz. & phosphatic calcite, plastic, soft, sparse shell fragments, sulfur smell, low permeability.

- 105-105.8 Calcareous Clay: very lt. gray (N8), argillaceous, arenaceous, 30% f.g. sand, subangular to subrounded, c.g. sand (5%), subrounded, 4% phosphate, plastic, soft, continuous, low permeability.
- 105.8-113.5 Dolomitic L.S.: lt. gray (N7), argillaceous, arenaceous, soft, mottled, fossiliferous. Contact based on lithology change, and an increase in burrowing and phosphate content.
- 105.8-109.2 Dolomitic L.S.: very lt. gray (N8) with lt. gray (N7) burrows, argillaceous, arenaceous, 30% f.-m.g. sand, subangular to subrounded, 20% clay, 10% large qtz. and phosphatized calcite grains (v.c. to 6 mm in diam.), 5% phosphate, 25% shell molds, sparse shell frags., mottled (*Callianassa* burrows), poorly indurated, plastic, fossiliferous, med. soft, low permeability.
- 109.2-112.2 Dolomitic L.S.: lt. gray (N7), argillaceous, arenaceous, 40% f-m.g. sand, subrounded to subangular, 20% clay, 15% v.c. qtz & phosphatized calcite grains, 20% shell molds & casts, 3% phosphate, fossiliferous, friable, low permeability.
- 112.2-113.5 Dolomitic L.S.: lt. gray (N7), alt. sand & clay lenses, 50% f.g. sand, subangular to subrounded, 25% clay, 10% v.c. qtz. and phosphatized calcite grains, 3% phosphate, .5% mica, sparse fossils, burrows present, friable, low permeability.
- 113.5-120.3 Dolomitic L.S.: lt. gray (N7), arenaceous, argillaceous, highly bioturbated from 117.2-119.5, high phosphate and coarse quartz grain content. Gradational contact based on increase bioturbation and phosphate content.
- 113.5-117.2 Dolomitic L.S.: lt. gray (N7) with med. lt. gray (N6) burrows, 40% v.f.-f.g. sand, 20% clay, 20% v.c. qtz. and phosphatized calcite, 3% particulate phosphate, 0.5% mica, abundant shell molds, fossiliferous (mostly pelecypods), some *Callianassa* burrows, friable, moderate hard, low permeability.
- 117.2-120.3 Dolomitic L.S.: lt. gray (N7) with med. lt. gray (N6) burrows, 35% v.f.-f.g. sand, subangular to subrounded, 20% clay, 20% v.c. qtz. and phos. calcite, subrounded, 10% weathered fossil molds & casts, highly bioturbated, poorly indurated, plastic, med. hard, continuous, low permeability. 20% of this section contains med. gray silty clay lenses w/ 20% v.c. qtz. grains.

- 120.3-127.6 Dolomitic L.S.: lt. gray (N7), arenaceous, argillaceous, fossiliferous, low permeability. Gradational contact based on decrease bioturbation, phosphate, and coarse quartz grains.
- 120.3-121.5 Dolomitic L.S.: lt. gray (N7), 35% v.f.-f.g. sand, subrounded to subangular, 20% clay, 7% v.c. qtz & phos. calcite grains, burrows present, med. hard, continuous, low permeability.
- 121.5-122.2 Core Loss
- 122.2-126.4 Dolomitic L.S.: lt. gray (N7), 35% f.g. sand, 20% clay, 30% shell molds, 5% v.c. qtz. & phos. calcite grains, .5% mica flakes, med. hard, fossiliferous (*Chesapecten* cf., and *Mercenaria prodroma* cf.), friable, tiny vugs present, low permeability.
- 126.4-126.6 Dolomitic L.S.: lt. gray (N7), argillaceous, arenaceous, 40% v.f.-f.g. sand, 15% clay, 7% v.c. qtz. & phos. calcite grains, 50% shell molds (clams & pelecypods), semiplastic, low permeability.
- 126.6-128.3 Dolomitic L.S.: lt. gray (N7), argillaceous, arenaceous, 40% f.-m.g. sand, subrounded to subangular, 30% clay, 10% v.c. qtz. & phos. calcite grains, 20% shell molds (pin shells, pelecypods), 5% phosphatic fossiliferous (brachiopod *Lingula*), continuous, bioturbated, low permeability.
- 128.3-135.9 Dolomitic L.S.: lt. gray (N7) argillaceous, arenaceous, highly bioturbated, increase in phosphate, low permeability. Gradational contact based on increase bioturbation, phosphate.
- 128.3-129.8 Dolomitic L.S.: lt. gray (N7), argillaceous, arenaceous, 45% f.-m.g. sand, subangular to subrounded, 45% clay, 7% v.c. qtz. & phos. calcite, 2% shell molds, bioturbated, low permeability.
- 129.8-130.9 Dolomitic L.S.: lt. gray (N7), argillaceous, arenaceous, 40% f.-m.g. sand, subrounded to subangular, 20% clay, 15% v.c. qtz. & phos. calcite grains, 15% shell molds, bioturbated, fossiliferous, low permeability.
- 130.9-131.6 Dolomitic L.S.: lt. gray (N7), argillaceous, arenaceous, 45% f.-m.g. sand, subrounded to subangular, 20% clay, 15% v.c. qtz. & phos. calcite grains, 10% shell molds & casts, bioturbated, poorly indurated, low permeability.
- 135.9-136.7 Core loss

- 136.7-145.7 Calcareous Sand: lt. gray (N7), poorly indurated loose quartz sand, poorly sorted, good permeability, fair effective porosity. Contact based on change in lithology.
- 136.7- 137.6 Calcareous Sand: lt. gray (N7), poorly sorted sand, 45% c.-v.c. sand, 35% m.g. sand, subangular to subrounded, 2% clay, poorly indurated, friable, good permeability, fair effective porosity.
- 137.6-139.1 Calcareous Sand: alternating layers of poorly sorted calcareous sand (lt. gray (N7)) & calcareous fat clay (very lt. gray (N8)), the clay lenses (30%) are about 1" in thickness, 35% c.g. sand, subrounded, 25% f.-m.g. sand, subangular to subrounded, 10% v.c. sand, subrounded, friable, poorly indurated, fair permeability, fair effective porosity.
- 139.1 -139.7 Calcareous Sand: lt. gray (N7), 60% c.-v.c. sand, subrounded, 30% f.-m.g. sand, subangular to subrounded, 2% clay, clean, friable, poorly sorted, poorly indurated, good permeability, fair effective porosity.
- 139.7-140 Dolomitic L.S.: very lt. gray (N8), arenaceous, argillaceous, 40% f.-m.g. sand, subrounded, 30% v.c.g. sand, subrounded, poorly sorted sand, 15% clay, med. hard, vugs present, low permeability.
- 140-141.1 Calcareous sand: lt. gray (N7), poorly sorted sand, 65% c.g. sand, subrounded, 20% f.-m.g. sand, subangular to subrounded, 10% v.c.g. sand, subrounded, 2% clay, 0.5% mica, poorly indurated to loose, friable, good permeability, fair effective porosity.
- 141.1-142 Core Loss
- 142-143.8 Calcareous Sand: lt. gray (N7), poorly sorted sand, 60% c.g. sand, subrounded, 15% f.-m.g. sand, subangular to subrounded, 5% v.c.g. sand, subrounded, 2% shell molds & casts, 5% thin tan gray fat clay lenses about 1/2 inch thick, friable, poorly indurated to loose, good permeability, fair effective porosity.
- 143.8-144.1 Dolomitic L.S.: very lt. gray (N8), alternating layers of calcareous poorly sorted sand and calcareous tan gray clay, 60% c.g. subrounded sand, 15% f.-m.g. subangular to subrounded sand, 5% c.g. subrounded sand, 10% calcareous clay, med. hard, friable, bioturbated, fair permeability, fair effective porosity.
- 144.1-145.7 Calcareous Sand: lt. gray (N7), poorly sorted sand, 60% c.g. rounded sand, 15% m.g. subangular sand, 5% v.c.g.

rounded sand, 5% calcareous tan gray clay (1/4" to 1.5" in thickness), poorly indurated to loose, good permeability, fair effective porosity.

- 145.7-155.5 Dolomitic L.S.: lt. gray (N7), arenaceous, argillaceous, bioturbated, soft, good confining unit. Contact based on lithology change.
- 145.7-148.2 Dolomitic L.S.: lt. gray (N7), 40% c.g. subrounded sand, 15% v.f.-m.g. subrounded, 5% v.c. subrounded sand, 15% clay, 3% shell molds, continuous, friable, some vugs, med. hard, low permeability
- 148.2-148.6 Dolomitic L.S.: lt. gray (N7), 40% c.g. subrounded sand, 15% v.f.-m.g. subrounded, 5% v.c. subrounded sand, 15% clay, 3% shell molds, poorly indurated to loose, low permeability.
- 148.6-150.3 Dolomitic L.S.: lt. gray (N7), 45% f.-m.g. sand, subrounded to subangular, 10% v.c.g. subrounded sand, 25% clay, 0.5% mica flakes, 0.5% large qtz. grains (8mm in diam.), 2% brachiopods, 20% shell molds, fossiliferous (*Chesapecten* cf., and brachiopod *Lingula*), bioturbated, continuous, low permeability.
- 150.3-153 Dolomitic L.S.: lt. gray (N7), 50% f.-m.g. sand, subrounded to subangular, 10% v.c.g. subrounded sand, 25% clay, 0.5% mica flakes, 0.5% large qtz. grains (8mm in diam.), 2% phosphate, 2% brachiopods, 3% shell molds, mottled, continuous, low permeability.
- 153-155.5 Dolomitic L.S.: lt. gray (N7), 40% f.-m.g. sand, subrounded to subangular, 15% v.c.g. sand, subrounded, 25% clay, 2% phosphate, 1% mica flakes, med.soft, continuous, mottled, low permeability, good confining unit.

Description of cuttings from Well KBMP 6, Site 2

Driller: Corps of Engineers, Savannah, GA

Latitude/Longitude: 30°43'10", 81°27'26"

Altitude: 6.86 ft. above mean low water

Total Depth: 170 ft.

(Colors were dry samples matched to the Rock Color Chart, GSA, 1984)

<u>Depth in ft. below land surface</u>	<u>Description</u>
Holocene to Pleistocene Undifferentiated	
0-10	Sand: Lt. olive gray (5Y6/1), v.f.-f.g., subangular, well sorted, 5% heavy minerals, trace of mica
10-20	Sand: same as previous section
20-30	Sand: Lt. olive gray (5Y6/1), v.f.-f.g., subangular, well sorted, 7% shell fragments, 5% heavy minerals, trace of mica.
30-40	Sand: Lt. gray (N7), v.f.-f.g., subangular, well sorted, 3% heavy minerals, 3% mica.
45-50	Sandy Clay: Med. lt. gray (N6), 35% v.f.-f.g. sand, subangular, 45% clay, 3% heavy minerals.
Pliocene Series	
50-61.5	Clayey Sand: Lt. gray (N7), v.f.-f.g., subangular, 10% shell fragments, 10% clay, 3% heavy minerals.
Middle Miocene Series Upper Charlton Formation	
61.5-170	Dolomitic Limestone: olive gray (5Y6/1), argillaceous, arenaceous, phosphatic, 20% granule size sand. Contact based on top of rock.
61.5-65	Dolomitic L.S.: Lt. olive gray (5Y6/1), 45% v.f.-f.g. sand, subangular, (wash down), 10% broken shells, 5% clay, 2% phosphate.
65-70	Dolomitic L.S.: Same as previous section
70-80	Dolomitic L.S.: Lt. olive gray (5Y6/1), 45% f.g. sand, subangular, 15% clay, 10% broken shell fragments, 5% heavy minerals, 2% phosphate.

- 80-90 Dolomitic L.S.: Yellow gray (5Y8/1), 40% f.-m.g. sand, subangular, 20% clay, 5% shell fragments, 5% heavy minerals, 2% phosphate, 1% mica, argillaceous.
- 90-100 Dolomitic L.S.: Lt. olive gray (5Y6/1), 40% f.-m.g. sand, subangular, 25% clay, 15% v.c. sand to fine gravel, subrounded, 5% heavy minerals, 5% phosphate, 1% mica, argillaceous.
- 100-110 Dolomitic L.S.: Lt. olive gray (5Y6/1), 40% f.-m.g. sand, subangular, 25% clay, 20% v.c. sand to fine gravel, subrounded, 7% phosphate, 3% heavy minerals, 1% mica, argillaceous.
- 110-120 Dolomitic L.S.: Lt. olive gray (5Y6/1), 40% f.-m.g. sand, subangular, 30% calcareous clay, 25% v.c. sand to fine gravel, subrounded, 5% shells, 5% phosphate, argillaceous.
- 120-130 Dolomitic L.S.: Lt. olive gray (5Y6/1), 40% f.-m.g. sand, subangular, 30% clay, 20% c. sand to fine gravel, subrounded, 7% phosphate, 3% heavy minerals, 1% mica, argillaceous.
- 130-140 Dolomitic L.S.: Lt. olive gray (5Y6/1), 40% clay, 35% f.-m.g. sand, subangular, poorly sorted, 20% c. sand to fine gravel, subrounded, 3% phosphate, 3% heavy minerals, 1% mica, argillaceous.
- 140-145 Dolomitic L.S.: Lt. olive gray (5Y6/1), 45% calcareous clay, 30% f.-m.g. sand, subangular, 20% v.c. sand to fine gravel, subrounded, 5% phosphate, 3% heavy minerals, argillaceous.
- 145-155 Dolomitic L.S.: Lt. olive gray (5Y6/1), 30% f.-m.g. sand, subangular, 45% calcareous clay, 20% v.c. sand to fine gravel, subrounded, 3% phosphate, argillaceous.
- 155-160 Dolomitic L.S.: Lt. olive gray (5Y6/1), 30% f.-m.g. sand, subangular, 30% v.c. sand to fine gravel, subrounded, 25% clay, 3% phosphate, argillaceous.
- 160-165 Dolomitic L.S.: Lt. olive gray (5Y6/1), 30% f.-m.g. sand, subangular, 45% calcareous clay, 20% v.c. sand to fine gravel, subrounded, 3% phosphate, 2% phosphate, argillaceous.
- 165-170 Dolomitic L.S.: Lt. olive gray (5Y6/1), 30% f.-m.g. sand, subangular, 50% clay, 15% v.c. sand to fine gravel, subrounded, 3% phosphate, 2% phosphate, argillaceous.

Description of cuttings from Well KBMP 10, Site 3

Driller: Corps of Engineers, Savannah, GA
 Latitude/Longitude: 30°44'51", 81°28'0"
 Altitude: 15.93 ft. above mean low water
 Total Depth: 133 ft.

(Colors were dry samples matched to the Rock Color Chart, GSA, 1984)

<u>Depth in ft. below land surface</u>	<u>Description</u>
Pleistocene Series	
5-10	Sand: Grayish orange (10YR7/4), v.f.-f.g., well sorted, angular to subangular, 10% shell fragments, 3% heavy minerals, 1% mica.
10-20	Sand: same as previous section
20-30	Sand: same as 0-10 section
30-35	Clayey Sand: Yellowish gray (5Y8/1), 50% v.f.g. silty sand, subangular, 40% gray clay chunks approximately 5mm in diameter, 3% shell fragments.
35-40	Clayey Sand: Yellowish gray (5Y8/1), 45% v.f.g. silty sand, subangular, 45% gray clay, 10% shell fragments, 10% heavy minerals.
40-45	Clayey Sand: Yellowish gray (5Y8/1), 50% gray clay, 40% v.f.g. silty sand, subangular, 10% shell fragments, 10% heavy minerals.
45-50	Clay: Lt. gray (N7), fat, clean, 10% oyster shells and other.
50-55	Clay: same as previous section.
55-60	Sandy Clay: Lt. gray (N7), 50% fat gray clay, 40% v.f.-f.g. sand, subangular, 15% broken shell fragments, 3% heavy minerals, 2% mica.
60-62	Sandy Clay: same as previous section
Pliocene Series	
Duplin Formation	
62-80	Sand: lt. gray (N7), poorly sorted, subangular to subrounded, grading into clayey sand and clay towards the base of this section,

good permeability from 65-72'. Contact based on change in lithology.

- 62-65 Clayey Sand: Lt. gray (N7), 55% f.-m.g. sand, subangular, 20% clay, 20% shell fragments often 2mm in diameter.
- 65-72 Sand: Lt. gray (N7), f.-c.g. sand, subangular to subrounded, poorly sorted, 25% of sand is granule in size, 25% coarse shell fragments, 3% clay, good permeability.
- 72-75 Clayey Sand: Med. lt. gray (N6), f.-c.g. sand, subangular to subrounded, poorly sorted, 25% coarse shell fragments, 20% clay, slightly calcareous.
- 75-80 Sandy Clay: Yellowish gray (5Y8/1), 40% clay, 30% f.-c.g. sand, subangular, poorly sorted, 15% limestone fragments, 15% shell fragments.

Middle Miocene Series

Upper Charlton Formation

80-133

Limestone, fractured at the top of rock becoming a very dense dolomite at 89'. From 100-132' sandy clay with dolomite fragments, phosphatic. A very dense dolomite is present at the base of this section. Contact based on top of rock.

- 80-88 Limestone: Very lt. gray (N8), 15% f.-c.g. sand, subangular, 15% broken shell fragments, 3% clay, fossiliferous.
- 89-95 Dolomite: Med. lt. gray (N6), very hard, slow drilling time.
- 95-100 Dolomite: Lt. gray (N7), 30% clay, 20% oyster, pelecypod & other shell fragments, 10% f.-c.g. sand, subangular to subrounded, 3% phosphate, argillaceous.
- 100-110 Sandy Clay: Lt. gray (N7), 40% gray clay, 30% v.f.-c. sand, subangular to subrounded, 20% dolomite fragments, 10% shell fragments, 5% phosphate (right on with gamma), slightly calcareous.
- 110-115 Sandy Clay: Lt. gray (N7), 40% gray clay, 25% m.-c. sand, subangular to subrounded, poorly sorted, 3% heavy minerals, 2% phosphate, slightly calcareous.
- 115-120 Sandy Clay: Lt. gray (N7), 40% gray clay, 40% v.f.-c. sand, subangular to subrounded, poorly sorted, 3% shell fragments, 3% heavy minerals, 1% phosphate, slightly calcareous.

- 120-132 Clayey Sand: Lt. gray (N7), 40% gray, fat, clay, 35% v.f.-c. sand, subangular to subrounded, poorly sorted, 10% fine gravel, subrounded, 7% oyster & other shell fragments, 5% phosphate, 1% heavy minerals, slightly calcareous.
- 133 Dolomite: Lt. gray (N7), 30% clay, 20% f.-c.g. sand, subangular, 15% gravel, subrounded, 5% shell fragments, 3% phosphate, argillaceous, hard, slow drill time.

APPENDIX C

Estimation of Hydraulic Conductivity Based on Grain Size Analysis

Masch and Denny (1966) presented a method in which the standard deviation of the sample is incorporated in the process of determining the hydraulic conductivity. Estimation of hydraulic conductivity is more accurate when the standard deviation of the gradation curve is taken into account. First, the gradation curve is plotted using Krumbein's ϕ units (see figure C1). Next, the standard deviation of the sample is calculated by:

$$s = \frac{d_{16} - d_{84}}{4} + \frac{d_5 - d_{95}}{6.6} \quad (C1)$$

Knowing the median grain size (d_{50}) derived from the grain size analysis (figure C1) and the standard deviation of the sample, the hydraulic conductivity may be estimated from graph C2. The curves in figure C2 were developed experimentally by testing a group of unconsolidated sand samples (Masch and Denny, 1966).

The method employed to approximate hydraulic conductivity and does not take into account factors such as natural particle arrangement, stratification, or the anisotropy of the zone. Also, the samples tested are not representative of the grain-size characteristics of the entire zone. Although these factors are not considered, the approximation for hydraulic conductivity based on grain size provides a suitable range of values for field samples.

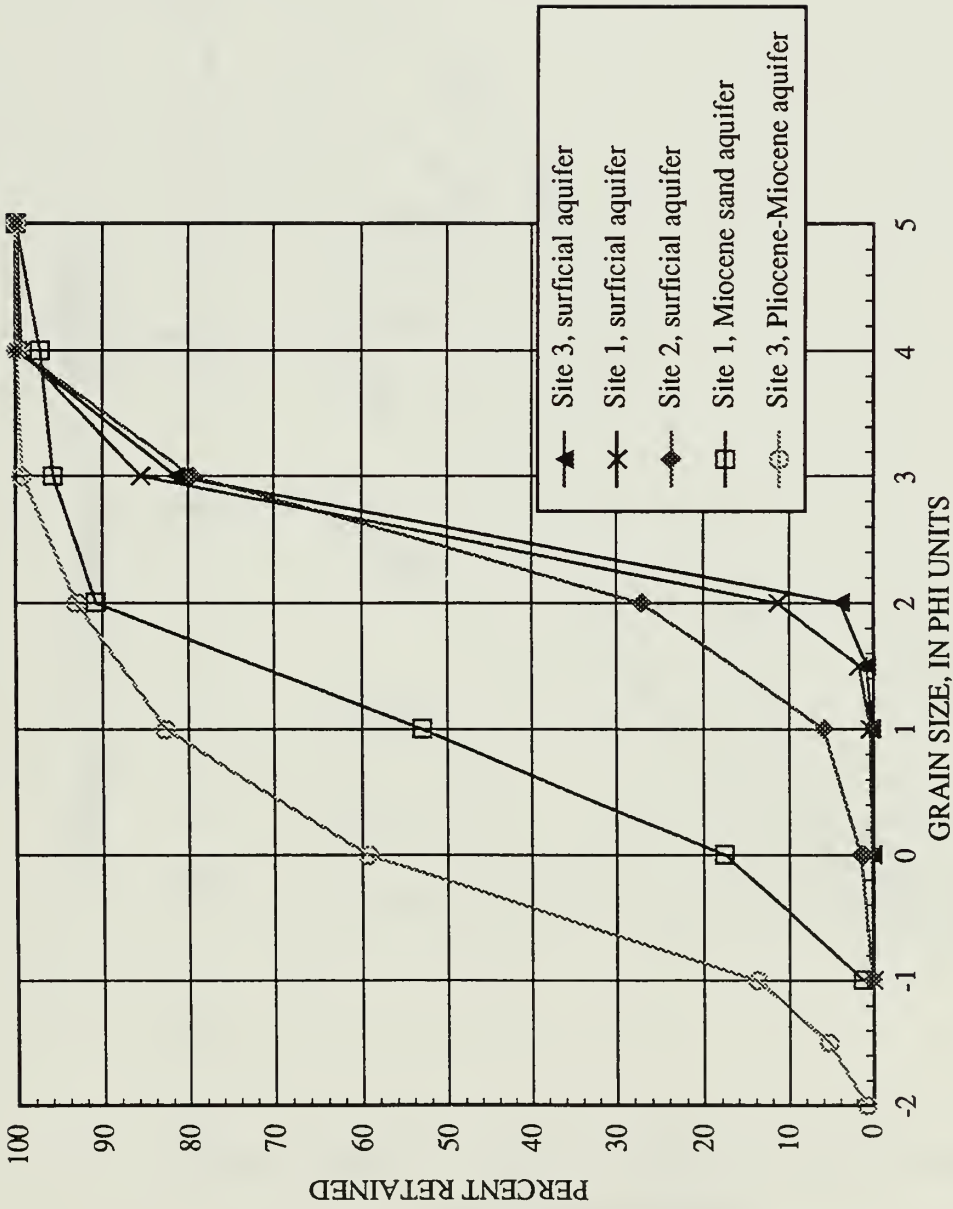
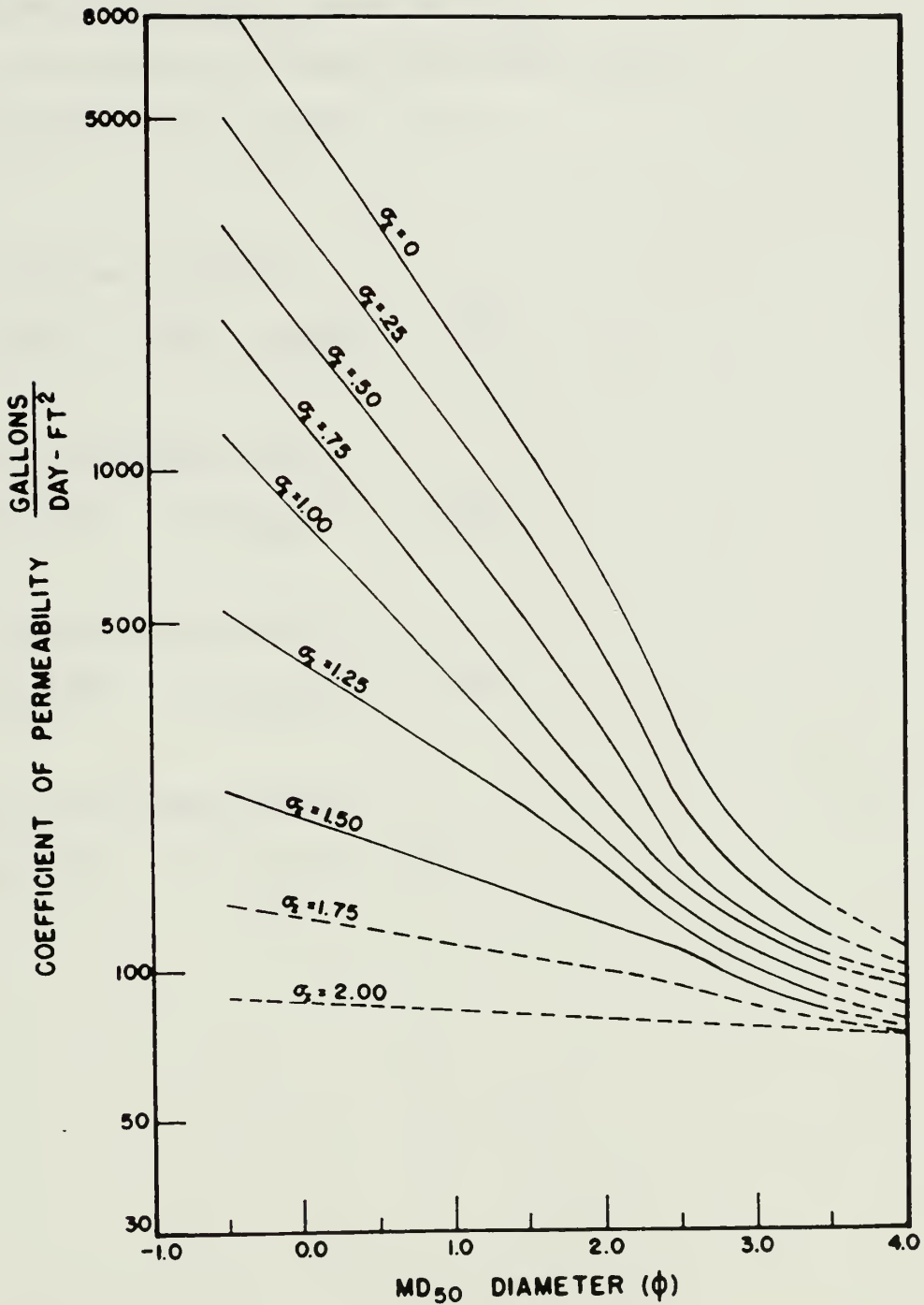


Figure C1. Grain size distribution curves, in phi units.



C2. Estimation of hydraulic conductivity once d_{50} and the standard deviation are known (Masch and Denny, 1966).

Calculation of the standard deviation of each sample.

Site 3, Pliocene sand of the Pliocene-Miocene aquifer, KBMP 9

$$\frac{1.15 - (-0.9)}{4} + \frac{2.3 - (-1.5)}{6.6} = 1.08$$

Site 1, Miocene sand, KBMP 1

$$\frac{1.8 - (-0.1)}{4} + \frac{2.85 - (-0.78)}{6.6} = 1.025$$

Site 2, Surficial aquifer, KBMP 5

$$\frac{3.21 - (1.45)}{4} + \frac{3.77 - (0.7)}{6.6} = 0.905$$

Site 1, Surficial Aquifer, KBMP 2

$$\frac{2.99 - (2.07)}{4} + \frac{3.65 - (1.65)}{6.6} = 0.533$$

Site 3, Surficial Aquifer, KBMP 8

$$\frac{3.12 - (2.15)}{4} + \frac{3.7 - (2.0)}{6.6} = 0.5$$

APPENDIX D

Density Corrections

Density Corrections

<u>Well number</u>	<u>Percent seawater</u>	<u>ρ_i (gm/cc)</u>	<u>ρ_i (lb/ft³)</u>
KBMP 01	32	1.008	62.93
KBMP 02	0.2	1.000	62.43
KBMP 03	68	1.017	63.49
KBMP 04	73	1.018	63.55
KBMP 05	3.0	1.001	62.49
KBMP 06	89	1.022	63.80
KBMP 07	4.2	1.001	62.49
KBMP 08	0.7	1.000	62.43
KBMP 09	0.2	1.000	62.43
KBMP 10	0.2	1.000	62.43
KBMP 11	5.2	1.017	62.49

The following equation was used to convert percent seawater to density:

$$\rho = (\text{percent seawater})(0.025 \text{ gm/cc}) + 1.0 \text{ gm/cc}$$

The freshwater head in a well containing saline water is calculated by the following equation:

$$H_{if} = \frac{\rho_i H_{ip} - z(\rho_i - \rho_f)}{\rho_f} \quad (D1)$$

(Luszczynski, 1961) where:

i = any point in ground water of variable density

H_{if} = fresh water head at i

H_{ip} = point water head at i

z = elevation of i , measured positively upward

ρ_i = water density at i

ρ_f = fresh water density

KBMP 01 (146 ft deep) 32% seawater

$$H_{if} = \frac{(62.93 \text{ lb/ft}^3) (0.66 \text{ ft}) - (-141.4 \text{ ft}) (62.93 \text{ lb/ft}^3 - 62.43 \text{ lb/ft}^3)}{62.43 \text{ lb/ft}^3}$$

$$H_{if} = 1.80 \text{ ft}$$

KBMP 03 (94 ft deep) 68% seawater

$$H_{if} = \frac{(63.49 \text{ lb/ft}^3) (0.15 \text{ ft}) - (-89.4 \text{ ft}) (63.49 \text{ lb/ft}^3 - 62.43 \text{ lb/ft}^3)}{62.43 \text{ lb/ft}^3}$$

$$H_{if} = 1.67 \text{ ft}$$

KBMP 04 (95 ft deep) 73% seawater

$$H_{if} = \frac{(63.55 \text{ lb/ft}^3) (3.87 \text{ ft}) - (-88.14 \text{ ft}) (63.55 \text{ lb/ft}^3 - 62.43 \text{ lb/ft}^3)}{62.43 \text{ lb/ft}^3}$$

$$H_{if} = 5.52 \text{ ft}$$

KBMP 05 (44 ft deep) 3% seawater

$$H_{if} = \frac{(62.49 \text{ lb/ft}^3) (4.41 \text{ ft}) - (-37.14 \text{ ft}) (62.49 \text{ lb/ft}^3 - 62.43 \text{ lb/ft}^3)}{62.43 \text{ lb/ft}^3}$$

$$H_{if} = 4.44 \text{ ft}$$

KBMP 06 (71 ft deep) 89% seawater

$$H_{if} = \frac{(63.80 \text{ lb/ft}^3) (3.83 \text{ ft}) - (-64.14 \text{ ft}) (63.80 \text{ lb/ft}^3 - 62.43 \text{ lb/ft}^3)}{62.43 \text{ lb/ft}^3}$$

$$H_{if} = 5.32 \text{ ft}$$

KBMP 07 (89 ft deep) 4.2% seawater

$$H_{if} = \frac{(62.49 \text{ lb/ft}^3) (2.55 \text{ ft}) - (-73.07 \text{ ft}) (62.49 \text{ lb/ft}^3 - 62.43 \text{ lb/ft}^3)}{62.43 \text{ lb/ft}^3}$$

$$H_{if} = 2.62 \text{ ft}$$

KBMP 11 (95 ft deep) 5.2% seawater

$$H_{if} = \frac{(62.49 \text{ lb/ft}^3) (2.55 \text{ ft}) - (-79.07 \text{ ft}) (62.49 \text{ lb/ft}^3 - 62.43 \text{ lb/ft}^3)}{62.43 \text{ lb/ft}^3}$$

$$H_{if} = 2.62 \text{ ft}$$

APPENDIX E

Leakage and Analytical Model Calculations

Steady state vertical leakage between the shallow aquifers.

The horizontal hydraulic conductivity for a clean clay based on table 2.2 from Freeze and Cherry (1979) is 1.0×10^{-2} ft/d. The vertical hydraulic conductivity is assumed to be a half an order of magnitude smaller than the horizontal hydraulic conductivity. Therefore the vertical hydraulic conductivity for the Pleistocene aquiclude is assumed to be 5.0×10^{-3} ft/d. The vertical hydraulic conductivity for the Hawthorn and Charlton Formations is 1.0×10^{-3} ft/d (Brown, 1984). The vertical hydraulic conductivity of the confining layer between the Pliocene sand and the Miocene limestone is 1.7×10^{-2} ft/d based on aquifer test results. All water levels were measured 6/28/90.

The leakage equation is expressed as:

$$q = \frac{K' \phi_{ext} - \phi}{b'}$$

q = the leakage rate or the volume of water flowing per unit time through a unit cross-sectional area [ft/d]

K' = vertical hydraulic conductivity of the confining layer [ft/d]

ϕ_{ext} = potentiometric head of the overlying or underlying zone [ft]

ϕ = potentiometric head in the aquifer [ft]

b' = confining layer thickness [ft] (Bear, 1979).

Where the leakage rate, q , is negative, groundwater is leaving the aquifer. Where the leakage rate is positive, groundwater is entering the aquifer.

Leakage from the surficial aquifer to the Pliocene-Miocene aquifer at site 3

Water levels above mean sea level : KBMP 8 = 4.93 ft

KBMP 9 = 2.48 ft

$$q = \frac{(5.0 \times 10^{-3} \text{ ft/d}) (2.45 \text{ ft})}{30 \text{ ft}}$$

$$q = 4.08 \times 10^{-4} \text{ ft/d}$$

Volumetric leakage for one square mile:

$$1 \text{ mi}^2 = 2.79 \times 10^7 \text{ ft}^2$$

$$(4.08 \times 10^{-4} \text{ ft/d}) (2.79 \times 10^7 \text{ ft}^2) = 1.14 \times 10^4 \text{ ft}^3/\text{d}$$

$$1.14 \times 10^4 \text{ ft}^3/\text{d} \times 7.481 \text{ gal/ft}^3 = 8.52 \times 10^4 \text{ gal/d}$$

Leakage from the Pliocene-Miocene aquifer to the surficial aquifer at site 2.

Water levels above mean sea level : KBMP 4 = 5.52 ft

$$\text{KBMP 5} = 4.44 \text{ ft}$$

$$q = \frac{(5.0 \times 10^{-3} \text{ ft/d}) (-1.08 \text{ ft})}{17 \text{ ft}}$$

$$q = -3.17 \times 10^{-4} \text{ ft/d}$$

Leakage from the Pliocene-Miocene aquifer to the surficial aquifer site 1.

Water levels above mean sea level : KBMP 3 = 1.67 ft

$$\text{KBMP 2} = 0.5 \text{ ft}$$

$$q = \frac{(1.0 \times 10^{-3} \text{ ft/d}) (-1.17 \text{ ft})}{56 \text{ ft}}$$

$$q = -2.09 \times 10^{-5} \text{ ft/d}$$

Leakage from the Miocene sand aquifer to the Pliocene-Miocene aquifer at site 1.

Water levels above mean sea level : KBMP 1 = 1.8 ft

$$\text{KBMP 3} = 1.67 \text{ ft}$$

$$q = \frac{(1.0 \times 10^{-3} \text{ ft/d}) (0.13 \text{ ft})}{42 \text{ ft}}$$

$$q = 3.1 \times 10^{-6} \text{ ft/d}$$

Leakage from the Charlton limestone (KBMP 7) to the Duplin sand (KBMP 9) at site 3.

K' was calculated from leakance values obtained through aquifer testing.

$$\text{Water levels above mean sea level : KBMP 9} = 2.48 \text{ ft}$$

$$\text{KBMP 7} = 2.62 \text{ ft}$$

$$q = \frac{(1.7 \times 10^{-2} \text{ ft/d}) (0.14 \text{ ft})}{8 \text{ ft}}$$

$$q = 2.97 \times 10^{-4} \text{ ft/d}$$

Volumetric leakage from the Charlton limestone to the Duplin sand for a one square mile area.

$$1 \text{ mi}^2 = 2.79 \times 10^7 \text{ ft}^2$$

$$(2.97 \times 10^{-4} \text{ ft/d}) (2.79 \times 10^7 \text{ ft}^2) = 8.29 \times 10^3 \text{ ft}^3/\text{d}$$

$$8.29 \times 10^3 \text{ ft}^3/\text{d} \times 7.481 \text{ gal/ft}^3 = 6.2 \times 10^4 \text{ gal/d}$$

The amount of recharge to the island is an estimated value based on results of Brown (1984). An annual water budget for the surficial aquifer was not determined during this study. Therefore the calculated recharge volume represents an approximate value which is applied to quantitatively define the system flow.

Total recharge to the surficial aquifer by precipitation for 1 year:

$$6 \text{ inches of recharge} \times 1 \text{ mi}^2 = 1.39 \times 10^7 \text{ ft}^3$$

$$1.39 \times 10^7 \text{ ft}^3 \times 7.481 \text{ gal/ft}^3 = 104 \times 10^6 \text{ gal/mi}^2$$

Seepage discharge from the surficial aquifer:

$$q = [K \frac{(h_1^2 - h_2^2)}{2L}]$$

(Raudkivi and Callander, 1976).

K = hydraulic conductivity of the surficial aquifer = 21 ft/d

h_1 = water level at site 3 = 4.93 ft

h_2 = water level at the seepage face = 0 ft

L = length from center of the island = 2640 ft

$$q = \frac{21 \text{ ft/d} [(4.93 \text{ ft})^2 - (0 \text{ ft})^2]}{2 (2640 \text{ ft})}$$

$$q = 0.096 \text{ ft}^2/\text{d}$$

Total discharge for the distance of 1 mile:

$$1 \text{ mile} = 5280 \text{ ft}$$

$$0.096 \text{ ft}^2/\text{d} \times 5280 \text{ ft} = 506.88 \text{ ft}^3/\text{d}$$

$$506.88 \text{ ft}^3/\text{d} \times 7.481 \text{ gal}/\text{ft}^3 = 3.79 \times 10^3 \text{ gal}/\text{d}$$

The calculated specific discharge along the seepage face near site 3 is valid given that a time-average mean is assumed where the water levels are at a constant altitude.

Analytical Model –

Recharge and discharge values were calculated for a 1 square mile area.

Total recharge from precipitation per year = $104 \times 10^6 \text{ gal}/\text{mi}^2$

Total recharge from precipitation per day = $2.85 \times 10^5 \text{ gal}/\text{mi}^2$

Total discharge along the seepage face $3.79 \times 10^3 \text{ gal}/\text{d} \times 2 = 7.58 \times 10^3 \text{ gal}/\text{d}$

Total discharge to the underlying Pliocene-Miocene age aquifer = $8.5 \times 10^4 \text{ gal}/\text{d}$

Discharge to the lakes and lowlying wetlands =

$$2.85 \times 10^5 \text{ gal}/\text{mi}^2 - 7.58 \times 10^3 \text{ gal}/\text{d} - 8.5 \times 10^4 \text{ gal}/\text{d} = 1.92 \times 10^5 \text{ gal}/\text{d}$$

APPENDIX F

Step Drawdown

Step drawdown test

The step-drawdown test was conducted by selecting five pumping rates or steps each lasting 1.5 hours and measuring drawdown in the pumped well. The data provided from the test were used to determine the specific capacity of the well and the optimum pumping rate.

The rates chosen for the step-drawdown test were based on the thickness of the aquifer and the estimated hydraulic conductivity. Estimated hydraulic conductivity values were obtained from Table 2.2 from Freeze and Cherry (1979). The five rates chosen were: 1.34, 2.67, 4.01, 5.35 and 6.69 ft³/min; the actual rates pumped were 1.47, 3.08, 3.61 and 4.68 ft³/min. The first three rates were conducted for 1.5 hours each. Thirty minutes into the fourth step (4.68 ft³/min.) the water level declined below the intake hose causing pumping to cease and the step-drawdown test to be discontinued.

The data provided by the three successful steps were used to determine the optimum pumping rate by comparing the specific capacities of each step. The specific capacity decreases as the degree of turbulent head loss increases. Based on the specific capacities calculated for the three rates, the optimum pumping rate for the aquifer test was 1.47 ft³/min. The rate used for the aquifer test was 1.54 ft³/min (see figure F1b).

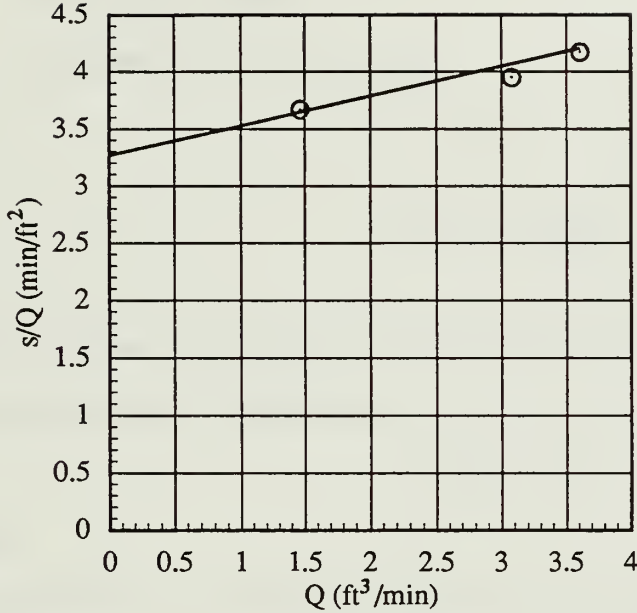
C.E. Jacob (1947) presented a method to evaluate the head loss resulting from turbulent flow in an artesian well by means of a step-drawdown test. As described by Theis (1935), drawdown in a confined aquifer under laminar flow conditions is expressed:

$$s = \frac{Q}{4\pi T} W(u) \quad (F1)$$

where

s = drawdown [ft]

A.



$B = 3.25 \text{ min/ft}^2$ (intercept)

$C = 0.25 \text{ min}^2/\text{ft}^5$ (slope)

B.

Q (ft ³ /min)	s (ft)	s (total)	s/Q (min/ft ²)	n	Q/s (ft ² /min)
1.47	5.4	5.4	3.67	89%	0.272
3.08	6.78	12.18	3.95	80%	0.253
3.61	2.9	15.08	4.17	78%	0.239

Figure F1. A. Plot of s/Q vs. Q to determine B and C values. B. Table of discharge, drawdown, percent of head loss due to laminar flow, and specific capacity.

Q = pumping [ft^3/min]

T = transmissivity [ft^2/min]

$W(u)$ = well function

Equation (F1) can be shortened to

$$s = BQ \quad (\text{F2})$$

$$\text{where } B = \frac{W(u)}{4\pi T}$$

Total drawdown in the discharging well includes both laminar flow and turbulent flow (Jacob, 1947) and is expressed as:

$$s = BQ + CQ^2 \quad (\text{F3})$$

where

B = the head loss in the formation per unit discharge (aquifer constant) [min/ft^2];

C = the head loss in the well due to turbulence per unit discharge squared (well loss constant) [min^2/ft^5]; and

Q = the discharge rate [ft^3/min]. By dividing equation (F3) by Q , the equation becomes

$$s/Q = CQ + B, \quad (\text{F4})$$

which is a linear equation. If s/Q and Q are plotted on arithmetic graph paper, the slope of the line formed equals C and the intercept equals B (see figure F1a for B and C values).

Once B and C are known, the percentage of total head loss due to laminar flow can be calculated by dividing the laminar head loss by the total head loss

$$n = \frac{BQ}{BQ + CQ^2} \times 100 \quad (\text{F5})$$

where n equals the efficiency of the discharging well (Driscoll, 1986).

For a pumping rate of 1.47 ft³/min., 89 percent of the head loss is attributable to laminar flow (see figure F1b for n values for each step). But the percentages calculated, n , do not represent true well efficiency. To derive the true well efficiency, the aquifer transmissivity must be determined by performing a constant-rate test. Then, the well efficiency is calculated by dividing the actual specific capacity, $(Q/s)_{\text{Actual}}$, by the theoretical specific capacity. The theoretical specific capacity is expressed as:

$$(Q/s)_{\text{Theoretical}} = T/2000 \quad (\text{F6})$$

(Driscoll, 1986). The theoretical specific capacity is an empirical equation derived by assuming an average well diameter (0.5 ft.), an average duration of pumping (24 hrs.), and typical storage coefficient value for a confined aquifer (1.0×10^{-3}) (Driscoll, 1986). The well efficiency calculated for KBMP 7 at a pumping rate of 1.54 ft³/min. is 82 percent (Calculations follow).

Step Drawdown Data

Head loss in well due to laminar flow (n). From Driscoll (1986), (n) is calculated from:

$$n = \frac{BQ}{BQ + CQ} \times 100$$

From the graph of Q vs. s/Q:

$$B = 3.25 \text{ min/ft}^2$$

$$C = 0.25 \text{ min}^2/\text{ft}^5$$

For Q = 1.47 ft³/min

$$n = \frac{(3.25 \text{ min/ft}^2)(1.47 \text{ ft}^3/\text{min})}{(3.25 \text{ min/ft}^2)(1.47 \text{ ft}^3/\text{min}) + (0.25 \text{ min}^2/\text{ft}^5)(1.47 \text{ ft}^3/\text{min})^2} = 89\%$$

For Q = 3.08 ft³/min

$$n = \frac{(3.25 \text{ min/ft}^2)(3.08 \text{ ft}^3/\text{min})}{(3.25 \text{ min/ft}^2)(3.08 \text{ ft}^3/\text{min}) + (0.25 \text{ min}^2/\text{ft}^5)(3.08 \text{ ft}^3/\text{min})^2} = 80\%$$

For Q = 3.61 ft³/min

$$n = \frac{(3.25 \text{ min/ft}^2)(3.61 \text{ ft}^3/\text{min})}{(3.25 \text{ min/ft}^2)(3.61 \text{ ft}^3/\text{min}) + (0.25 \text{ min}^2/\text{ft}^5)(3.61 \text{ ft}^3/\text{min})^2} = 78\%$$

Casing storage effects from (Driscoll, 1986)

$$t_c = \frac{0.6 (d_c^2 - d_p^2)}{Q/s}$$

d_c = diameter of casing = 4 inches

d_p = diameter of pump/discharge pipe = 5/8 inch

$$t_c = \frac{0.6 [(4)^2 - (5/8)^2]}{11.5/5.0} = 4.1 \text{ minutes}$$

at 4.1 minutes $s = 4.68$ ft

$$t_c = \frac{0.6 [(4)^2 - (5/8)^2]}{11.5/4.68} = 3.81 \text{ minutes}$$

at 3.81 minutes $s = 4.62$ ft

$$t_c = \frac{0.6 [(4)^2 - (5/8)^2]}{11.5/4.62} = 3.76 \text{ minutes}$$

at 3.76 minutes $s = 4.62$ ft

At 3.76 minutes the casing storage effects become negligible

OR

$$V = \pi r^2 h = (3.14) (0.166 \text{ ft})^2 (75.83 \text{ ft}) = 6.56 \text{ ft}^3 = 49.07 \text{ gal}$$

$$\frac{49.07 \text{ gal}}{11.5 \text{ gpm}} = 4.26 \text{ minutes}$$

At 4.26 minutes the casing storage effects become negligible

Pumping well efficiency

$$T = 650 \text{ ft}^2/\text{d} = 4863 \text{ gpd/ft}$$

Total drawdown after 371 minutes = 5.7 ft
(after this time water levels fluctuate with the tides)

$$(Q/s)_{\text{actual}} = 11.5 \text{ gpm} / 5.7 \text{ ft} = 2.0 \text{ gpm/ft}$$

$$(Q/s)_{\text{theoretical}} = T/2000 = \frac{4863 \text{ gpd/ft}}{2000} = 2.43 \text{ gpm/ft}$$

$$E = \frac{\text{actual specific capacity}}{\text{theoretical specific capacity}} = \frac{2.0}{2.43} = 82\% \text{ efficient}$$

APPENDIX G

Derivation of the Diffusion Equation

The diffusion equation is a combination of the Darcy's law and the principle of continuity. Darcy's law is expressed as:

$$Q = -K A \frac{\Delta h}{\Delta L} \quad (G1)$$

where:

Q = discharge rate [ft^3/d]

K = hydraulic conductivity [ft/d]

A = area [ft^2]

h = head [ft]

L = length [ft]

Dupuit (1848) made the assumption that within the cone of depression of a pumping well the head throughout a vertical line in the aquifer is constant and may be represented by the water level at a given point in the aquifer. If the aquifer is homogeneous and horizontal, then by the law of continuity ($Q_1 - Q_2 = 0$) virtually equal quantities of water are discharged from a pumping well as are discharged through any two concentric cylinders within the cone of depression. Under these conditions Darcy's law may be expressed as a first order differential equation where:

$$Q_1 = -2 \pi r_1 K b \left(\frac{dh}{dr_1} \right) \quad [\text{ft}^3/\text{d}] \quad (G2)$$

and

$$Q_2 = -2 \pi r_2 K b \left(\frac{dh}{dr_2} \right) \quad [\text{ft}^3/\text{d}] \quad (G3)$$

where

r_1 = distance from pumping well to the first concentric circle [ft]

Q_1 = discharge at r_1 [ft^3/d]

r_2 = distance from pumping well to the second concentric circle [ft]

Q_2 = discharge at r_2 [ft^3/d]

b = saturated thickness of aquifer [ft]

For steady state flow:

$$Q_1 - Q_2 = 0 \quad (G4)$$

For transient flow:

$$Q_1 - Q_2 = SA \frac{\partial h}{\partial t} \quad (G5)$$

S = Storage coefficient [dimensionless]

combining equations (G2) and (G3) yields:

$$Q_1 - Q_2 = -2 \pi K b \left(r_1 \left(\frac{\partial h}{\partial r} \right)_1 - r_2 \left(\frac{\partial h}{\partial r} \right)_2 \right) \quad (G6)$$

because $K_b = T$ equation (G6) may be expressed:

$$Q_1 - Q_2 = -2 \pi T \left(\left(r \frac{\partial h}{\partial r} \right)_2 - \left(r \frac{\partial h}{\partial r} \right)_1 \right) \quad (G7)$$

rearranging the equation in general form becomes:

$$Q_1 - Q_2 = 2 \pi T \frac{\partial (r \frac{\partial h}{\partial r})}{\partial r} \Delta r \quad (G8)$$

by substituting equation (G5) into equation (G8) results in:

$$S 2 \pi r \frac{\partial h}{\partial t} = 2 \pi T \left(r \frac{\partial^2 h}{\partial r^2} + \frac{\partial h}{\partial r} \right) \quad (G9)$$

dividing both sides of the equation by $2\pi Tr$ results in the partial differential equation for nonsteady flow or the diffusion equation:

$$\frac{1}{r} \frac{\partial h}{\partial r} + \frac{\partial^2 h}{\partial r^2} = \frac{S}{T} \frac{\partial h}{\partial t} \quad (G10)$$

(Lohman, 1972).

To solve the diffusion equation for nonsteady radial flow boundary conditions must be satisfied and are as follows:

$$\begin{aligned} h(r,t) \\ h(r,0) = h_0 \quad \text{for } r \geq 0 \\ h(\infty,t) = h_0 \quad \text{for } t \geq 0 \end{aligned}$$

If the rate of pumping is constant and the boundary conditions are applied, the equation (in SI units) may be expressed as:

$$s = \frac{Q}{4\pi T} \int_u^\infty \frac{e^{-u}}{u} du \quad (G11)$$

where

$$u = \frac{r^2 S}{4Tt}$$

expanding equation (G11)

$$s = \frac{Q}{4\pi T} \int_u^\infty \frac{1 - u + \frac{u^2}{2!} - \frac{u^3}{3!} \dots}{u} du \quad (G12)$$

dividing by u gives

$$s = \frac{Q}{4\pi T} \int_u^{\infty} \left(\frac{1}{u} - 1 + \frac{u}{2!} - \frac{u^2}{3!} \dots \right) du \quad (G13)$$

by integrating, the equation becomes

$$s = \frac{Q}{4\pi T} \left[\log_e u - u + \frac{u^2}{2 \cdot 2!} - \frac{u^3}{3 \cdot 3!} \dots \right]_u^{\infty} \quad (G14)$$

by applying the limits and solving equation (G14) results in

$$s = \frac{Q}{4\pi T} \left[-\text{Euler constant} - \left(\log_e u - u + \frac{u^2}{2 \cdot 2!} - \frac{u^3}{3 \cdot 3!} \dots \right) \right] \quad (G15)$$

or

$$s = \frac{Q}{4\pi T} \left[-.577216 - \log_e u + u - \frac{u^2}{2 \cdot 2!} + \frac{u^3}{3 \cdot 3!} \dots \right] \quad (G16)$$

for values of $u \leq 0.01$ equation (G16) may be terminated to the second term:

$$s = \frac{Q}{4\pi T} \left[-0.577216 - \log_e \frac{r^2 S}{4Tt} \right] \quad (G17)$$

or

$$s = \frac{Q}{4\pi T} \left[-\log_e \frac{4}{2.25} + \log_e \frac{4Tt}{r^2 S} \right] \quad (G18)$$

by converting to common log the equation becomes:

$$T = \frac{2.30Q}{4\pi s} \log_{10} \frac{2.25Tt}{r^2 S} \quad (G19)$$

in equation (G19) T, Q, S, and r are constants and the equation may be written :

$$T = \frac{2.30Q}{4\pi s} \left[\log_{10} \frac{2.25Tr}{S} + \log_{10} t \right] \quad (G20)$$

by differential calculus the equation becomes:

$$T = \frac{2.30Q}{4\pi ds/d\log_{10} t} \quad (G21)$$

By changing from derivatives to finite values the equation becomes:

$$T = \frac{2.30Q}{4\pi \Delta s / \Delta \log_{10} t} \quad (G22)$$

(Lohman, 1972) where

$\Delta s / \Delta \log_{10} t$ = the slope of the line (m) on semilogarithmic paper. Equation (G22) may be expressed as (Bixel and Van Poollen, 1967):

$$T = \frac{2.30Q}{4\pi m} \quad (G23)$$

APPENDIX H

Aquifer Test Data and Calculations for Transmissivity and Storage Values

Static water level = 2.76 ft above sea level

Time, in minutes	Drawdown, in feet	*Drawdown, in feet		Time, in minutes	Drawdown, in feet	*Drawdown, in feet
0.5	1.34	1.34		191	5.27	5.54
1	3.65	3.65		221	5.29	5.58
1.5	4.14	4.14		251	5.32	5.62
2	4.35	4.35		281	5.37	5.66
3	4.55	4.55		311	5.42	5.69
4	4.68	4.68		371	5.51	5.7
5	4.8	4.8		431	6.12	6.16
6	4.86	4.86		491	6.23	6.13
7	4.93	4.93		551	6.29	6.07
8	4.99	4.99		611	6.32	6.06
9	5.01	5.01		671	6.3	6.12
10	5.06	5.06		731	6.19	6.15
15	5.14	5.14		791	6.08	6.18
20	5.24	5.24		851	5.89	6.13
25	5.25	5.25		911	5.71	6.06
30	5.28	5.28		971	5.57	6
35	5.3	5.3		1031	5.53	5.99
40	5.31	5.31		1151	5.76	6.08
45	5.31	5.31		1271	5.92	6.11
50	5.32	5.32		1391	6.15	6.06
55	5.31	5.31		1514	6.09	6.03
60	5.33	5.33		1574	6.02	6.1
65	5.34	5.34		1601	5.68	5.82
70	5.33	5.33		1721	5.54	5.83
75	5.34	5.34		1841	5.66	5.93
80	5.35	5.35		1961	5.92	5.89
85	5.33	5.33		2301	6.14	6.07
90	5.36	5.36		2391	5.86	6.15
95	5.34	5.34		2514	5.61	6.04
100	5.32	5.46		3634	5.84	6.26
130	5.3	5.49		2754	6.15	6.14
160	5.3	5.54		2814	6.19	6.04

* Drawdown data corrected for tidal and barometric fluctuations

Table H1. Drawdown data for KBMP 7, December 8, 1989.

Water level at maximum drawdown = 3.28 ft below sea level

Time, in minutes	Recovery, in feet	*Recovery, in feet		Time, in minutes	Recovery, in feet	*Recovery, in feet
1	4.16	4.16		80	5.61	5.61
1.5	4.39	4.39		85	5.63	5.63
2	4.52	4.52		90	5.64	5.64
2.5	4.61	4.61		95	5.65	5.65
3	4.69	4.69		100	5.67	5.67
3.5	4.75	4.75		130	5.74	5.74
4	4.8	4.8		150	5.79	5.79
4.5	4.85	4.85		180	5.87	5.79
5	4.91	4.91		210	5.94	5.79
6	4.97	4.97		240	6.03	5.79
7	5.03	5.03		270	6.11	5.82
8	5.07	5.07		300	6.17	5.85
9	5.11	5.11		360	6.2	5.87
10	5.15	5.15		420	6.13	5.82
11	5.17	5.17		480	6	5.8
12	5.2	5.2		540	5.91	5.89
14	5.23	5.23		600	5.84	5.99
15	5.25	5.25		660	5.79	6.08
20	5.34	5.34		720	5.77	6.11
25	5.39	5.39		780	5.78	6.04
30	5.42	5.42		840	5.87	5.98
35	5.46	5.46		900	6.03	5.97
40	5.49	5.49		960	6.24	6.01
45	5.5	5.5		1020	6.44	6.07
50	5.52	5.52		1080	6.57	6.13
55	5.55	5.55		1140	6.55	6.1
60	5.56	5.56		1260	6.24	6.02
65	5.58	5.58		1380	6.03	6.16
70	5.59	5.59		1500	5.94	6.23
75	5.61	5.61		1700	5.66	5.73

* Recovery data corrected for tidal and barometric fluctuations

Table H2. Recovery data for KBMP 7, December 10, 1989.

Static water level = 3.05 ft above sea level

Time, in minutes	Drawdown, in feet	*Drawdown, in feet		Time, in minutes	Drawdown, in feet	*Drawdown, in feet
1	0.01	0.01		220	0.97	1.22
2	0.18	0.18		250	0.98	1.23
3	0.31	0.31		280	1.01	1.25
4	0.4	0.4		340	1.05	1.21
5	0.5	0.5		400	1.17	1.25
6	0.56	0.56		460	1.24	1.19
7	0.6	0.6		520	1.35	1.18
8	0.64	0.64		580	1.41	1.19
9	0.7	0.7		640	1.42	1.19
10	0.73	0.73		700	1.37	1.24
15	0.81	0.81		760	1.29	1.28
20	0.88	0.88		820	1.19	1.31
25	0.91	0.91		880	0.99	1.23
30	0.95	0.95		940	0.82	1.16
35	0.96	0.96		1000	0.73	1.11
40	0.99	0.99		1120	0.79	1.13
45	0.97	0.97		1240	1.07	1.17
50	1.01	1.01		1360	1.22	1.1
55	1.02	1.02		1480	1.27	1.2
60	1.02	1.02		1600	1.16	1.28
65	1.02	1.02		1720	1.01	1.27
70	1.02	1.02		1840	1.1	1.31
75	1.02	1.02		1960	1.31	1.29
80	1.02	1.02		2080	1.45	1.2
85	1	1.12		2200	1.49	1.29
90	0.99	1.13		2320	1.27	1.31
95	0.99	1.12		2440	0.95	1.27
100	0.99	1.14		2560	0.86	1.24
130	0.99	1.2		2680	1.1	1.28
160	0.98	1.21		2800	1.3	1.24
190	0.96	1.2				

* Drawdown data corrected for tidal and barometric fluctuations

Table H3. Drawdown data for KBMP 11, December 8, 1989.

Water level at maximum drawdown = 1.81 ft above sea level

Time, in minutes	Recovery, in feet	*Recovery, in feet		Time, in minutes	Recovery, in feet	*Recovery, in feet
1	0.14	0.14		95	1.18	1.18
2	0.28	0.28		100	1.19	1.26
3	0.4	0.4		120	1.22	1.27
4	0.48	0.48		150	1.28	1.26
5	0.54	0.54		180	1.34	1.27
6	0.59	0.59		210	1.4	1.28
7	0.64	0.64		240	1.48	1.3
8	0.69	0.69		270	1.59	1.37
9	0.72	0.72		360	1.69	1.42
10	0.74	0.74		420	1.61	1.34
15	0.85	0.85		480	1.51	1.34
20	0.91	0.91		540	1.44	1.42
25	0.95	0.95		600	1.34	1.47
30	0.99	0.99		660	1.32	1.57
35	1	1		720	1.3	1.6
40	1.01	1.01		780	1.31	1.55
45	1.01	1.01		840	1.39	1.49
55	1.08	1.08		900	1.46	1.44
60	1.09	1.09		960	1.86	1.53
65	1.1	1.1		1020	1.99	1.59
70	1.11	1.11		1080	1.96	1.57
75	10.1	10.1		1140	1.73	1.54
80	1.13	1.13		1260	1.54	1.62
85	1.13	1.13		1334	0.99	
90	1.15	1.15				

* Recovery data corrected for tidal and barometric fluctuations

Table H4. Recovery data for KBMP 11, December 10, 1989.

Static water level = 2.67 ft above sea level

Time, in minutes	Drawdown, in feet	*Drawdown, in feet	Time, in minutes	Drawdown, in feet	*Drawdown, in feet
1	0.2	0.2	281	0.95	1.19
2	0.21	0.21	341	1.09	1.25
3	0.25	0.25	401	1.11	1.17
4	0.33	0.33	461	1.2	1.15
4.5	0.39	0.39	521	1.31	1.14
5	0.46	0.46	581	1.37	1.15
5.5	0.5	0.5	641	1.37	1.14
6	0.54	0.54	701	1.32	1.19
7	0.57	0.57	761	1.21	1.2
7.5	0.6	0.6	821	1.1	1.22
8	0.65	0.65	881	0.92	1.16
9	0.67	0.67	941	0.76	1.1
10	0.68	0.68	1001	0.66	1.04
15	0.81	0.81	1121	0.73	1.07
20	0.88	0.88	1241	1.05	1.15
25	0.91	0.91	1361	1.2	1.08
30	0.93	0.93	1481	1.23	1.16
35	0.95	0.95	1601	1.1	1.22
40	0.96	0.96	1721	0.97	1.23
45	0.97	0.97	1841	1.07	1.28
50	0.97	0.97	1961	1.26	1.26
55	0.98	0.98	2081	1.18	1.18
86	0.97	0.97	2201	1.23	1.23
101	0.91	1.06	2321	1.17	1.17
131	0.93	1.13	2441	1.23	1.23
161	0.9	1.13	2561	1.18	1.18
191	0.86	1.11	2681	1.23	1.23
221	0.86	1.12	2801	1.16	1.16
251	0.9	1.15			

* Drawdown data corrected for tidal and barometric fluctuations

Table H5. Drawdown data for KBMP 12, December 8, 1989.

Water level at maximum drawdown = 1.51 ft above sea level

Time, in minutes	Recovery, in feet	*Recovery, in feet	Time, in minutes	Recovery, in feet	*Recovery, in feet
1	0.09	0.09	74	1.17	1.17
2	0.18	0.18	79	1.19	1.19
3	0.25	0.25	84	1.19	1.19
4	0.31	0.31	89	1.21	1.21
4.5	0.38	0.38	94	1.23	1.23
5	0.42	0.42	99	1.23	1.28
5.5	0.48	0.48	120	1.28	1.32
6	0.54	0.54	150	1.34	1.33
6.5	0.56	0.56	180	1.41	1.34
7	0.6	0.6	210	1.49	1.36
7.5	0.62	0.62	240	1.57	1.39
8	0.67	0.67	270	1.64	1.41
8.5	0.67	0.67	300	1.67	1.41
9	0.72	0.72	360	1.75	1.45
10	0.75	0.75	420	1.7	1.43
10.5	0.75	0.75	480	1.59	1.42
11	0.8	0.8	540	1.49	1.47
14	0.86	0.86	600	1.42	1.55
19	0.92	0.92	660	1.38	1.63
24	0.98	0.98	720	1.36	1.65
29	1.01	1.01	780	1.35	1.65
34	1.03	1.03	840	1.41	1.51
39	1.07	1.07	900	1.54	1.49
44	1.08	1.08	960	1.92	1.59
49	1.1	1.1	1020	2.08	1.68
54	1.12	1.12	1080	2.07	1.67
59	1.14	1.14	1140	1.83	1.64
64	1.14	1.14	1260	1.61	1.52
69	1.16	1.16	1330	1.54	1.54

* Recovery data corrected for tidal and barometric fluctuations

Table H6. Recovery data for KBMP 12, December 10, 1989.

Calculations for transmissivity and storage values of the Pliocene-Miocene aquifer using the Hantush-Jacob leaky method (1955).

$$T = \frac{Q}{4\pi s} W(u)$$

$$S = 4 T \frac{t/r^2}{1/u}$$

$$K'/b' = 4 T v^2/r^2$$

KBMP 11 Drawdown

$$T = \frac{1.54 \text{ ft}^3/\text{min}}{4 \pi (0.51 \text{ ft})} (1.0)$$

$$T = 0.240 \text{ ft}^2/\text{min}$$

$$T = 346 \text{ ft}^2/\text{d}$$

$$S = 4 (346 \text{ ft}^2/\text{d}) \frac{(9.38 \times 10^{-4} \text{ d})/(247 \text{ ft})^2}{1.0/1.0}$$

$$S = 2.12 \times 10^{-5}$$

$$K'/b' = 4 (346 \text{ ft}^2/\text{d}) \frac{(0.2)^2}{(247 \text{ ft})^2}$$

$$K'/b' = 9.07 \times 10^{-4} \text{ ft/d/ft}$$

KBMP 11 Recovery

$$T = \frac{1.54 \text{ ft}^3/\text{min}}{4 \pi (0.35 \text{ ft})} (1.0)$$

$$T = 0.350 \text{ ft}^2/\text{min}$$

$$T = 504 \text{ ft}^2/\text{d}$$

$$S = 4 (504 \text{ ft}^2/\text{d}) \frac{(4.38 \times 10^{-4} \text{ d})/(247 \text{ ft})^2}{1.0/1.0}$$

$$S = 1.44 \times 10^{-5}$$

$$K'/b' = 4 (504 \text{ ft}^2/\text{d}) \frac{(0.1)^2}{(247 \text{ ft})^2}$$

$$K'/b' = 3.3 \times 10^{-4} \text{ ft/d/ft}$$

KBMP 12 Drawdown

$$T = \frac{1.54 \text{ ft}^3/\text{min}}{4 \pi (0.75 \text{ ft})} (1.0)$$

$$T = 0.163 \text{ ft}^2/\text{min}$$

$$T = 235 \text{ ft}^2/\text{d}$$

$$S = 4 (235 \text{ ft}^2/\text{d}) \frac{(1.58 \times 10^{-3} \text{ d}) / (168 \text{ ft})^2}{1.0/1.0}$$

$$S = 5.27 \times 10^{-5}$$

$$K'/b' = 4 (235 \text{ ft}^2/\text{d}) \frac{(0.35)^2}{(168 \text{ ft})^2}$$

$$K'/b' = 4.08 \times 10^{-3} \text{ ft/d/ft}$$

KBMP 12 Recovery

$$T = \frac{1.54 \text{ ft}^3/\text{min}}{4 \pi (0.65 \text{ ft})} (1.0)$$

$$T = 0.189 \text{ ft}^2/\text{min}$$

$$T = 271 \text{ ft}^2/\text{d}$$

$$S = 4 (271 \text{ ft}^2/\text{d}) \frac{(1.46 \times 10^{-3} \text{ d}) / (168 \text{ ft})^2}{1.0/1.0}$$

$$S = 5.6 \times 10^{-5}$$

$$K'/b' = 4 (271 \text{ ft}^2/\text{d}) \frac{(0.24)^2}{(168 \text{ ft})^2}$$

$$K'/b' = 2.21 \times 10^{-3} \text{ ft/d/ft}$$

Straight line calculations:

Transmissivity calculated from second straight line (Bixel and Van Poolen, 1967)

$$T_1 = \frac{2.3 Q}{4 \pi s}$$

Transmissivity calculated from third straight line

$$T_2 = \frac{T_1 (2m_1 - m')}{m'}$$

Diffusivity (Streltsova, 1988)

$$\eta = \frac{r^2}{2.246 (t_0)}$$

Storage (Freeze and Cherry, 1979)

$$S = \frac{T}{\eta}$$

KBMP 11 drawdown

2nd curve

$$T_1 = \frac{2.3 \times 1.54 \text{ ft}^2/\text{min}}{4 \pi \times 0.8 \text{ ft}} = 0.353 \text{ ft}^2/\text{min} = 507 \text{ ft}^2/\text{d}$$

$$K = \frac{T}{b} = \frac{507 \text{ ft}^2/\text{d}}{7 \text{ ft}} = 72.4 \text{ ft/d}$$

$$V_s = \frac{K i}{\eta} = \frac{72.4 \text{ ft/d} (5.52 \text{ ft} - 2.59 \text{ ft})}{0.30 \times 10,660 \text{ ft}} = 0.066 \text{ ft/d}$$

$$\eta = \frac{(247 \text{ ft})^2}{2.246 (1.25 \text{ min})} = 21730.7 \text{ ft}^2/\text{min}$$

$$S = \frac{507 \text{ ft}^2/\text{d}}{21730.7 \text{ ft}^2/\text{min} \times 1440 \text{ min/d}} = 1.62 \times 10^{-5}$$

3rd curve

$$T_2 = \frac{507 \text{ ft}^2/\text{d} (2 (0.8) - 0.33)}{0.33} = 1951.2 \text{ ft}^2/\text{d}$$

KBMP 11 Recovery

2nd curve

$$T_1 = \frac{2.3 \times 1.54 \text{ ft}^2/\text{min}}{4 \pi \cdot 0.62 \text{ ft}} = 0.454 \text{ ft}^2/\text{min} = 653 \text{ ft}^2/\text{d}$$

$$K = \frac{653 \text{ ft}^2/\text{d}}{7 \text{ ft}} = 93.2 \text{ ft/d}$$

$$V_s = \frac{K i}{\eta} = \frac{93.2 \text{ ft/d} (5.52 \text{ ft} - 2.59 \text{ ft})}{0.30 \cdot 10,660 \text{ ft}} = 0.085 \text{ ft/d}$$

$$\eta = \frac{(247 \text{ ft})^2}{2.246 (0.63 \text{ min})} = 43116.5 \text{ ft}^2/\text{min}$$

$$S = \frac{653 \text{ ft}^2/\text{d}}{43116.5 \text{ ft}^2/\text{min} \times 1440 \text{ min/d}} = 1.05 \times 10^{-5}$$

3rd curve

$$T_2 = \frac{653 \text{ ft}^2/\text{d} (2 (0.62) - 0.38)}{0.38} = 1477.8 \text{ ft}^2/\text{d}$$

KBMP 12 drawdown

2nd curve

$$T_1 = \frac{2.3 \times 1.54 \text{ ft}^2/\text{min}}{4 \pi \cdot 0.93 \text{ ft}} = 0.303 \text{ ft}^2/\text{min} = 436 \text{ ft}^2/\text{d}$$

$$K = \frac{436 \text{ ft}^2/\text{d}}{7 \text{ ft}} = 62.3 \text{ ft/d}$$

$$V_s = \frac{K i}{\eta} = \frac{62.7 \text{ ft/d} (5.52 \text{ ft} - 2.59 \text{ ft})}{0.30 \cdot 10,660 \text{ ft}} = 0.057 \text{ ft/d}$$

$$\eta = \frac{(168 \text{ ft})^2}{2.246 (1.75 \text{ min})} = 7180.8 \text{ ft}^2/\text{min}$$

$$S = \frac{436 \text{ ft}^2/\text{d}}{7180.8 \text{ ft}^2/\text{min} \times 1440 \text{ min/d}} = 4.2 \times 10^{-5}$$

3rd curve

$$T_2 = \frac{436 \text{ ft}^2/\text{d} (2 (0.93) - 0.33)}{0.33} = 2021 \text{ ft}^2/\text{d}$$

KBMP 12 recovery

2nd curve

$$T_1 = \frac{2.3 \times 1.54 \text{ ft}^2/\text{min}}{4 \pi \times 1.07 \text{ ft}} = 0.264 \text{ ft}^2/\text{min} = 379.5 \text{ ft}^2/\text{d}$$

$$K = \frac{379.5 \text{ ft}^2/\text{d}}{7 \text{ ft}} = 54.2 \text{ ft/d}$$

$$V_s = \frac{K i}{\eta} = \frac{54.2 \text{ ft/d} (5.52 \text{ ft} - 2.59 \text{ ft})}{0.30 \times 10,660 \text{ ft}} = 0.049 \text{ ft/d}$$

$$\eta = \frac{(168 \text{ ft})^2}{2.246 (2.1 \text{ min})} = 5983.9 \text{ ft}^2/\text{min}$$

$$S = \frac{379.5 \text{ ft}^2/\text{d}}{5983.9 \text{ ft}^2/\text{min} \times 1440 \text{ min/d}} = 4.4 \times 10^{-5}$$

3rd curve

$$T_2 = \frac{379.5 \text{ ft}^2/\text{d} (2 (1.07) - 0.45)}{0.45} = 1425 \text{ ft}^2/\text{d}$$

KBMP 7 drawdown

$$T_1 = \frac{2.3 \times 1.54 \text{ ft}^2/\text{min}}{4 \pi \times 0.63 \text{ ft}} = 644 \text{ ft}^2/\text{d}$$

KBMP 7 recovery

$$T_1 = \frac{2.3 \times 1.54 \text{ ft}^2/\text{min}}{4 \pi \times 0.62 \text{ ft}} = 654 \text{ ft}^2/\text{d}$$

Streltsova (1988) straight line method

Transmissivity calculated from second straight line

$$T_1 = \frac{2.3 Q}{4 \pi s}$$

Transmissivity calculated from third straight line

$$T_2 = \frac{T_1 (2m_1 - m')}{m'}$$

KBMP 11 Drawdown

$$T_1 = \frac{2.3 \times 1.54 \text{ ft}^2/\text{min}}{4 \pi \times 0.8 \text{ ft}} = 0.353 \text{ ft}^2/\text{min} = 507 \text{ ft}^2/\text{d}$$

$$T_2 = \frac{507 \text{ ft}^2/\text{d} (0.8 - 0.33)}{0.33} = 722 \text{ ft}^2/\text{d}$$

KBMP 11 Recovery

$$T_1 = \frac{2.3 \times 1.54 \text{ ft}^2/\text{min}}{4 \pi \times 0.62 \text{ ft}} = 0.454 \text{ ft}^2/\text{min} = 653 \text{ ft}^2/\text{d}$$

$$T_2 = \frac{653 \text{ ft}^2/\text{d} (0.62 - 0.38)}{0.38} = 412 \text{ ft}^2/\text{d}$$

KBMP 12 Drawdown

$$T_1 = \frac{2.3 \times 1.54 \text{ ft}^2/\text{min}}{4 \pi \times 0.93 \text{ ft}} = 0.303 \text{ ft}^2/\text{min} = 436 \text{ ft}^2/\text{d}$$

$$T_2 = \frac{436 \text{ ft}^2/\text{d} (0.93 - 0.33)}{0.33} = 792 \text{ ft}^2/\text{d}$$

KBMP 12 Recovery

$$T_1 = \frac{2.3 \times 1.54 \text{ ft}^2/\text{min}}{4 \pi \times 1.07 \text{ ft}} = 0.264 \text{ ft}^2/\text{min} = 379.5 \text{ ft}^2/\text{d}$$

$$T_2 = \frac{380 \text{ ft}^2/\text{d} (1.07 - 0.45)}{0.45} = 522 \text{ ft}^2/\text{d}$$

APPENDIX I

Tidal Effects

Tidal Efficiency

Water levels in wells penetrating confined aquifers respond to nearby fluctuating tides due to the compression and expansion of the overlying confining layers as the load of the tidal water changes. Well tidal efficiency is the effectiveness of a well's response to fluctuating tides measured in percentage. The tidal efficiency decreases with the depth of a well and the distance from the tidal body. Well construction and the hydrogeology of the screened interval also are factors in the degree of tidal efficiency (Gregg, 1966). A poorly constructed well in a low permeable zone will have a low tidal efficiency.

The tides on Cumberland Island are nearly semidiurnal and range from 6 to 8 feet. They are measured by a continuous tide-stage recorder operated by the USGS. The recorder is located at the Dungeness dock on the west side of Cumberland Island.

Along the west coast, the island is affected by channel tides and on the east coast by ocean tides. These tides probably do not have the same magnitude at the same time which causes asymmetrical water-level changes in the confined aquifers. This difference in tide stage could not be accounted for in calculations since tidal data are not available on the ocean side of the island.

The tidal efficiency equation takes into account the barometric pressure change and is expressed as:

$$\text{T.E.} = \frac{\text{barometric change} - \text{water level change}}{\text{barometric change} - \text{tidal change}} \quad (\text{I1})$$

(Gregg, 1966).

The tidal efficiency was calculated for one-half of a tide cycle for each of the wells. The change in tide was corrected to its freshwater equivalent by multiplying the tidal change by the seawater density (1.025 gm/cm³) and dividing by the freshwater density (1.0 gm/cm³) as shown below:

$$\text{tidal change} = \text{uncorrected tidal change (ft)} \times \frac{1.025 \text{ ft. seawater/unit weight}}{1.000 \text{ ft. freshwater/unit weight}} \quad (12)$$

(Gregg, 1966).

The drawdown and recovery data for each of the monitoring wells does not form a smooth curve or straight line after about 100 min. from the initial pumping or recovery time due to the influence of tidal fluctuations. During the first 100 min. of drawdown and recovery, the data were not corrected for tidal fluctuation because the magnitude of the drawdown and recovery had a greater impact on water levels than did the tidal effects. The data were corrected for tidal fluctuations by calculating the tidal efficiency; multiplying this value by the tide level; then subtracting or adding the new value to the water level, depending on high or low tidal fluctuations, respectively. This technique minimized the tidal fluctuations in the data, but did not entirely alleviate them. This is partially due to the variation of lag time from one-half of a tide cycle to the next half of a tide cycle (high to low tide or vice versa) ranging from 0.5 to 1.5 hours. The time lag was "ignored" during tidal efficiency calculations by matching the high and low ocean tides with the high and low water levels by a shift in time. Variations in lag time made it difficult to choose corresponding tide levels between half tides. Also, because the tidal fluctuation data were recorded in 15-minute intervals, the corresponding tide level could not be matched exactly to the water level for a given time.

The tidal efficiencies calculated for KBMP 7 (9.4 percent), KBMP 11 (7.9 percent), and KBMP 12 (8.2 percent) were in close agreement, which is logical since these wells are in the same zone and are located relatively close. The tidal efficiency for KBMP 9 (7.2 percent) is located close to those wells tapping the limestone zone. Although this well

penetrates a different type of lithology, the well construction is similar to KBMP 7 and is located close to the previously mentioned wells.

Well KBMP 10 has a tidal efficiency of 1.4 percent. Although it is located in the same area as the other wells and the well construction is similar, the hydrogeology is much different. The well taps a zone that has a low hydraulic conductivity. Therefore, propagation of tidal fluctuations is not as effective in this zone.

The tidal efficiency is calculated by:

$$\text{T.E.} = \frac{\text{barometric change} - \text{water level change}}{\text{barometric change} - \text{tidal change}} \quad (13)$$

The tidal efficiency was calculated for one-half of a tide cycle for each of the wells. The change in tide was corrected to its freshwater equivalent by multiplying the tidal change by the seawater density (1.025 g/cm³) and dividing by the freshwater density (1.0 g/cm³) as shown below:

$$\text{tidal change} = \text{uncorrected tidal change (ft)} \times \frac{1.025 \text{ ft. seawater/unit weight}}{1.000 \text{ ft. freshwater/unit weight}} \quad (14)$$

(Gregg, 1966).

The tide intensity and lag varied from each tide cycle which caused the calculated tidal efficiency to vary for a well for each tide cycle. The tidal efficiency was calculated for each well for 3 or 4 half tide cycles. The average value was assumed for the well tidal efficiency.

KBMP 7 tidal efficiency:

8/12/89-9/12/90

change in barometric pressure = 0 ft.

change in water level = (6.32 ft. - 5.53 ft.) = 0.79 ft.

change in tide level = (-2.75 ft. + 4.92 ft.) = 7.67 ft. x 1.025 ft. seawater/unit

weight = 7.86

$$\frac{0.79 \text{ ft.}}{7.86 \text{ ft.}} = 10.1\%$$

11/12/90

change in barometric pressure = 0 ft.

change in water level = (19.54 ft. - 20.35 ft.) = 0.81 ft.

change in tide level = (-3.72 ft. + 4.86 ft.) = 8.58 ft. x 1.025 ft. seawater/unit

weight = 8.79

$$\frac{0.81 \text{ ft.}}{8.79 \text{ ft.}} = 9.2\%$$

10/12/90-11/12/90

change in barometric pressure = 0 ft.

change in water level = (5.53 ft. - 6.15 ft.) = 0.62 ft.

change in tide level = (-1.76 ft. + 4.92 ft.) = 6.68 ft. x 1.025 ft. seawater/unit

weight = 6.85

$$\frac{0.62 \text{ ft.}}{6.85 \text{ ft.}} = 9.1\%$$

The average tidal efficiency for KBMP 7 is 9.4%.

KBMP 11 tidal efficiency:

8/12/90-9/12/90

change in barometric pressure = 0.01 ft.

change in water level = 0.69 ft.

change in tide level = 7.67 ft. x 1.025 ft. seawater/unit weight = 7.86

$$\frac{0.01 - 0.69 \text{ ft.}}{0.01 - 7.86 \text{ ft.}} = 8.7\%$$

9/12/90-10/12/90

change in barometric pressure = 0.01 ft.

change in water level = 0.63 ft.

change in tide level = 8.35 ft. x 1.025 ft. seawater/unit weight = 8.56

$$\frac{0.01 - 0.63 \text{ ft.}}{0.01 - 8.56 \text{ ft.}} = 7.3\%$$

9/12/90

change in barometric pressure = 0 ft.

change in water level = 0.51 ft.

change in tide level = 6.68 ft. x 1.025 ft. seawater/unit weight = 6.85

$$\frac{0.51 \text{ ft.}}{6.85 \text{ ft.}} = 7.5\%$$

11/12/90

change in barometric pressure = 0 ft.

change in water level = 0.69 ft.

change in tide level = 8.58 ft. x 1.025 ft. seawater/unit weight = 8.79

$$\frac{0.69 \text{ ft.}}{8.79 \text{ ft.}} = 7.8\%$$

The average tide efficiency for KBMP 11 is 7.8%.

KBMP 12 tide efficiency 8/12/90-9/12/90:

change in barometric pressure = 0.01 ft.

change in water level = 0.71 ft.

change in tide level = 7.67 ft. x 1.025 ft. seawater/unit weight = 7.86

$$\frac{0.01 - 0.71 \text{ ft.}}{0.01 - 7.86 \text{ ft.}} = 8.9\%$$

9/12/90

change in barometric pressure = 0 ft.

change in water level = 0.57 ft.

change in tide level = 6.68 ft. x 1.025 ft. seawater/unit weight = 6.8 ft.

$$\frac{0.57 \text{ ft.}}{6.8 \text{ ft.}} = 8.4\%$$

11/12/90

change in barometric pressure = 0 ft.

change in water level = 0.73 ft.

change in tide level = 8.58 ft. x 1.025 ft. seawater/unit weight = 8.79 ft.

$$\frac{0.73 \text{ ft.}}{8.79 \text{ ft.}} = 8.3\%$$

The average tide efficiency for KBMP12 is 8.5%

The tide efficiency for KBMP 9:
8/12/90-9/12/90

change in barometric pressure = 0.01 ft.

change in water level = 0.52 ft.

change in tide level = 7.67 ft. x 1.025 ft. seawater/unit weight = 7.86 ft.

$$\frac{0.01 - 0.52 \text{ ft.}}{0.01 - 7.86 \text{ ft.}} = 6.5\%$$

9/12/90

change in barometric pressure = 0 ft.

change in water level = 0.53 ft.

change in tide level = 6.68 ft. x 1.025 ft. seawater/unit weight = 6.8 ft.

$$\frac{0.53 \text{ ft.}}{6.8 \text{ ft.}} = 7.8\%$$

9/12/90-10/12/90

change in barometric pressure = 0.01 ft.

change in water level = 0.67 ft.

change in tide level = 8.35 ft. x 1.025 ft. seawater/unit weight = 8.56

$$\frac{0.01 - 0.67 \text{ ft.}}{0.01 - 8.56 \text{ ft.}} = 7.7\%$$

11/12/90

change in barometric pressure = 0 ft.

change in water level = 0.60 ft.

change in tide level = 8.58 ft. x 1.025 ft. seawater/unit weight = 8.79 ft.

$$\frac{0.60 \text{ ft.}}{8.79 \text{ ft.}} = 6.8\%$$

The average tide efficiency for KBMP 9 is 7.2%.

The tide efficiency for KBMP 10 8/12/90-9/12/90:

change in barometric pressure = 0.01 ft.

change in water level = 0.19 ft.

change in tide level = 7.67 ft. x 1.025 ft. seawater/unit weight = 7.86 ft.

$$\frac{0.01 - 0.19 \text{ ft.}}{0.01 - 7.86 \text{ ft.}} = 2.3\%$$

9/12/90

change in barometric pressure = 0 ft.

change in water level = 0.06 ft.

change in tide level = 6.68 ft. x 1.025 ft. seawater/unit weight = 6.8 ft.

$$\frac{0.06 \text{ ft.}}{6.8 \text{ ft.}} = 0.9\%$$

9/12/90-10/12/90

change in barometric pressure = 0.01 ft.

change in water level = 0.09 ft.

change in tide level = 6.99 ft. seawater/unit weight = 7.16 ft.

$$\frac{0.01 - 0.09 \text{ ft.}}{0.01 - 7.16 \text{ ft.}} = 1.1\%$$

11/12/90

change in barometric pressure = 0 ft.

change in water level = 0.09 ft.

change in tide level = 8.58 ft. x 1.025 ft. seawater/unit weight = 8.79

$$\frac{0.09 \text{ ft.}}{8.79 \text{ ft.}} = 1.0\%$$

The average tide efficiency for KBMP 9 is 1.3%

APPENDIX J

Calculations for Potential Seawater Intrusion

The following equation is used to determine the net volume of water exiting the Pliocene-Miocene aquifer in the channel.

$$\frac{V}{A} = \frac{K}{\Delta L} \left[\left(\frac{m_1 t^2}{2} + b_1 t \right)_0^3 + \left(\frac{m_2 t^2}{2} + b_2 t \right)_3^9 + \left(\frac{m_3 t^2}{2} + b_3 t \right)_9^{15} + \left(\frac{m_4 t^2}{2} + b_4 t \right)_{15}^{20} + \left(\frac{m_4 t^2}{2} + b_4 t \right)_{20}^{21} + \left(\frac{m_5 t^2}{2} + b_5 t \right)_{21}^{24} \right] \quad (J1)$$

The total volume of water exiting the Pliocene-Miocene aquifer into the channel is calculated by:

$$\frac{V}{A} = \frac{K}{\Delta L} \left[\left(\frac{m_1 t^2}{2} + b_1 t \right)_0^3 + \left(\frac{m_2 t^2}{2} + b_2 t \right)_3^9 + \left(\frac{m_3 t^2}{2} + b_3 t \right)_9^{15} + \left(\frac{m_4 t^2}{2} + b_4 t \right)_{15}^{20} \right] \quad (J2)$$

The total volume of seawater entering the Pliocene-Miocene aquifer from the channel is calculated by:

$$\frac{V}{A} = \frac{K}{\Delta L} \left[\left(\frac{m_4 t^2}{2} + b_4 t \right)_{20}^{21} + \left(\frac{m_5 t^2}{2} + b_5 t \right)_{21}^{24} \right] \quad (J3)$$

Well site 3

$$K = 2.3 \text{ ft/hr}$$

$$\Delta L = 5405.7 \text{ ft.}$$

$$\begin{aligned} \frac{V}{A} = & \frac{2.3 \text{ ft/hr}}{5405.7 \text{ ft.}} \left[\left[\frac{1.66 \text{ ft/hr} (3\text{hr})^2}{2} + (0 \text{ ft.})(3 \text{ hr}) - 0 \right]_0^3 + \right. \\ & \left. \left[\frac{-0.8 \text{ ft/hr} (9\text{hr})^2}{2} + 7.3\text{ft} (9\text{hr}) - \frac{-0.8 \text{ ft/hr} (3\text{hr})^2}{2} + 7.3\text{ft} (3\text{hr}) \right]_3^9 + \right. \\ & \left. \left[\frac{0.76 \text{ ft/hr} (15\text{hr})^2}{2} + -6.7\text{ft} (15\text{hr}) - \frac{0.76 \text{ ft/hr} (9\text{hr})^2}{2} + -6.7\text{ft} (9\text{hr}) \right]_9^{15} + \right. \\ & \left. \left[\frac{-0.96 \text{ ft/hr} (20\text{hr})^2}{2} + 19.2\text{ft} (20\text{hr}) - \frac{-0.96 \text{ ft/hr} (15\text{hr})^2}{2} + 19.2\text{ft} (15\text{hr}) \right]_{15}^{20} \right] + \end{aligned}$$

$$\frac{V}{A} = \frac{2.3 \text{ ft/hr}}{5405.7 \text{ ft}} \quad 48.99 \text{ ft.hr.}$$

$$\frac{V}{A} = 0.02 \text{ feet per 20 hours}$$

$$\frac{V}{A} = \frac{2.3 \text{ ft/hr}}{5405.7} \left[\frac{-0.96 \text{ ft/hr} (21\text{hr})^2}{2} + 19.2\text{ft} (21\text{hr}) - \frac{-0.96 \text{ ft/hr} (20\text{hr})^2}{2} + 19.2\text{ft} (20\text{hr}) \right]_{20}^{21}$$

$$\left[\frac{0.33 \text{ ft/hr} (24\text{hr})^2}{2} + -8.0\text{ft} (24\text{hr}) - \frac{0.33 \text{ ft/hr} (21\text{hr})^2}{2} + -8.0\text{ft} (21\text{hr}) \right]_{21}^{24}$$

$$\frac{V}{A} = \frac{2.3 \text{ ft/hr}}{5405.7 \text{ ft}} \quad 2.21 \text{ ft.hr.}$$

$$\frac{V}{A} = 0.001 \text{ feet per 4 hours}$$

The net volume of flushing over a 24 hour period is $0.019 \text{ ft}^3/\text{ft}^2/\text{d}$



As the nation's principal conservation agency, the Department of the Interior has responsibility for most of our nationally owned public lands and natural and cultural resources. This includes fostering wise use of our land and water resources, protecting our fish and wildlife, preserving the environmental and cultural values of our national parks and historical places, and providing for enjoyment of life through outdoor recreation. The department assesses our energy and mineral resources and works to ensure that their development is in the best interests of all our people. The department also promotes the goals of the Take Pride in America campaign by encouraging stewardship and citizen responsibility for American Indian reservation communities and for the people who live in island territories under U.S. administration.

